

# **CONTRACTOR REPORT**

SAND96-2205  
Unlimited Release  
UC-1211

## **Final Project Report: High-Energy Rotor Development, Test and Evaluation**

FloWind Corporation  
990 A Street, Suite 300  
San Rafael, California 94901

Prepared by Sandia National Laboratories Albuquerque, New Mexico 87185  
and Livermore, California 94550 for the United States Department of Energy  
under Contract DE-AC04-94AL85000

Printed September 1996

Issued by Sandia National Laboratories, operated for the United States Department of Energy by Sandia Corporation.

**NOTICE:** This report was prepared as an account of work sponsored by an agency of the United States Government. Neither the United States Government nor any agency thereof, nor any of their employees, nor any of their contractors, subcontractors, or their employees, makes any warranty, express or implied, or assumes any legal liability or responsibility for the accuracy, completeness, or usefulness of any information, apparatus, product, or process disclosed, or represents that its use would not infringe privately owned rights. Reference herein to any specific commercial product, process, or service by trade name, trademark, manufacturer, or otherwise, does not necessarily constitute or imply its endorsement, recommendation, or favoring by the United States Government, any agency thereof or any of their contractors or subcontractors. The views and opinions expressed herein do not necessarily state or reflect those of the United States Government, any agency thereof or any of their contractors.

Printed in the United States of America. This report has been reproduced directly from the best available copy.

Available to DOE and DOE contractors from  
Office of Scientific and Technical Information  
PO Box 62  
Oak Ridge, TN 37831

Prices available from (615) 576-8401, FTS 626-8401

Available to the public from  
National Technical Information Service  
US Department of Commerce  
5285 Port Royal Rd  
Springfield, VA 22161

NTIS price codes  
Printed copy: A06  
Microfiche copy: A01

SAND96-2205  
Unlimited Release  
Printed September, 1996

**FINAL PROJECT REPORT:**

**HIGH ENERGY ROTOR**

**DEVELOPMENT, TEST AND EVALUATION**

by

**FLOWIND CORPORATION**

990 A Street, Suite 300  
San Rafael, CA 94901

**SANDIA CONTRACT: AB-7292**

**ABSTRACT**

Under the auspices of the "Government/Industry Wind Technology Applications Project" ["Letter of Interest" (LOI) Number RC-1-11101], FloWind Corp. has successfully developed, tested, and delivered a high-energy rotor upgrade candidate for their 19-meter Vertical Axis Wind Turbine. The project included the demonstration of the innovative extended height-to-diameter ratio concept, the development of a continuous-span single-piece composite blade, the demonstration of a continuous blade manufacturing technique, the utilization of the Sandia National Laboratories developed SNLA 2150 natural laminar flow airfoil and the reuse of existing wind turbine and wind power plant infrastructure.

This report and its accompanying figures are printed as supplied to Sandia National Laboratories by FloWind.

## Contents

-	List of Figures	vii
-	List of Tables	viii
-	Glossary of Terms	ix
-	Executive Summary	1
-	Introduction	2
I.	Configuration Optimization	3
	I.1 Baseline Design Objectives	
	I.2 Structural Design Criteria	
	I.3 System Modeling Methodology	
	I.4 Optimized Machine Design	
II.	Detailed Design	13
	II.1 Structural System Design	
	II.2 Rotor Component Design Methodology Using the VAWT System Model	
	II.3 "A" Blade and Laminate	
	II.4 Root Joint	
	II.5 Struts	
	II.6 Upper Bearing	
	II.7 Lower Bearing	
	II.8 Rotor Stand	
	II.9 Foundation	
	II.10 Guy Cables and Anchors	
	II.11 Microprocessor	
III.	Supporting Laboratory Tests	22
	III.1 Blade Material Coupon Ultimate Property Testing	
	III.2 Additional Blade Property Testing	
	III.3 Blade Root Fatigue Testing	
	III.4 Blade Thermal Coefficient of Expansion	
IV.	Parts Procurement	23
	IV.1 Competitive Bidding	
	IV.2 Vendor Qualification	
	IV.3 First Article Inspection	
	IV.4 Quality Control	
	IV.5 Shipment	

V.	Site Preparation	24
	V.1 Site Prep - Construction	
	V.2 Site Prep - Testing	
VI.	Turbine Assembly, Installation, Commissioning	27
	VI.1 Component Weight	
	VI.2 Component Assembly and Erection	
	VI.3 Commissioning	
VII.	Turbine Instrumentation & Test Planning	28
	VII.1 Test Bed Site Selection	
	VII.2 Data Acquisition System and Data Signal Network	
VIII.	Test & Evaluation	30
	VIII.1 Data Acquisition Primary Data Types	
	VIII.2 Data Analysis Software Tools	
	VIII.3 Turbine to Meteorological Tower Correlation	
	VIII.4 Test Matrix Results Summary	
IX.	Design Modifications & Planning for Fleet Deployment	40
	- Final Summary	42
	- References	44

## List of Figures

<u>Figure No#</u>	<u>Figure Description</u>
Figure 1	SNLA 2150 27" airfoil vs NACA0015 28" airfoil
Figure 2	17 & 19 Meter NACA 0015 Clean vs Dirty Power Curve
Figure 3	Laminate S/N Curve
Figure 4	Steel S/N Curve
Figure 5	3D 17 EHD & 19-m
Figure 6	Campbell Diagram (60.89 rpm) with SNLA2150 blade
Figure 7	Blade Total Stress Outer Surface - Gravity Only
Figure 8	Blade Total Stress Inner Surface - Gravity Only
Figure 9	Blade Total Stress Outer Surface - Gravity & Omega
Figure 10	Blade Total Stress Outer Surface - Gravity & Omega
Figure 11	Blade Flatwise Dynamic RMS Stress
Figure 12	Blade Edgewise Dynamic RMS Stress
Figure 13	"A" Blade Airfoil Cross-Section
Figure 14	Deformation, Gravity Plus High Wind
Figure 15	NISA Blade FEA Model
Figure 16	Upgrade Root Joint Iteration Number 1
Figure 17	Upgrade Root Joint Iteration Number 1
Figure 18	Upgrade Root Joint - Flatwise Moment Stress
Figure 19	Upgrade Root Joint - Flatwise Moment Stress
Figure 20	Upgrade Root Joint - Axial Moment Stress
Figure 21	Upgrade Root Joint - Axial Moment Stress
Figure 22	Upgrade Root Joint - Edgewise Moment Stress
Figure 23	Upgrade Root Joint - Edgewise Moment Stress
Figure 24	Root Joint Bolt Interface Model, Iteration Number 0
Figure 25	Root Bolt Model, Iteration Number 1, Flatwise Response
Figure 26	Root Bolt Model, Iteration Number 1, Flatwise Response
Figure 27	Root Bolt Model, Iteration Number 1, Edgewise Response
Figure 28	Root Bolt Model, Iteration Number 1, Edgewise Response
Figure 29	V-Strut Model
Figure 30	V-Strut Model
Figure 31	V-Strut, Edgewise Force at Blade
Figure 32	V-Strut, Flatwise Moment at Blade
Figure 33	Upper Bearing Assembly FEA Model
Figure 34	Base Structure (pedestal model)
Figure 35	Guy Anchor Foundation
Figure 36	Test Site Layout
Figure 37	17 EHD Strain Gage Locations
Figure 38	Strain Gage Listing (original layout), STRGGMP3.wk4, p.1.

**List of Figure  
(concluded)**

<u>Figure No#</u>	<u>Figure Description</u>
Figure 39	Strain Gage Listing (original layout), STRGGMP3.wk4, p.2.
Figure 40	Test matrix
Figure 41	Predicted mode shape and frequency, 1st tower bending
Figure 42	Measured mode shape and frequency, 1st tower bending
Figure 43	Predicted mode shape and frequency, 1st propeller, brakes applied
Figure 44	Measured mode shape and frequency, 1st propeller, brakes applied
Figure 45	Predicted mode shape and frequency, 1st flatwise blade, asymmetric
Figure 46	Measured mode shape and frequency, 1st flatwise blade, asymmetric
Figure 47	Time Series, FW1121942058, Start Up Small Drive Shaft vs. 19-m Start Up
Figure 48	Time Series, FW0617941434, (stop record)
Figure 49	Measured Loads, V - Struts, 58.5 rpm, 0902 1901
Figure 50	Time History, TB00
Figure 51	Frequency Spectrum TB00
Figure 52	Loads Correlation, Pre-Tensioned Struts
Figure 53	Loads Correlation, Blade Stresses
Figure 54	Dynamic RMS Value vs Wind Speed, LSTA
Figure 55	Dynamic RMS Value vs Wind Speed, LRE1
Figure 56	Dynamic RMS Value vs Wind Speed, URF1
Figure 57	Coast Down Plot, 4/5/94
Figure 58	Measured vs Predicted Power Curve, SNLA Airfoil
Figure 59	Measured Power Curves, 60 rpm, 58.5 rpm, 51.8 rpm
Figure 60	Altamont Pass 19-m Wake Test
Figure 61	"B" Blade Turbine Campbell Diagram
Figure 62	"B" Blade Flutter Damping Coefficients
Figure 63	Viscous Flow Schematic ( $\alpha=0$ )

**List of Tables**

<u>Table No#</u>	<u>Figure Description</u>	<u>Page</u>
Table 1	Turbine Design Configuration Summary	10
Table 2	Summary of Configuration Changes	11



## Glossary of Terms and Definitions

$\alpha$	Angle of Attack
asl	above sea level
Cl	Coefficient of Lift
Cd	Coefficient of Drag
DAS	Data Acquisition System
EHD	Extended Height-to-Diameter
hp	horse power
Hz	Hertz
kg	kilogram
kip	kilo pounds per square inch
kW	kiloWatt
kWh	kiloWatt-hour
lbs	pounds
m	meter
m/s	meter per second
mph	miles per hour
NACA00##	National Advisory Committee for Aeronautics (symmetrical airfoil series), ## = airfoil thickness/chord length
psi	pounds per square inch
rad/sec	radians per second
Re	Reynolds Number
rpm	revolutions per minute
SNLA####	Sandia Natural Laminar Flow Airfoil Series (stall regulated), #### = first two ## (airfoil thickness/chord length), second two ## (maximum thickness location as a % of chord)
Vac	Volts alternating current
VAWT	Vertical Axis Wind Turbine
Vdc	Volts direct current
yd <sup>3</sup>	cubic yards

## FORWARD

The program cited in this report was conducted by FloWind Corp. under the auspices of the "Government/Industry Wind Technology Applications Project" ["Letter of Interest" (LOI) Number RC-1-11101] issued by National Renewable Energy Laboratory (NREL) on April 26, 1991. Responses to this LOI were due in July, 1992. FloWind submitted the proposal entitled "High Energy Rotor Development, Test and Evaluation," Its objective was to "develop, construct, test and evaluate a high energy rotor and related improvements..." for retrofitting their fleet of 19-m VAWTs. After a complete review of all of the proposals, the FloWind proposal was one of several selected for funding. Since Sandia National Laboratories (SNL) was the DOE "lead lab" for vertical-axis wind technology, DOE, NREL and SNL wind program management decided that the contract with FloWind should be placed and managed by the SNL Wind Energy Program.

FloWind submitted an updated proposal to SNL on May 29, 1992 and a fixed-cost contract was signed on July 23, 1992. The project was essentially completed on April 4, 1995 when FloWind conducted a final project review for selected SNL and NREL personnel at the National Wind Test Center, Boulder, CO.

The LOI required that the proposer cost-share the project. The initial proposal called for FloWind to contribute approximately 54 percent of the total cost of the project. As reported by FloWind, the cost of developing the process for making pultruded wind turbine blades were significantly higher than originally anticipated. The final cost for this project required a cost-share of 90 percent by FloWind.

H. J. Sutherland  
Technical Monitor  
August 20, 1996

## **Executive Summary**

FloWind's 17 EHD project as described in response to LOI Solicitation number RC-1-11101 entitled, "High Energy Rotor Development, Test and Evaluation" and administered under Sandia National Laboratories contract #AB-7292, embarked with the following objectives 1) develop, 2) construct, 3) test, and 4) evaluate a high-energy rotor and related improvements to the 19-meter VAWT.

FloWind Corporation, with partial funding from the Department of Energy, has successfully developed, tested and delivered a high-energy rotor upgrade candidate for the 19-meter Vertical Axis Wind Turbine. This effort included demonstration of the innovative extended height-to-diameter ratio concept, continuous-span single-piece composite blade, continuous process blade manufacturing, utilization of the Sandia National Laboratories developed SNLA 2150 natural laminar flow airfoil, and reuse of existing wind turbine and wind power plant infrastructure. In parallel with this project, and ultimately utilized by it, FloWind developed the ANSYS 5.0 PC based "Vertical Axis Wind Turbine Analysis System."

The SNLA 2150 configured turbine has met the structural requirements of the upgrade but did not meet energy projections. Performance predictions using the Eppler Airfoil Program System, and wind tunnel testing did not accurately quantify transition bubble drag. FloWind's field testing, the first commercial application of this airfoil, identified both desirable and undesirable aerodynamic characteristics. The unpublished revision of the Eppler code was successfully used to model the degradation of the SNLA 2150 due to laminar bubble formation and to design a new blade profile, identified as the "B" blade, which will be installed during the spring of 1995.

With the EHD concept proven, FloWind has committed to rapid development, testing and ultimate deployment of an alternative airfoil to further improve the output of the 17 EHD. To this end, FloWind has purchased a pultrusion machine and set up a blade manufacturing facility in Mojave, CA. Commercial application of the EHD is scheduled for 1995.

## Introduction

FloWind Corporation embarked on the development of a 19 meter high energy rotor upgrade to: 1). take advantage of the premium energy prices under existing power purchase agreements with two major California utilities (PG&E and SCE), 2). re-use existing 19 meter structural, mechanical and electrical infrastructure, and 3). effectively eliminate the design shortcomings which greatly influenced fatigue and mechanical component life of first generation VAWTs; i.e., improve reliability.

To take fullest advantage of the power purchase contracts, the upgrade design had to provide maximum energy capture using the existing 19 meter infrastructure and turbine sites.

Analyses were performed to identify candidate upgrade sites at FloWind's Tehachapi and Altamont Pass wind power plants. Approximately 169, 19 meter sites have been identified as upgrade candidates. The upgrade development focused on initial installation in Tehachapi where 90% of the 19 meter VAWT fleet is installed.

Desired infrastructure "re-use" included the following wind power plant and turbine infrastructure;

- o pad mount transformers and turbine electrical infrastructure
- o turbine foundation and anchors
- o turbine support system (guy cables, bearings and base structure)
- o turbine drive train components (drive shaft, gearbox and generator)
- o turbine control and switchgear assemblies
- o brake hydraulic system
- o mast sections
- o brake system.

This left the following components for detailed consideration;

- o blade; profile, geometry, material, manufacturing method, and connection techniques
- o strut; location, quantity, geometry and material
- o brake calipers; configuration and quantity.

To address the design shortcomings of the first generation equipment, FloWind evaluated the operating histories of both the Altamont and Tehachapi 17 and 19 meter VAWT fleets. From the historical performance and service data, FloWind determined which mechanical and structural assemblies were candidates for retrofit or redesign. A cost/benefit evaluation was performed to focus the engineering efforts on those assemblies that would yield the best return for the upgrade dollar spent.

Most of the effort ultimately focused on rotor geometry, blade profile and material, and blade manufacturing techniques.

## **I. CONFIGURATION OPTIMIZATION**

### **Plan**

Propose a turbine geometry that; 1). yielded significant increases in annual energy delivered, 2). took fullest advantage of the installed wind turbine and wind power plant infrastructure and 3). improved fatigue resistance and component reliability.

### **Accomplishments**

Developed batch processing of proposed airfoil configurations. Developed the following configurations for ultimate consideration; 1). a fiberglass blade without splices, and 2). a three bladed high height to diameter rotor geometry.

### **I.1. Baseline Design Objectives**

#### **I.1a. Double Baseline 19-meter VAWT Annual Energy Production**

FloWind's 19-m VAWT in Tehachapi delivers annual energy levels ranging between 225,000 kWh to 450,000 kWh. Local terrain, wind resource and micrositing effects have resulted in a 50% difference in annual energy production from the lowest to the highest producing sites. FloWind's Tehachapi site has an average elevation of 4,200 feet asl but varies by as much as 1,000 feet.

To achieve the above energy goal, immediate consideration was given to optimum rotor geometries. Rotor configuration was optimized based on the following variables:

- I.1a1. Airfoil performance (NACA 0015,0018,and 0021, and SNLA 1850 and 2150)  
The baseline FloWind 19-m wind turbine utilizes the 28 inch chord, NACA 0015 (15% thick) airfoil profile. See Figure 1. The performance of this profile is significantly affected by surface roughness due to dirt and bug residue buildup. The impact on performance of a typical 19-m turbine in Tehachapi is shown in Figure 2. To mitigate the effects of dirt and bug residue, FloWind initiated two programs, blade cleaning and application of Vortex Generators (VGs). Through these programs, FloWind quantified the effects of both cleaning the blades and installing VGs (depending upon both chordwise and spanwise placement). With this knowledge, FloWind has developed confidence in the ability to enhance or alter turbine performance under specific operating scenarios.

Two series of blade profiles have been used in the development of commercial scale VAWTs. They are the NACA and the SNLA airfoils. The NACA series has been used on both prototype and commercially sold units and the SNLA series has been used on prototypes only. The NACA series is not suitable for the EHD VAWT upgrade. Both peak  $C_1$  vs  $\alpha$  and structural requirements for reasonable solidities preclude its use. Initial evaluation of the SNLA series airfoils revealed desirable performance qualities including stall angle. The

thicker 2150 section, when used with a 27-inch chord provided the desired theoretical aerodynamic performance and structural stiffness requirements for the selected blade material. Additionally, the 2150 was expected to yield reduced roughness sensitivity.

I.1a2. Rotor Solidity (Blade chord and Number)

Achieving optimum blade solidity required consideration of likely composite blade material section properties, blade performance (coefficients of lift and drag) and the effect of blade quantity on torque ripple. Aerodynamic torque ripple is decreased by a factor of about 4 using 3 vs. 2 blades; assuming equal solidity. The frequency increase from 2/rev to 3/rev is insignificant compared to the load reduction. Additionally, blade manufacturing technique and limitations played heavily on the likely blade candidates.

I.1a3. Rotor Diameter (Swept Area, Peak Torque, Down Wind Wake Profile)

Rotor diameter impacts the following;

- a. Row spacing (down wind wake deficits)
- b. Turbine side to side spacing
- c. Rotor swept area
- d. Peak torque
- e. Bend-into-place blade stresses

I.1a4. Rotor Height (Swept area, Solidity, Down-wind Wake)

To achieve greater swept area without greatly impacting peak power, FloWind had to consider unconventional turbine designs. Height-to-diameter ratios of 1.3 to 1 (a circle being 1 to 1) were used for the existing aluminum bladed VAWT fleet. However, to take advantage of the existing infrastructure, increased diameter could not be considered without significantly reducing solidity. In order to keep a realistic size chord, a greater rotor height was the solution to increased energy capture. By stretching or elongating the Darrius rotor, peak power could be achieved while swept area could be greatly increased.

I.1a5. Rotor Speed (Tip Speed)

To reduce peak gearbox torque, the rotor speed of the EHD was increased to 60 rpm. This allowed reuse of the existing drive train with minimal modification to the gearbox; i.e., a new high-speed pinion was required.

I.1a6. Peak Power

The FloWind 19-m was rated 300 kW at sea level but installed at 4,200 asl. The result was that the 300-kW peak generating capacity was reduced to 258 kW. This combined with the reduced aerodynamic performance due to blade roughness, resulted in average peak power output of approximately 240 kW. A primary objective of the upgrade was to reuse the existing infrastructure and

achieve its peak capacity; i.e., 300 kW. In fact it could be slightly increased as a result of the improved insulation class applied to each wind turbine generator during routine reconditioning. The winding insulation class has been increased from F to H as a result of the retrofit.

**I.1b. Reuse Existing Electrical Infrastructure to Capacity**

The existing electrical infrastructure includes 1) underground 480 Vac electrical, 2) pad mount transformers, and 3) existing control and signal wiring. This limits the peak generator output of the wind turbine. A detailed evaluation of the infrastructure included:

1. **Existing conductors**  
Analysis of the original 300-kW and the 320-kW, 440 VAC electrical conductor requirements yielded an increased line current of 29 amperes under the worst case scenario (full load without kVAR correction). This additional current is well within the limits of the existing conductors.
2. **kVAR Correction**  
Review of kVAR correction capacitor requirements showed that the maximum recommended correction was already installed on the Tehachapi 19-meter machines for the 300-kW case (80 kVARs).
3. **Transformers**  
Pad mount transformers are currently undersized 32% at rated power (four 19-meter machines at 300 kW and .91 power factor). With four EHD's installed on the same pad mount transformer, it would be undersized by 40%. This falls within the typical transformer sizing "rule-of-thumb". At rated power, the transformer is experiencing maximum air cooling, which accounts for the undersized rating.
4. **Generator overload protection**  
The existing overload protection circuit (a heat sensing element) requires adjustment only. The 320-kW rating is an additional 6.6% higher than the original 300 kW.
5. **Starter/Contactor**  
The NEMA 4 and 5 motor contactors are adequately sized for the additional inrush requirements of the EHD.
6. **600 Amperes Molded Circuit Breaker**  
Locked rotor current for the EHD during start up is 760 A. This is within the intermittent rating of the 600-A breaker which is a minimum of six times full load current.

### **I.1c. Maximum Reuse of Existing Turbine Components**

The FloWind 19-m VAWT assembly was broken down by subassembly and reviewed for structural and performance integrity as follows:

1. Upper bearing assembly
2. Mast
3. Guy cable and anchor support system
4. Lower bearing and support structure
5. Brakes and hydraulic
6. Drive shaft and couplings
7. Gearbox
8. Generator
9. Controller
10. Turbine Foundation

This is discussed in further detail in section II.

### **I.1d. Improve Long Term Fatigue Life and Component Reliability**

Although chosen mainly for low manufacturing cost, fiberglass pultrusions designed for structural applications also provide potential for extended fatigue life. "In-service" cracking and joint problems with the existing 19-m machines have added impetus to the move away from aluminum, and toward a single-piece continuous blade. Light weight is also beneficial in reducing component costs for root joints, mast, and struts.

Low modulus material is desirable so that dynamic stresses in reaction to aerodynamic operating loads are reduced. Stress concentrations due to machine internal loads can also be reduced because lower modulus material distributes stresses more readily.

Fibrous composites are also relatively resistant to fatigue, in comparison with metals, due to high strains to yield and toughness. Further, fabrication methods, such as pultrusion, that can possibly increase product uniformity and thereby increase fatigue resistance and reliability by reducing scatter in fatigue strength compared with hand layups.

Despite the benefits of composites, some parts are too complex to be economically made of composites and must be made of metal. An important objective has been to maximize reliability of all metal component parts. This is facilitated by 1) accuracy load predictions for components from the system model, 2) extensive use of finite element models at the component level, 3) high fidelity fatigue cumulative damage analysis with large margins of safety, and 4) follow-up testing in the lab and on operating machines, leading to fatigue damage prediction adjustments. (Reference Figures 3 and 4.)

## **I.2. Structural Design Criteria**

The critical structural design criterion is high reliability over the desired 20-year machine life. A theoretical reliability of 0.999 has been used for component design, along with conservative



assumptions about machine availability, run time, loading environments, and material fatigue properties. To achieve such a high reliability objective naturally requires static stresses that are low in relation to the ultimate strength, and dynamic stresses that are only a few ksi. A number of loading conditions are considered in the overall evaluation of fatigue reliability, relating to static and dynamic stresses, as outlined below. An important feature of machine design has been to minimize nominal stresses in joints during operation by detailed geometrical "tuning" to account for all loading conditions.

**I.2a. Bend into place blade loading**

The low modulus of fiberglass laminates allows the bending into place approach. As a rule of thumb, we have sought to maintain blade stresses for bending into place less than 10 ksi, compared to ultimate strength of 40 to 70 ksi, depending on laminate design. Other components are not greatly affected, except bending into place begins the loading considered for geometrical tuning.

**I.2b. Gravity**

Gravity on the whole machine is evaluated.

**I.2c. Centrifugal loading**

Quasi-static centrifugal load is considered, with a geometrical tuning objective of minimizing strut tension and moment at the blade, and root joint stresses (by controlling tension and moment in proper proportion).

**I.2d. Aerodynamic loading**

For design purposes, the blade loading due to an 18-mph mean Rayleigh wind environment was simulated by multiple analyses at several wind speeds. Loads are developed on the blades using a modified version of Sandia's FORCE (and SLICEIT) code, and analysis is done in the frequency domain. From these results, fatigue analysis of blades and mast using rainflow counting and Miner's rule of cumulative damage is done.

In addition, a critical ultimate loading condition has been high wind survival. The wind level was chosen as 120 mph, representing a conservative 20-year maximum based on Tehachapi site data. The machine designs of interest were subjected to elastic instability analyses as a result of this load, and this was a major factor in strut positioning and blade rigidity requirements. This load has not been critical for stresses.

A corollary requirement has been to avoid machine resonances at multiples of running speed by at least 5% in frequency. Campbell diagrams (fan plots) have been used to evaluate this in an approximate manner, and it has been difficult to avoid resonances from 0 to 5 Hz for all modes. However, the fatigue requirement above already effectively ensures against problem resonances, because large responses from resonance would lead to inadequate life. If a non-participatory mode is near

resonance, it is not considered a problem as long as fatigue life is high. It has also been necessary to consider the possibility of frequency variation, leading to using "worst case Campbell diagram" system models for fatigue evaluation.

### **I.3. System Modeling Methodology Summary**

The entire analysis is performed with the ANSYS finite element program. ANSYS solution options for static and dynamic analyses are driven by a system of APDL (ANSYS Parametric Design Language) macros developed especially for VAWT analysis and optimization. Two FORTRAN programs are automatically called by ANSYS macros to perform specialized aerodynamic load and beam section properties analysis, respectively.

The following discussion summarizes analysis details used for the F17 EHD modeling effort. Some program options that are available are not described because they are not used for this particular project (for example, the option of tapered chord blades).

#### **I.3a. Model Construction**

The user enters model information into the macro file FWINPUT.MAC. The exact nodal coordinates of blade and mast are not necessarily directly entered. Instead, overall model dimensional data is used in later macros to build the model automatically.

Particular model features include:

1. Tapered 3-D beam elements for blades and mast (not tapered for EHD).
2. Cables modeled as individual tension elements, including angle to ground.
3. Upper and lower bearing mass and stiffness models.
4. Lower foundation stiffness model.
5. Drive shaft torsion beam and coupler joints.
6. Equivalent stiffness, mass, and damping of drive train/generator system.
7. Single beam element struts from mast to blades.
8. Root joints modeled as multi-axial equivalent stiffness on stiff links from mast.
9. Stress stiffening of blades and mast.
10. Centrifugal softening of blades and mast.
11. Gyroscopic (coriolis) effects of blades and mast.
12. Aeroelastic (flutter) stiffness, mass, and damping of blades.

The model is built automatically. Then the user may supply the file FWMANUAL.MAC, in which special changes to the model can be made if desired. For the EHD, this is used to: 1) adjust node positions for struts, 2) input special stiffness matrices for root joints, and 3) add strut preloading to achieve exact strut length for minimum blade stress during operation.

It is also important to note that the EHD model has initially straight blades. The analysis system includes simulation of blades being pushed into position, and these

stresses are included in fatigue analysis as part of the quasi-static mean stress.

**I.3b. Blade Installation**

The first analysis for the EHD is bending the blades into position. This is a large deflection nonlinear analysis with the struts temporarily excluded. The stress and load results are saved for later use. The model geometry is updated to the bent shape.

**I.3c. Gravity Load**

The bent shape model, with struts replaced, is loaded with gravity and cable preloads. The cable preloads are achieved using initial strains. The struts also have initial strains so that their true unloaded length is properly accounted for, despite the bent shape of the blade that was determined without the struts (and determines initial length of the struts).

A large deflection nonlinear static analysis is used. This analysis is "new", not a "prestressed restart" from the bending into shape. This is a necessary method due to the change in status of the struts. However, the initial geometry does use the bent into place shape from the previous step, and bent into place loads are carried forward for stress stiffening effect in dynamic analysis.

**I.3d. High Wind Load**

The gravity analysis is restarted and aero loads added to simulate high wind load. Aerodynamic loads on the mast and struts are calculated using simple drag coefficient models. Loads on the blades are computed using the FWAEROLD FORTRAN aerodynamic code. FWAEROLD is a modified and adapted version of Sandia Labs' FORCE code, which uses double-multiple-streamtube theory.

All of the loading calculations, including the FORTRAN execution, are automated. The loads are applied in a large deflection nonlinear analysis. If the loads are too high, the solution will diverge and the run is automatically stopped.

**I.3e. Centrifugal Load**

The gravity model is also restarted with centrifugal loads added. Large deflection nonlinear analysis is used, and centrifugal load is applied by specifying rotation rate. Because this is a restart, the strut initial strains are still active, and if well chosen, they result in near zero static load at the blade ends of the struts after centrifugal loads are applied (a design objective). This results in low static stresses in the blades at the struts, and minimizes quasi-static stresses in the struts themselves. This is an important design feature to enhance fatigue life, especially of the metallic components.

**I.f. Dynamic Model Preparation**

Blade and mast internal loads from the bending into shape, gravity, and centrifugal conditions are collected for later use in stress stiffening models. The stress stiffening matrices for beam elements use the common formulation documented in the ANSYS

theoretical manual, but it is implemented manually in macros (i.e., not using the ANSYS automatic option). Using the manual approach provides greater modeling flexibility, the option to change the model details, and provides a major efficiency increase for the entire analysis, to be discussed in later sections.

The final centrifugal load deflections are used to update model geometry for all subsequent dynamic analysis, including calculation of all aerodynamic blade forces for dynamic response analysis. Aerodynamic blade forces are calculated for all desired combinations of wind speed and rpm, and are stored in frequency domain form for later use in harmonic response analysis. Again, the FWAEROLD FORTRAN code is automatically executed.

### **I.3g. Zero rpm Modal Analysis**

Complex modal analysis is first done using zero rpm conditions. Usually, no stress stiffening effects (also termed "differential stiffening" or "centrifugal stiffening") are included in this analysis. Later modal analysis at non-zero rpm does, however, include stress stiffening and for low rotation rates, this provides a clear indicator of the effect of the initial mast compression and blade installation forces on vibration frequencies.

On the other hand, for comparison with static modal test data, special modeling is used to account for nominal mast compression and other test conditions, such as brakes applied. This provides a more accurate modal frequency prediction for correlation purposes. It has been found that whether brakes are on or off is critical to proper comparison of torsional rotor modes, and also has some influence on modes involving mast bending.

The option (usually taken) exists to incorporate damping into the complex modal analysis. Normally, an assumption of 2% for all modes is assumed. This does not affect the mode frequencies significantly. The main reason for using complex modal analysis is to make the output consistent with the later modal analyses at non-zero rpm, which can only be solved using a more complex method (due to Coriolis and other non-symmetric effects).

### **I.3h. Finite rpm Modal Analysis**

For increments of rpm, complex modal analysis is performed including all the special effects of interest (structural damping, aeroelastic terms, centrifugal softening, coriolis, stress stiffening). The full speed geometry, as updated from the centrifugal analysis, is always used (this is an approximation used for efficiency). Stress stiffening is based on internal loads that are appropriately scaled from the omega analysis and added to the gravity and bent into shape data. This precludes the need to perform a separate omega analysis and store its results for each rpm, and is a major time and disk space savings for total analysis.

### **I.3i. Harmonic Response Analysis**

A full harmonic analysis (i.e., full matrix representation) is performed for each wind speed/rpm combination. Solutions are done for frequencies up to the 7th harmonic of running speed, but this is adjustable. This analysis includes all the special effects mentioned for modal analysis. Loads were derived before in step I.3f, based on deterministic aerodynamic analysis. It is very important to note that this is a full matrix analysis. It is *not* based on modal superposition or any matrix reduction method; which are not advisable with special mass effects such as gyroscopics. The full matrix approach ensures no deficiencies in simulating total structural compliance or mass distribution. This is an important enhancement that, to our knowledge, has never been used in the past for VAWT wind machine analyses.

### **I.3j. Postprocessing Options**

- Static loading stress and deflection responses. Deformed geometry, displacement vector, and blade stress contour plots are automated.
- Campbell Diagram (from plot). The frequency data from complex model analysis is plotted as a Campbell diagram.
- Model shape plots. The real part of each extracted vibration mode is plotted in orthogonal and isometric views. The real part is the major part of lightly damped models, and modal character can be determined.
- Harmonic response forces. Postprocessing optional routines allow automated viewing of time domain response forces and moment's anywhere in the model via an EXCEL spreadsheet workbook.
- Blade/mast fatigue analysis. Blade and mast harmonic response stresses are covered to the time domain, and a complete fatigue analysis at every blade and mast node is performed via rainflow counting method. Miner's rule is used to accumulate fatigue damage for multiple wind speeds. A mean S-N curve with statistical scatter is used against a specified reliability and lifetime for fatigue calculations. The Modified Goodman method is used to account for mean stress.
- Component fatigue analysis. The EXCEL response force workbook has been enhanced to perform component fatigue analysis in a semi-manual manner. Stresses per unit component load are normally available from separate detailed models (FEM or not). These coefficients are entered into a spreadsheet, and then time domain component stresses are calculated using the appropriate modal force and moment data from the harmonic response analysis. The stress result, in Von Mises form, is rainflow counted and fatigue damage fraction is calculated. Results for multiple wind speeds are combined using Miner's rule.

### **I.4. Optimized Machine Design**

Tables 1 and 2 summarize the design that resulted from weighing all the design requirements, with some modifications due to test findings that will be described later. Further changes planned, mainly to improve aerodynamic performance, are described in section IX. Reference Figure 5 for a geometrical comparison.

**Table 1 - TURBINE DESIGN CONFIGURATION SUMMARY**

	<u>19 m</u>	<u>17 EHD</u>
Diameter	19.2 m (63.0 ft)	<u>17 m (55.8)</u>
Turbine Assembly Height	30.8 m (101 ft)	<u>53.85 m (176.7 ft)</u>
Base Height	4.6 m (15 ft)	4.6 m (15 ft)
Height to Diameter Ratio	1.31 : 1	<u>2.78 : 1</u>
Swept Area	316 m <sup>2</sup> (3402 ft <sup>2</sup> )	<u>536 m<sup>2</sup> (5762 ft<sup>2</sup>)</u>
Rotor Speed	5.4 rad/sec (51.8 rpm)	<u>6.4 rad/sec (60.89 rpm)</u>
Rotor Frequency (1/rev)	.86 Hz	<u>1.05 Hz</u>
Rotor Weight	9,500 kg (20,900 lbs)	<u>17,823 kg (39,210 lbs)</u>
Blade Weight/Foot	9.3 kg (20.3 lbs)	9.3 kg (20.3 lbs)
Blade Weight (All blades)	1,855 kg (4,080 lbs)	<u>4,374 kg (9,622 lbs)</u>
Blade Quantity	2	<u>3</u>
Blade Profile	NACA 0015	<u>SNLA 2150</u>
Blade Chord	.71 m (28")	<u>.69 m (27")</u>
Blade Material	Aluminum (6063)	<u>FRP (Fiberglass Reinforced Plastic)</u>
Blade Fabrication Process	Extrusion	<u>Pultrusion</u>
Blade Attachment Method	Bolted	<u>Bonded</u>
Blade Segments	3/blade	<u>1/blade</u>
Blade to Blade Joints	2/blade	<u>0/blade</u>
Blade Span	30.6 m (100.5')	<u>48.2 m (158')</u>
Blade Shape	Prebent Troposkein	<u>Bent-In-Place Troposkein</u>
Blade Installed Preload	0 psi	<u>9,000 psi</u>
Struts Quantity	2/blade	2/blade
Strut Depth	15%	<u>20%</u>
Strut Construction	Welded Rectangular Tube	<u>Welded Pipe</u>
Capacity Wind Speed	18.3 m/s (41 mph)	<u>15 m/s (34 mph)</u>
Buckling Wind Speed	71.4 m/s (160 mph)	<u>53.6 m/s (120 mph)</u>
Peak Power (4200 ASL)	240 kW	<u>327 kW</u>
Generator Voltage	480 Vac	480 Vac
Generator Speed	1800 rpm	1800 rpm
Generator Configuration	Induction	Induction
Generator Housing	Open Drip Proof	Open Drip Proof
Generator Insulation Class	F	<u>H</u>
Power Factor	95%	95%
Gearbox Type	3 Stage Vertical Shaft	3 Stage Vertical Shaft
Gearbox Rating	400 Hp	400 Hp
Drive Shaft Diameter	6.7"	<u>8.2"</u>
Service Brake Configuration	Fixed (Hydraulic)	<u>Floating (Hydraulic)</u>
Service Brake Caliper Qty.	2 Sets of 6	<u>2 Sets of 3</u>
Park Brake Configuration	Floating Caliper (Spring)	Floating Caliper (Spring)
Park Brake Caliper Qty.	1 Set of 3	1 set of 3
Guy Cable Angle	35 - 40 Degrees	<u>55 - 60 Degrees</u>
Guy Cable Diameter	2.86 cm (1.125")	2.86 cm (1.125")
Guy Cable Length	67 m (220 ft)	83 m (270 ft)
Guy Cable Tension	12-16 kips	<u>14-16 kips</u>
Guy Cable Weights	As Required	Not Required With Dampers
Guy Cable Tethers Location	Not Required	40% of Length From Anchor End.
Guy Cable Damping Coefficient	Not Required	30-70 in/sec (range 3-150)
Guy Cable Anchors	Deadman	Deadman
Guy Cable Anchor Concrete	13.3 yds <sup>3</sup>	<u>13.3 yds<sup>3</sup></u>
Turbine Base Structure	Pipe & Angle Design	Pipe & Angle Design
Turbine Base Foundation	Deadman	Deadman
Foundation Concrete	32.5 yds <sup>3</sup>	32.5 yds <sup>3</sup>
Complete Turbine Weight	15,371 kg (33,816 lbs)	<u>23,868 kg (52,510 lbs)</u>
Annual Energy Ratio (19-m=1)	1.0	<u>2.0 - 2.5</u>
Dynamic Class	<sup>1</sup> Stiff	<sup>2</sup> Soft

<sup>1</sup> Operating frequency resonant crossings above run speed (51.8 rpm or .86 Hz)

<sup>2</sup> Operating frequency resonant crossings below run speed (60.89 rpm or 1.05 Hz)

Note: Configuration changes for the 17 EHD case are underlined and in bold.

**Table 2 - Summary of Configuration Changes**

<u>Category</u>	<u>From - To</u>	<u>Difference</u>
Reduced Diameter	19.2 to 17 m	- 2.2 m, (7.2 ft)
Increased Height	30.8 m to 53.9 m	+ 23.1 m, (75.7 ft)
Increased Height to Diameter Ratio	1.31:1 vs 2.78:1	
Increased Swept Area	336 m <sup>2</sup> vs 532 m <sup>2</sup>	+ 196 m <sup>2</sup> , (2,360 ft <sup>2</sup> )
Increased Rotor Speed/Rotating Frequency	5.4 to 6.4 rad/sec	+ 1 rad/sec, (9 rpm)
Increased Rotor Weight	15,371 to 23,868 kg	+ 8,497 kg, (18,693 lbs)
Increased Blade Weight	2,030 to 4,374 kg	+ 2,344 kg, (5,157 lbs)
Increased Number of Blades (Increased Solidity)	2 to 3	+ 1
Stall Regulated Blade Profile	NACA 0015 to SNLA2150	
Reduced Chord	28 to 27"	- .03 m, (1")
Blade Material	Al to FRP	
Improved Blade Manufacturing Process	Extrusion to Pultrusion	
Single Piece Blade (No Blade Splices)	2 to 0 blade splices	
Blade To Root Joint	Bolted to Bonded root joint	
Increased Blade Span	100.5 ft to 158 ft	+ 17.5 m, (57.5 ft)
Blade Spanwise Configuration	Preformed to Bent-into-place shape	
Increased Strut Depth	15 to 20%	+ 5%
Low Cost Strut Configuration	Square to round tube construction	
Reduced Capacity Wind Speed	18.3 to 15 m/s	- 3.3 m/s
Increased Annual Energy	1.0 - 2.5	
Increased Peak Power (Fully Utilize Drive Train)	300 to 327 kW	+ 27 kW
Increased Generator Insulation Class	F to H	
Service Brake Calipers	Mico (fixed) to Tolomatics (floating)	
Reduction in Number of Service Brake Calipers	12 to 6 (1 for 2 swap)	
Increased Guy Cable Angle (Original Anchors)	40 to 60 degrees	+ 20 degrees
Rotor Dynamics	From dynamically stiff to soft rotor	

## **II. DETAILED DESIGN**

### **Plan**

1). Utilize available design and modelling tools and techniques, to accomplish a detailed structural and mechanical design of a cost effective 19 meter turbine upgrade. This included procedures, specifications, and drawings for fabrication and assembly of tooling, and new and used parts for retrofit, and 2). Develop a single piece (continuous span) composite blade design including manufacturing tooling.

### **Accomplishments**

1). Integrated ANSYS based VAWT System model into both optimization and design phases of project, 2). successfully designed a geometry and related hardware to operate within the static and dynamic frequency environment of the system, 3). designed a composite blade and tooling which takes advantage of the pultrusion process for continuous manufacturing, and 4). re-used the majority of the existing turbine and electrical infrastructure.

## II.1. Structural System Design

The ANSYS based VAWT Analysis System was used to perform static and dynamic analysis in an automated manner. The main interest at the system level is to have a good Campbell diagram that avoids resonances, which will also minimize component stresses. See Figure 6 for the final 52 rpm Campbell diagram.

The most important area of the Campbell diagram is near 2/rev, where the lower second tower (2T) mode is above 2/rev. The lower 2T mode involves mast bending (about 3/4 wave length) along with flatwise bending of the blades in concert, modified by the strut influence (see later modal test comparison). The main tuning factor for this mode is the strut placement, and it is also affected by cable stiffness (tension).

Another cluster of mode crossing are near 5/rev, but it is found that these higher flatwise modes are not readily excitable, due to the relative phase of blade motion, which does not synchronize with aero forces. Other mode placement is excellent, with no chance of mode resonance. For example, the modes below 5/rev all involve fundamental flatwise blade motion, and even if the frequencies were lower by some effect, they would still be well separated from excitations.

Several machine configurations were tested in which cable tensions were changed, struts were changed, and gearbox ratios were changed. Initially, the design was set for 60.89 rpm to achieve full power. In this case, the 2T mode near 2/rev was most critical, but no resonance problems were observed, except for guy cables. The guy cables were ultimately damped with tethers.

The 60.89 rpm gearbox failed prematurely due to poor gear quality. Then, a 58.5 rpm gearbox was used. The slightly lower speed was chosen to separate the 2T mode from 2/rev an additional amount. However, due to simultaneous strut changes, the 58.5 rpm machine was actually nearer resonance, but not unduly close.

Finally, it was decided to return to the original 52 rpm gearbox from low cost upgrade, with an airfoil change to recover peak power. The final "A" blade testing was done with this speed. In this case, the Campbell Diagram of Figure 6 is very good.

The high-wind case is checked to avoid elastic instability, and fatigue cumulative damage in the blades and mast are automatically calculated. Damage fractions are on the order of 0.01 for blades and mast for the A blade, and so further factors for turbulence, wind shear, and uncertainty can be tolerated.

In addition, the system-level component forces and moments are outputs of the analysis, and are used to perform detailed fatigue analysis of components, as described in the next section.



## **II.2. Rotor Component Design Methodology Using The VAWT System Model**

### **II.2a. Approach**

Components are modeled as accurate stiffness and mass representations in the system model to ensure proper system responses and to allow determination of component interface loads (forces and moments). This is done with the minimum number of finite elements necessary to maintain system model computational efficiency. For example, the struts are simulated as single beams, and root joints as 6 degree-of-freedom stiffness matrices.

In addition, detailed component models are used 1) to determine the parameters for the simplified system representations, and 2) to provide a means of detailed stress prediction. Each component model is exercised with individual components of interface forces or moments, and a matrix of stress influence coefficients are collected to encompass all important stress "risers", or stress concentration points.

An extensive EXCEL spreadsheet analysis package has been developed for postprocessing the static and dynamic results from the ANSYS system solutions. An important part of this system involves using the component stress data to transform system loads (forces and moments) to component stresses, which are in turn used for fatigue analysis.

### **II.2b. Procedure**

The steps in the process for a typical component are as follows:

1. Build a finite element detailed model of the component.
2. Determine equivalent properties of the detailed model for use in the system as a simpler model. This can be done, for example, by calculating equivalent beam properties for the strut by using end loading cases and beam formulas.
3. Exercise the detailed model for all interface force and moment components. Extract stress components for all critical stress riser points, and collect into a stress coefficient data base.
4. Move to the spreadsheet system. For a given wind speed of interest, ANSYS solution forces and moments are read in for the component interface location, and are transformed from frequency to time domain.
5. For a selected stress riser of the component, the stress influence coefficients are used to transform six components of interface force and moment to six components of stress at a point, in the time domain, including all static conditions.

6. The component stresses are converted into von Mises stress in cases where stress is not uniaxial.
7. Rainflow counting is used to determine stress ranges or cycles for fatigue analysis.
8. Fatigue cumulative damage is calculated using a mean S-N curve and standard deviation of log life for the material, reliability objective, and lifetime in years. Mean stresses are accounted for by the modified Goodman correction. This is approximately valid for composites as long as static compressive and tensile stresses are treated equally. For steel, compressive stress does not effect fatigue life.

The blades and mast are sufficiently described in the system model as beams with appropriate properties. For these components, fatigue analysis using rainflow counting is implemented within the automated ANSYS macro system. The methodology, although completely automated, is identical to that described above. Thus, the spreadsheet system and separate component models are not necessary. However, the root joint and strut are addressed with detailed models.

The root joint area is covered with two different models. The first model includes a detailed representation of a fiberglass blade bonded within the clamshells, which are in turn bolted to the "tuning fork" plate, which is fixed to the mast flange.

The second model has no blade and clamshell detail, but simulates greater detail of the mast flange bolted connection, including individual bolts with preload. This model was developed to help diagnose and solve bolt loosening that was observed in the original EHD prototype.

### **II.3. "A" Blade and Laminate**

FloWind's original objective in the development of a fiberglass VAWT blade was 1) elimination of stress concentrations due to splices, 2) elimination of struts, and 3) the improvement of overall component reliability; i.e., fatigue life. These requirements posed significant challenges to the development of the EHD blade. First, traditional blade fabrication processes did not yield a product having uniform cross-sectional properties over the proposed span of a VAWT blade. Second, variable blade geometry was considered desirable if traditional FRP manufacturing techniques were to be utilized to allow the elimination of struts. Finally, there was no history with a product of this size (if done in one piece) or similar application available for comparison.

An economic evaluation of available FRP manufacturing techniques was performed. The processes included traditional hand lay-up, resin transfer molding, filament winding and pultrusion. Fabricated prototype material costs ranged from \$5 to \$28 per pound depending

on the process and internal blade structure proposed. Pultrusion became the clear choice for the following reasons;

- Continuous process (no splices, and length limited to shipping and handling).
- Minimal labor requirements.
- Highly regular material properties (without exotic pre-pregs etc.)
- High fiber to resin ratio without vacuum bagging or autoclaving parts.
- Portability.
- Minimal emissions.

Selection of the pultrusion process however resulted in the following;

- Constant cross section (no variable blade chord).
- Limited number of existing manufacturers.

Details of the constant cross section blade geometry are addressed below. For manufacturing, FloWind identified a pultrusion industry member who was interested in prototyping the first set of "A" blades. This manufacturer is located in the San Francisco Bay area, which further facilitated development of this product.

Once the manufacturing process was selected, details of the "A" blade laminate design were addressed. These details included the following:

### **II.3a. Blade bend into place stresses**

To avoid blade splice connections and the associated reduction in reliability, the EHD blade is manufactured as a single piece approximately 48.2 m (158 feet) long without curvature. It is then sprung into position during installation. The resulting bend-into-place stresses are limited to 30% of ultimate strength. The bend-into-place shape provides for additional high wind buckling benefit.

### **II.3b. Handling Loads (gripping, shipping and installation)**

The blade is gripped and pulled during manufacture as part of the process. The loads associated with this process have been considered in the design of the gripping tool. Once the blade is fully manufactured, it must be removed from the process line and handled for subassembly of blade strut and root plates and then packaged for shipment. Special racks contoured for the blade profile have been prepared for packaging and support during shipment.

### **II.3c. Shipping Loads**

Shipment of 48.2-m long VAWT blades requires special support and transportation equipment. A large shipping truss has been manufactured to provide spanwise support for as many as 18 blades during a single shipment. The blades are loaded in groups of three onto the shipping truss mounted on the specially configured semi tractor and trailers. Portable gantry cranes and all terrain cranes were used in the loading and

off-loading of blade packages.

### **II.3d. Installation Loads**

The highest loads experienced by the single-piece blade are during installation onto the rotor. Conventional installation of two-bladed FloWind VAWT rotors was done following complete assembly on the ground. The three-bladed EHD requires special installation considerations. The rotor mast is assembled and erected as a single piece. The blades are then installed individually. The process requires the blades be lifted from the horizontal into the vertical position and then prebent and attached to the mast. These loads, although highest, are acceptable because they do not exceed about one-fourth of ultimate load.

### **II.3e. Operating Loads**

The effect of gravity, spin, and aerodynamics induces static and dynamic loads in the blades. The predominant stress, however, is bending into place, followed by centrifugal stretching/bending and finally, dynamic response. Figures 7 through 12 show typical predicted stresses for the A blade.

### **II.3f. High Wind Buckling**

Without the ability to vary blade section geometry, tailoring of the roots to transmit 100% of the blade loads into the mast could not be accomplished. Therefore, struts were required. These were sized and positioned to minimize their influence on rotor drag and still provide adequate high wind buckling resistance. Figure 13 shows a cross-section of the "A" blade. The "A" blade buckling limit is 145 mph with struts. Figure 14 shows the response shape at 130 mph (magnified).

### **II.3g. Panel buckling**

Panel stiffness is adequate to prevent buckling. The blade cross-sectional design includes spanwise shear webs which provide adequate panel support. Detailed blade segments were modelled by FEM to evaluate buckling resistance.

### **II.3h. Modulus**

Blade elastic moduli are variable depending upon the laminate fiber to resin ratio and laminate material makeup, fiber orientation, and resin system properties. Typical modulus values for VAWT blade designs range from 3.5 to 5.0 Mpsi. The A blade equivalent value is near 4.0 Mpsi, predicted by ANSYS FEA (Figure 15) and laminate theory and verified in tests.

### **II.3i. Weight and Rigidity**

The blade rigidity is determined by the equivalent section modulus and moments of inertia. Skin and web thickness were determined to meet design rigidity goals within the airfoil envelope. Blade weight was a by-product of this sizing.

## II.4. Root Joint

The basic EHD blade root attachments are designed after the highly successful 17-m two-bladed rotor root design. The blade-to-mast attachment is significantly softer in flatwise bending than the original 19-m root design. In addition, all root blade loads are transmitted via adhesive rather than bolts, further improving fatigue performance. However, two through bolts with phenolic inserts were added for adhesive creep protection in the prototypes.

The root joint transmits virtually all of the tensile centrifugal blade loads, and also transmits a small portion of the edgewise motive power forces. Smaller flatwise static and dynamic loads are also transmitted.

The root joint assembly has been analyzed using ANSYS FEM. The model shown in Figures 16 and 17, includes a segment of the A blade and the adhesive interface between blade and clamshell. Individual component loads on the root, applied at the blade exit from the root, were analyzed for stress responses. For example, the stresses shown in Figures 18 and 19 occur in response to a reference level flatwise moment of 10,000 in-lb, and the results look similar for a flatwise shear force. The plate bend stress concentration can be clearly seen, and the blade is seen to have no significant stress concentration at the clamshell exit. Figures 20 and 21 show similar data for axial force, where the offset centroid of the blade can be seen to cause the trailing edge stress to be higher, but stress concentration is minimal. Figures 22 and 23 show data for edgewise moment.

An additional model, shown in Figure 24, was used to investigate flange and flange bolt detail stresses. Bolts were individually modeled with torque preload, and component loads were again applied. Figures 25 and 26 show flatwise response, while Figures 27 and 28 show edgewise response.

Stresses per unit component load were taken from these model results for use in prediction of operating stresses. The system level operating static and dynamic loads at the root joint exit were combined with these stress per unit load "influence coefficients" to convert forces to component stresses. This was done for all stress riser points found in the models, and time domain von Mises stresses in the metallic parts were predicted for a full revolution of the rotor.

The time domain stress data were in turn processed into stress cycle means and ranges via rainflow counting for a series of wind speeds. Then the cycle data were used in a cumulative fatigue damage calculation. It was desired to have a total fatigue damage fraction below 0.01 for 20 years in order to provide margin for effects of turbulence and other uncertainty.

## II.5. Struts

Analyses of the struts were performed similar to the root joint analyses discussed above. There was an evolution of strut designs during the test program due to some stress

concentration problems. Figures 29 and 30 show the most recent so-called "V-strut" configuration model, which was ultimately used. Figure 31 shows stresses for a reference level 1000-lb edgewise force at the strut end, which is the motive power load, and is the most important loading on the strut. Figure 32 shows flatwise moment response, which is also significant. This model indicated the need to extend the blade end gussets to reduce stress concentration, and again, fatigue analysis was performed.

The blade/strut clamshells were not modeled because the load levels at this interface were low compared to the blade/root clamshell interface area, and very low stresses in clamshell, blade, and adhesive are expected. The mast end of the strut is the more heavily loaded region. Bolt holes have been completely eliminated from the basic EHD strut to blade attachments. An elastomer interface exists between the blade and each of the two halves of a steel clamshell. The connection carries no radial static load during operation due to centrifugal force tuning of strut geometry.

## II.6. Upper Bearing

The upper bearing assembly was analyzed and determined to be within the limits of the operating criteria. A finite element model was prepared for the cone and bearing housing. The analysis was performed and no changes to the bearing support structure were required. Reference Figure 33 for an upper bearing FEA model drawing.

An 18-mph Weibull distribution with a shape factor of 1.5 was used for bearing life calculations. The wind and load distributions were

Wind Speed m/s (mph)	Operating Hours	Radial Bearing		Thrust Bearing	
		Radial Load(lbs)	Thrust Radial Load(lbs)	Thrust Load(lbs)	Thrust Load(lbs)
6.3 (14)	953	1,898	3,436	1,538	76,299
9.4 (21)	1,426	3,494	6,324	2,830	76,299
12.5 (28)	1,156	5,070	9,176	4,107	76,299
15.6 (35)	921	6,895	12,481	5,585	76,299
18.8 (42)	519	8,668	15,689	7,021	76,299
21.9 (49)	244	10,442	18,899	8,458	76,299
25.0 (56)	143	12,304	22,270	9,966	76,299

Bearing life (hours) was calculated and determined to be as follows:

	Basic Life	Life with Lube Factor
Upper radial bearing life	57,000	84,200
Upper thrust bearing	46,100	66,500

## II.7. Lower Bearing

The 19-m lower bearing life was calculated based upon the operating wind distribution used for the upper bearing case. The wind and load distributions were as follows:

Wind Speed m/s (mph)	Operating Hours	Radial Load (lbs)	Thrust Load
6.3 (14)	953	1,358	109,300
9.4 (21)	1,426	2,934	109,300
12.5 (28)	1,156	4,045	109,300
15.6 (35)	921	5,199	109,300
18.8 (42)	519	6,470	109,300
21.9 (49)	244	8,093	109,300
25.0 (56)	143	9,677	109,300

The life calculation results were

	Basic Life	Life with Lube Factor
Lower thrust bearing life (hours)	80,800	136,000

## II.8. Rotor Stand

The FloWind 19-m rotor stand (pedestal) design was reviewed for the three basic loading conditions: 1) survival wind (130 mph) along the X-axis, 2) survival wind (130 mph) along the Y-axis and 3) peak momentary torque of 285,000 Lb-ft (3 brake sets applied simultaneously) with a vertical load of 102.1 kips and a wind load of 15.0 kips in the negative Y-direction. The existing pedestal design was determined to be suitable for the 17 EHD. Reference Figure 34--rotor stand model. Further details are available in D'Amato (19).

## II.9. Foundation

The two primary load conditions considered were 1) survival wind speed of 130 mph at 86% of sea level air density, and 2) emergency shutdown torque on the pedestal of 285,000 lb.ft. with an aerodynamic load on the machine of 30,000 lb. Dead weight load for the mast and blades is 40,400 lbs. The existing foundation with 32.5 yd<sup>3</sup> of concrete was reviewed in conjunction with the soils report and determined to be sufficient. Further details are available in D'Amato (19).

## **II.10. Guy Cables and Anchors**

The safety factor for the guy cables was calculated to be 2.11, which satisfied the applicable structural standard. The guy cable anchor beam departure angle relative to horizontal had to be increased to 60 degrees to accommodate re-use of existing anchor locations with sufficient stiffness at the upper bearing connection. This was accomplished with the method detailed in Figure 35. Further details are available in D'Amato (19).

## **II.11. Microprocessor**

Control algorithm changes were made to accommodate a higher rotor inertia by allowing a longer startup time. The higher rotor speed with the 60-rpm gearbox required a higher overspeed limit and a modified limit for the low-speed vs. high-speed tachometer disagree check. For increased safety during testing, one of the inputs to the microprocessor was reconfigured to accept an alarm signal based on the accelerometer channels. The alarm signal was the output from a dedicated programmable controller which sampled the x- and y-accelerator channels, computed the resultant magnitude and averaged it over a specified period. If the average exceeded a specified threshold of 0.7g or if an instantaneous resultant sample exceeded a higher threshold of 1.8 g, the turbine would shut down and latch.

## **III. SUPPORTING LABORATORY TESTS**

### **Plan**

Execute hardware and material property testing to adequately characterize the performance of specific components for use on the upgrade system.

### **Accomplishments**

Blade material property and blade root joint testing was accomplished. The blade material property testing confirmed adequacy of predicted blade properties. Root testing resulted in a review of the root joint design and subsequent modifications.

### **III.1. Blade Material Coupon Ultimate Property Testing**

Basic material property testing for modulus, shear, tensile strength and compressive strength were performed by the pultrusion manufacturer. The results satisfied design requirements.

### **III.2. Additional Blade Property Testing**

The following additional tests were performed to qualify blade quality: Tg to determine extent of cure, Barcoll to measure hardness, and dye wicking to determine porosity (wetout).



### **III.3. Blade Root Fatigue Testing**

Initial full-scale blade-root-fatigue testing was accomplished under separate and unrelated funding by Sandia National Laboratories as part of a condition monitoring research effort.

Test fixturing consisted of a root joint cantilevered with a 10-20 ft segment of blade. The cantilever point was then vibrated radially, and the system resonated, resulting in large flatwise moments in the root joint. The sample was vibrated until failure.

The joint failed at a cycle count about 5-10 times less than predicted. It appeared that the load level for accelerated testing introduced an unexpected failure mode strongly driven by flatwise moment. The tuning fork tang cracked near the base, in line with the nearest clamshell belt hole. Heating was observed at this location in check-out testing.

In actual operation, the joint has relatively large (75,000 lbs) static tensile load along the blade, and flatwise moments are small. Thus, the observed failure mode is not likely in service. However, the test failure indicates that the joint could be improved by 1) moving bolt holes away from the fork tang end, and 2) by extending the clamshells further past the tang end. These changes are planned for production root joints.

In addition, the results indicate that more modeling detail may be needed for bolt holes and potential separation of mating parts.

### **III.4. Blade Thermal Coefficient of Expansion**

Prior to installation of blade strain gages, thermal properties were required to determine gage factors. FloWind's initial strain gage contractor instrumented and tested blade coupons for thermal properties.

## **IV. PARTS PROCUREMENT**

### **Plan**

1). Manufacture EHD prototype using existing job shops, hardware vendors, and fabricators, following vendor qualification and competitive bid exercises, and 2). design and develop pultruded blade manufacturing tooling. Note, special considerations were required for; 1). upgrading hardware in the field for re-use on the EHD, and 2). manufacturing and shipping single piece pultruded blades.

### **Accomplishments**

Developed the techniques and tooling to manufacture continuous span fiberglass VAWT blades. Developed the infrastructure and methodology and executed the transport of 160+ foot long flexible fiberglass blades. Establish and executed procedures and logistics for rework of existing hardware for maximum economic

benefit including upper bearing and mast sections.

#### **IV.1. Competitive Bidding**

FloWind's standard practice for procurement includes solicitation for competitive bids from a minimum of three qualified vendors.

#### **IV.2. Vendor Qualification**

New vendors are pre-qualified for capabilities prior to issuance of a purchase order for parts. Facilities including manpower, equipment, buildings, and machine tools are reviewed for the required capacity or capability.

#### **IV.3. First Article Inspection**

Standard procurement practice calls for "first article" inspection. Workmanship and tolerances are reviewed and approved or modified prior to full-scale production of each assembly.

#### **IV.4. Quality Control**

FloWind maintains quality control through the above procedures (IV.1, IV.2., & IV.3) and through documentation prior to release of component drawings. The drawing data base and practices are maintained through application of current standards and practices. FloWind design and CAD based drafting adheres to applicable ANSY Y14.4 standards for design, drawing and annotation.

#### **IV.5. Shipment**

EHD hardware includes existing components and new sub-assemblies, several of which require additional or special handling. Existing hardware is shipped from the site for rework and returned as new EHD assemblies. This includes both the mast and upper bearing assemblies. Refer to sections II.3b & 3c for blade shipment requirements.

### **V. SITE PREPARATION**

#### **Plan**

Modify the proposed test site to provide for; 1). turbine assembly and erection, including bonding blade attachment hardware to the blades, 2). test instrumentation and infrastructure and 3). rework existing guy anchors to meet the new guy cable departure angle requirements.

#### **Accomplishments**

Construct all-weather facility to bond blade roots on test site including staging area for 150 foot long mast and 160 foot long blades. Prepare construction and instrumentation infrastructure and modify turbine guy anchors.

## **V.1. Site Prep - Construction**

### **V.1a. Site Selection**

Tehachapi turbine #258 was selected as one of four candidates for EHD testing. Selection criteria included historical turbine and meteorological performance in the following categories:

1. Average power output and total energy produced.
2. Average wind speed, wind speed extremes and monthly averages during initial prototype testing.
3. Historical component fatigue damage.
4. Suitability for down wind wake deficit measurements.
5. Site accessibility.
6. Proximity of upwind machines (none).

Reference Figure 36 - Site map.

The first two site candidates selected excelled in the first three categories but posed significant problems regarding accessibility. They are located on the Horned Toad region of the Cameroon Ridge VAWT project. These sites could become inaccessible for short durations during the winter months, but more importantly, they offered limited access. The EHD blade shipment would not be able to make the winding decent from upper Cameroon Ridge. Turbine 258 offered the next most aggressive leading edge site for testing.

### **V.1b. Decommissioning**

Turbine 258 was decommissioned, lowered and disassembled. The rotor mast sections and upper bearing were then shipped to Washington state for rework. The gearbox was removed and shipped to Los Angeles for retrofit.

### **V.1c. Preparation**

A modification to the existing guy anchors required adjustment of the exiting angle. This has been discussed in Section II.10. The modification was executed after removal of the topsoil and exposure of the anchor at the top of the concrete.

Site preparation for the construction phase of the EHD required additional working areas to accommodate a 45.7-m (150-ft) mast and required assembly equipment. A heated clean room for bonding blade roots was constructed and a staging area for both final treatment and support of the 48.2-m (158-ft) blades was prepared. Temporary power and office facilities were installed.

The scale of the EHD prototype required additional construction equipment for material handling and lifting. This included all terrain hydraulic cranes, boom truck and an all terrain fork lift.

## **V.2. Site Prep - Testing**

### **V.2a. Infrastructure and Power**

EHD testing required installation of necessary test infrastructure for turbine structural and electrical performance and meteorological correlation testing. Turbine 258 was selected as a test bed candidate for both its historical performance and location on the leading edge of Cameroon Ridge. A 41.2-m (135-ft) tall reference meteorological tower and sensors were installed in preparation for EHD testing:

The test site is located at an area of complex terrain; the wind accelerates directly upwind of the turbine as it comes up out of the canyon and over the ridge. The upwind reference meteorological tower was installed two rotor diameters' upwind of the rotor location but shifted north approximately 100 ft along the ridge such that ground elevation is at approximately the same level as the base of the turbine to give a reading more representative of that seen at the turbine.

Teledyne anemometers were mounted at 50 ft (19-m equator height and 17-m EHD) lower strut level), 93 ft (17-m EHD equator height) and 131 ft (17-m EHD upper strut level). A wind vane and vertical wind speed sensor were also mounted at the 93 ft level. The shear exponent at the site was calculated and found to be very low.

A turbine-meteorological correlation test was conducted to determine the difference between the meteorological tower and turbine site. An anemometer was mounted on the blade and the turbine was oriented so the blade-mounted sensor experienced the minimum interference effects due to the blade. For the second part of the test, the sensors from the meteorological tower and the blade were swapped to eliminate any effects from the sensors themselves. Results are discussed later in section "Turbine to Meteorological Tower Correlation."

Underground conduit, conductor (power and signal wires) were run from the D4 instrumentation and test trailer to the following;

1. Guy cable anchors numbers 1, 2, & 3.
2. Reference meteorological tower.
3. Turbine foundation/controller.

Termination boxes/panels were installed at each of the above three locations.

Sandia's D4 test trailer was sited and anchored.

A modal test trailer was temporarily sited for initial static testing.

Power for testing was supplied via 480 Vac conductors (SO cable) to both the test trailers and associated instrumentation.

#### **V.2b. Instrumentation**

Onsite installation and calibration of the following instrumentation were performed in preparation for EHD testing;

Strain gage installation was completed for the mast, root mounting plates and struts once the components were received on site. Reference Figure 37--Strain gage location drawing, and Figures 38 and 39 channel summary.

Calibration of the blade strain gages was performed on site by an outside subcontractor prior to blade installation. Weights were attached at both ends of the blade and strains were measured using strain gages and a portable data acquisition system. Blade deflections were measured at both the ends and of intermediate locations. Calibration was possible using the known determinate loading and beam theory assumption for fiber strains. Manpower and equipment availability made calibration of the 48.2-m blade instrumentation manageable.

### **VI. TURBINE ASSEMBLY, INSTALLATION, COMMISSIONING**

#### **Plan**

Assemble, install and commission EHD turbine components as they become available. Additional consideration had to be given to the extended length mast and single piece blade, "in-air" installation requirements.

#### **Accomplishments**

Assembly and installation of the 150' long mast and upper bearing assemblies prior to delivery of the blade sections. The mast was assembled and erected as a complete assembly without difficulty. The remaining rotor components including blades and struts were assembled and installed uneventfully.

#### **VI.1. Component Weight (Turbine 258 and alternate)**

Prior to assembly, each of the rotor components (prototype #2) was weighed using the spring dynamometer provided by Sandia. The prototype #1 components are considered identical to #2 within the resolution of the scale. Component weight was measured for future reference in the event an imbalance was measured in the system during testing.

## VI.2. Component Assembly and Erection

Assembly of the EHD occurred in stages and required additional equipment above that of typical VAWT installations. The mast, upper bearing and guy cable system was assembled on the ground and erected onto the base structure in a single lift. The guy cables were then tensioned to specifications. The blades were erected vertically, one at a time, using additional lifting equipment. Once vertical, the blade was pre-bent for bolt-up using a winch and cable system. Once the blades were installed, the struts immediately followed.

## VI.3. Commissioning

Operational commissioning was performed on all turbine subsystems. This included guy support system (cable tensions and frequency), subassembly fasteners (torque), preliminary brake performance testing (response time, torque and rotor inertia), startup control sequence verification (start time, wye-delta switch, relay and control logic), and startup power requirements (volts, amperes, & vars).

## VII. TURBINE INSTRUMENTATION & TEST PLANNING

### Plan

Select the one of the most interesting sites at FloWind's Tehachapi wind power plant for testing the EHD prototype. Selection criteria included the existing turbine's performance and meteorology. Install and calibrate meteorology and performance instrumentation at the test bed and on the rotor components as required. Interface turbine and meteorological instrumentation to the trailer based SANDIA D-4 instrumentation and data acquisition system. Establish a test matrix for evaluation of the EHD structural and aerodynamic performance characteristics.

### Accomplishments

- 1). Installed instrumentation as required, 2). interfaced to the D4 and 3). developed a test matrix for characterizing the EHD performance.

### VII.1. Test Bed Site Selection Criteria

Location	- Leading edge of Cameroon Ridge.
Access	- Easily accessible from main road
Wind Distribution	- Rayleigh 18 mph
Shear Exponent	- .04
Turbulence	- .08 TI
Temperature	- 0° to 110° F
Recorded High Wind Peaks	- 46.9 m/s (105 mph)

## VII.2. Data Acquisition System and Data Signal Network

### VII.2a. Rotor Based System

The rotor based system is composed of termination panel, pulse code modulator (PCM), battery power pack (strain gage power supply), and telemetry system.

### VII.2b. Ground Based System

The ground based system comprises controller signal network, termination panel, and underground wiring, meteorological signal network and the D4 Signal Receiving and data acquisition system. This includes termination panels with lightning/surge protection, signal conditioning, anemometry (wind speed, wind direction, temperature and pressure), control signals, regulated power supplies, signal digitizer, and multiplexer, HP1000 A series and data acquisition software, PC data logger, Nomad data logger and telemetry system.

### VII.2c. Instrumentation Calibration

NIST traceable calibrations were performed on power curve instrumentation including current transformers, power transducers, and meteorological instruments. Structural blade instrumentation calibrations are discussed in section (V.2b). Strut and mast calibrations were based upon gage location and gage factors due to difficulty of true load calibration (in fact, strut is an indeterminate structure).

Instrumentation including strain gages, accelerometers, speed sensors, thermocouples, and transducers were installed on the following components or in the following locations (also refer to Figures 37, 38, 39):

Rotor (strain gages)  
Blades - At the root, strut, equator, and root clam shells.  
Struts - At the mast mount, blade mount, and on the structural tubes.  
Blade mount - At the fork fillets and center bend.  
Mast - At the center and lower flanges.  
Upper bearing - Accelerometers on the bearing cap.

Rotor Support (strain gages)  
Guy cables - On the clevises at the anchor end of the cables.

Brake System (pressure transducers)  
In the "A" service brake hydraulic line.  
In the "B" service brake hydraulic line.

Generator Windings (thermocouples)

Controller Signals  
Turbine control (start, stop and emergency stop)

Rotor speed  
Generator speed  
Generator power  
Generator reactive power  
Generator current  
Generator voltage

Meteorological Towers

Wind speed (upper strut level)	131'
Wind speed (equator level)	93'
Wind speed (19-m turbine equator level)	50'
Wind direction	93'
Vertical wind speed	93'

Atmospheric

Temperature  
Barometric Pressure

Each test or battery of tests required recording output from a subset of the channels connected to the above instrumentation. The data was collected as both bins and time series data and used to analyze turbine aerodynamic and structural performance and transients. It was used to quantify the structural, aerodynamic, mechanical and electrical performance of the system. Figure 40 details the general test matrix, and the next section describes summaries of each of the tests noted.

**VIII. TEST & EVALUATION**

Plan

Execute the proposed structural, aerodynamic, electrical and mechanical test matrix following static Modal testing of the EHD structure by SANDIA. Modify system and test requirements as the test progressed and data became available.

Accomplishments

Performed tests to characterize the rotor structural, aerodynamic, electrical and mechanical performance. Characterized the drive train response using the 8.2 inch (diameter) drive shaft and determined that the original shaft was suitable.

Significant Changes

1). Operated the turbine first at approximately 60 rpm using a retrofit gearbox fitted with cut rather than ground gears. Then operated the turbine with two different gearboxes fitted for approximately 58 and 52 rpm. The latter two gearboxes were fitted with ground rather than cut gears. These changes were made to a). characterize the performance using a gearbox with ground gears and b). to operate at a lower rpm



to avoid a gear retrofit if suitable, 2). added tethers and dampers to the guy cables to mitigate resonance conditions, 3). replaced the original struts (pre-tensioned) with struts using tubular construction having a "V" geometry, and 4). welded the "moveable strut mounting ring" permanently to the mast. The original strut mounting configuration allowed modifications to the strut location and geometry if resonance avoidance was required.

FloWind's EHD wind turbine development program included the following general categories of testing:

- Structural - validation of static and dynamic code predictions.
- Aerodynamic - validation of airfoil and rotor performance code predictions.
- Mechanical - emphasis on performance and reliability of existing hardware.
- Electrical - emphasis on performance and reliability of existing hardware.

### **VIII.1. Data Acquisition Primary Data Types**

Primary data was collected on the HP1000A using the menu-driven options, as prepared by Sandia National Laboratories. In general, data was collected and stored as both time series data and bins data. Other than for specific short-term tests, time series data was sampled and stored at 20 Hz, which ensured that any frequency content up to 10 Hz would not be subject to aliasing. This easily covered all significant frequency modes observed in both rotating and stationary frames. Bins data was stored as 10-second averages. Filtering for rpm and wind direction in the Bins Master File ensured all bins data contained values collected with the turbine at full speed and wind from prevailing direction.

Problems were encountered with the rotating frame signals; drop-outs due to multipath reflection/transmission in the telemetry data caused spikes in the data that had to be cleaned up as part of data processing. Data files were transferred from the HP1000A system over a serial link to a PC, where they were backed up to tape for easy transferring of data to another location.

### **VIII.2. Data Acquisition Analysis Software Tools**

Whenever possible the HP1000A menu-driven routines were used to reduce and summarize data in both time and frequency domains, and as bins data. The ability to easily combine separate bins files together for viewing results was a great aid. However, in order to clean up data with drop-outs, the binary data was converted to ASCII for use with either a spreadsheet program or Windats (written by SERI) or data analysis software Gauss. A conversion program was written in C to prompt the user to select channels of interest and give the option of pre-averaging the data.

### **VIII.3. Turbine to Meteorological Tower Correlation**

The ASME /ANSI PTC 42 Wind Turbine Performance Test Code does not require that a wind-speed correlation test be done if the meteorological tower is less than four rotor diameters from the turbine and certain geometrical relationships between anemometer level, equator level and terrain are met. Although not required for the test site, this test was done to verify that the initial discrepancy between predicted and measured power curves was not due to wind speed measurement at the meteorological tower being drastically different from that

at the turbine.

An anemometer was mounted on the blade with a 10 ft boom, and the turbine was oriented so that the blade-mounted sensor experienced the minimum interference effects due to the blade; the blade was pointed upwind so that the minimum blade surface area was exposed to the wind and so that the angle of attack was close to zero. Data was collected at the 93 ft level on the meteorological tower and from the blade. Data was sampled at 1 Hz and stored as one-minute averages over a 5-60 mph wind speed range. For the second part of the test, the sensors from the met tower and blade were swapped to minimize any effects from small differences in the sensors themselves. Data was collected over a 17-70 mph range. The ratio of each one-minute average and the average of the ratios was determined.

Results: (1) Blade: meteorological tower difference = 3.12% (before sensors swapped)  
(2) Blade: meteorological tower difference = 3.38% (after sensors swapped)

A difference of up to 2% would be well within the tolerance of the sensors; the closeness of these ratios suggests that the particular sensors being used are very close to each other in sensitivity and that the difference between meteorological tower and blade is 3%.

**VIII.4. Test Matrix Results Summary (Refer to Figure 40 for Test Matrix)**

**VIII.4a. Blade Bend Into Place Stresses**

Objective: Measure the magnitude of the bend into position stresses only.

Procedure: Pre-bend blade on the ground (horizontally), measure and record strain gage output using the data acquisition system (DAS).

Results: This test was not accomplished. Test number VIII.4b was better accomplished. Full-scale blade strain gage calibrations, discussed earlier, verified blade bending properties.

**VIII.4b. Blade Bend Into Place + Gravity**

Objective: Measure installation stresses during assembly of the blade to the rotor.

Procedure: Measure and record output of blade and root joint strain gages during assembly using the DAS.

Results: Assembly stresses were measured and were in good agreement with predicted levels (within about 5%).

**VIII.4c. Guy Cable & Mast Assembly Stresses**

Objective: Obtain mast and cable stresses during installation.

Procedure: Measure and record output of mast and cable strain gages during installation using DAS to establish baseline zeros and pre-loaded conditions.

Results: The DAS system was unavailable during mast installation, therefore mast baseline strain gage zeros are in the pre-loaded condition. Guy cable tensions are measured using calibrated instrumented turnbuckles (a total of 6 units). Thus cable and mast pre-loading are well known.

**VIII.4d. Turbine Static Modal Testing**

**Objective :** Confirm model predictions of turbine 0 rpm modal response.

**Procedure:** Instrument, excite (using a stepped force input) and measure major turbine modal frequencies.

**Results:** Sandia's modal test data shows measured results in good agreement with predictions. Carne (1) details the results of these tests. Figures 41 and 42 show predicted and measured shapes for the first tower mode shape. Figures 43 and 44 show predicted and measured shapes for the first propeller mode with the brakes applied. Figures 45 and 46 show predicted and measured shapes for the first flatwise asymmetric blade mode. The frequency results are compared below:

**MODAL FREQUENCIES - 0 RPM**

Description	Test	Analysis	Comments
1T - first mast bend + flatwise/edgewise	1.07-1.08	1.09	2 modes. Required brakes on stiffness to correlate
1P - First twist or propeller with brakes	1.40	1.47	1 modes
2T - 2nd mast bend + flatwise/edgewise	2.31	2.22	2 modes
1F - First flatwise blades	2.17	2.40	3 modes
3T - 3rd mast bend + flatwise/edgewise	2.87	2.54	2 modes
F HIGH - Local flatwise at ends	3.19	3.06	1 mode
F HIGH - Local flatwise at ends	3.31	3.33	1 mode
2P - 2nd twist or propeller with brakes	3.51	3.46	1 mode
HIGHER - Mixed Mode shape	4.14	4.53	Mode shape match more difficult
HIGHER - Mixed mode shape	4.65	4.78	Mode shape match more difficult

**VIII.4e. Turbine Baseline Losses**

**Objective:** Determine baseline turbine system losses (aero,mechanical, & electrical).

**Procedure:** Measure turbine electrical and mechanical power levels in low wind speeds.

**Results:** Electrical power has been measured for low-wind operation. Predictions of strut and blade drag, mechanical losses in very low lift conditions were made

by extrapolating from measured 19-m turbine losses and accounting for extended blade length, extra blade and different rotor speed. Measured power consumption for the 17-m EHD closely matched predictions at both 52 rpm and 58.5 rpm.

**Motoring Losses**

19 m @ 52 rpm

Total consumption in 0-8 mph winds	32 kW
Gearbox losses	10 kW
Generator losses	5 kW
Rotor losses (struts and blades)	17 kW

Predicted 17m EHD losses @ 52 rpm

Gearbox losses	10 kW
Generator losses	5 kW
Rotor losses (multiply by 1.6 for blade length) (Multiply again by 1.5 for 3rd blade)	40.8 kW
Total (estimate high as struts not factored separately)	55.8 kW
Measured	50.0 kW

Predicted 17 m EHD losses @ 58.5 rpm

Gearbox losses	12 kW
Generator losses	6 kW
Rotor losses X rpm <sup>2</sup> ratio	51.6 kW
Total Prediction	69.6 kW
Measured	70.0 kW

**VIII.4f. Turbine Start Transients**

**Objective:** Identify significant mechanical, electrical and structural transients associated with turbine start up and modify system accordingly.

**Procedure:** Measure electrical, mechanical and structural sensors and transducers of interest during turbine start-up (over the full operating wind-speed range).

**Results:** The start transient structural behavior for the EHD is decidedly benign. It is in fact difficult to discern traverse of most resonant crossings that are indicated on the Campbell diagram. The initial design for 60.89 rpm operation included a larger drive shaft of 8.2 inch diameter compared to the original 6.7 inch shaft used for the F19. The sole reason for using this larger shaft was to avoid the first propeller or drive train mode resonance during start. In fact, this mode was not observed during start.

The only structural responses of interest included, first, relatively minor resonance of the lowest 1T + F mode at low speed as it crossed 2/rev. Second, there was an audible drive train buzz at high frequency at about 1/2 to

3/4 speed. Third, a lesser drive train mode, possibly a gearbox shaft bending mode, occurred just before full speed. Finally, there was some minor increase in structural response as the machine decelerated just after reaching full speed. None of these events resulted in significant loads or stresses measured in the test.

Because of the benign nature of the start, and the cost of fabricating new drive shafts, tests were performed with the original 6.7 inch drive shaft in late 1994. The objective was to determine whether the resonance during start might be tolerable. Figure 47 shows the rpm transient for this case, in comparison with that of the F19 production turbine. The amplitude of oscillation is substantially less for the EHD than for the F19, and no problems were observed during testing, except that the resonance is audibly noticeable. Thus, it appears that the drive train mode is tolerable with the original drive shaft. It is hoped that future testing will include a torque instrumented drive shaft so that final determination can be made of the torque loads during this transient.

**VIII.4g.** Turbine Stopping Transients

**Objective:** Identify significant mechanical, electrical and structural transients associated with the turbine stopping, and modify system accordingly.

**Procedure:** Measure electrical, mechanical and structural sensors and transducers of interest during turbine stop (over the full operating wind speed range).

**Results:** No significant transients associated with the turbine stop sequence have been identified. The brake configuration has been redesigned and retrofit for reduced maintenance and to allow for increased brake disc runout due to the additional rotor height. Also see section IX.1c for further discussion. Figure 48 illustrates a typical braking time series plot.

**VIII.4h.** Turbine Brake System Performance

**Objective:** Confirm turbine brake performance predictions

**Procedure:** Measure turbine stop time and system pressure for each braking condition over the full range of operating wind speeds.

**Results:** The brakes existing on the 19-m turbine were found to be adequate (stopping time/torque/disk temperature) for stopping the turbine safely and with the same level of redundancy, i.e., two independent sets of hydraulically applied service brakes and a third set of spring-applied, hydraulically released parking brakes. However, during testing it was found that the taller tower exacerbated the runout of the brake disk. Part of this runout was due to thermal effects; if the turbine had been standing in the sun before being operated, the side of the tower exposed to sunlight expanded more than the side in the shade. Until these effects evened out, the disk periodically impacted the fixed calipers, increasing the rotational stiffness and resulting in higher rotor system frequencies and a changed Campbell diagram. The higher system frequency mode became much closer to a driving frequency and resulted in intermittent

resonance. Turbine brake performance is within predictions for the one and two brake stop in wind speeds to 60 mph. Figure 48 illustrates a typical braking time series plot. The existing high-maintenance brake calipers were replaced with a floating caliper design and prototypes of a new design are being tested. See section IX.1c.

**VIII.4i. Turbine Dynamic Response**

**Objective:** Confirm turbine dynamic model predictions.

**Procedure:** Measure and record turbine structural performance using strain gages, accelerometers and transducers to correlate structural response to turbine output and wind input on the rotor. Identify operating modal response and component dynamic stresses.

**Results:** Figure 49 illustrates a typical test results table for selected channels. The zero rpm offset column simply indicates the strain gage reading at zero rpm and is not meaningful on its own. Figure 50 is an example of measured results compared to analysis of a time history plot and shows the mast midspan bending strain gage (in line with blade #1). There is a slight difference between rotor speed and analytical speed due to induction motor slip. Figure 51 illustrates a typical spectral plot for a rotating frame channel. Figure 52 compares stress test results and predictions for two strain gages on the original pre-tensioned strut design. Figure 53 compares measured and predicted stresses for blade edgewise and flatwise channels, located near the V-strut, and for mast stress. Figures 54, 55, 56 illustrate dynamic stress comparisons between measured and predicted values vs wind speed for the 1) lower strut trailing axial, 2) blade at lower root edgewise bending, and 3) blade at upper root flatwise bending strain gage channels; all three sets of data are for the V-strut case operating at 58.5 rpm. Dynamic rms levels correlate very well with predictions for the final V-strut design. For the earlier tension strut design, the analysis showed higher levels in some instances than seen in tests. We were having some rod slacking trouble that may have been altering the calibration, and the strut tubes were bowed in installation which may have modified load carrying or stiffness behavior of the strut.

It is important to note that predictions and test rms results match well even though the predictions do not include stochastic turbulence. This is indicative of the dominance of deterministic aerodynamic forces in the machine response. Observed responses show that the dominant deterministic forcing establishes the cycles of stress, and turbulence only serves to vary the peak levels from cycle to cycle. The crest factors (max amplitude divided by rms level), are greater in the test, as would be expected, and these factors can be used to easily adjust fatigue analysis based on deterministic amplitudes..

**VIII.4j.**      Coast (spin) Down Tests

**Objective:**    Identify excessive airfoil drag.

**Procedure:**    Measure and record turbine speed, power and wind speed (as a minimum) in low wind conditions. Disengage electrical power and allow turbine to coast to a stop once the turbine has achieved full speed operation.

**Results:**        Deceleration of the turbine rotor did not show effects of excessive drag induced by blade or blade support components. Rotor drag was more easily quantified during low wind operation (see VIII.4e Turbine Baseline Losses). Figure 57 shows the deceleration of the rotor during a coast down vs time for a given wind speed.

**VIII.4k.**      Turbine Electrical Power Performance

**Objective:**    Confirm predicted power curve for a clean blade condition.

**Procedure:**    Record turbine power output over the full range of operating wind speeds.

**Results:**        The power curve for the EHD with the SNLA2150 airfoil fell short of predictions in low to moderate wind speeds. In high wind speeds it did reach design peak power. Subsequent performance predictions of the SNLA2150 using the output from the most recent (as yet unpublished) Eppler code, which quantifies the effect of transition or laminar bubble drag, showed a striking correlation to measured power curve results. Figure 63 illustrates the laminar separation bubble condition (reference 31) on an SNLA1850 airfoil, the same family as the SNLA2150 airfoil. Figure 58 shows the original and most recent power curve predictions with the measured power curve. Figure 59 illustrates power curve measurements at the three different rotor speeds at which the 17-m EHD was tested. Note the improved low wind performance at low wind speeds with the slower rotor speed and corresponding peak power reduction.

**VIII.4l.**      Parked Stress (multiple orientation)

**Objective:**    Correlate wind excited modal response to the predicted response, and check the stress level.

**Procedure:**    Measure and record turbine strain gage, accelerometer and transducer signals with turbine parked at different orientations relative to the wind and perform analysis to identify modal response.

**Results:**        Wind excited stresses are negligible. Wind excited modal testing has been useful for checking the effect of rotor component changes on natural frequencies. The response peaks are clearly seen in output spectra. Data was taken in wind speeds up to 60 mph.

**VIII.4m.**      Dynamically Balance Turbine

**Objective:**    Identify and reduce loads resulting from eccentricity or an unbalanced condition of the operating 17-m EHD due to component variations.

**Procedure:**    Measure the periodic response of the EHD due to rotor component imbalance and add corrective weights as required.

**Results:** Measurements were taken by an outside contractor. No significant imbalance was identified. This is also confirmed in the spectral plots for the upper bearing accelerometer channels taken as a routine part of the EHD data set.

**VIII.4n.** Turbine Iced Dynamic Response

**Objective:** Determine the effect of iced blades on the dynamic response of the rotor.

**Procedure:** Measure and record turbine structural performance of the EHD in an iced condition using strain gages, accelerometers and transducers to correlate structural response to turbine output and wind input on the rotor.

**Results:** The EHD has not been operated at full speed in iced conditions.

**VIII.4o.** Wind Only Start From 0 rpm

**Objective:** Determine rate of acceleration and time to achieve operating speeds due to wind only starting from 0 rpm.

**Procedure:** Measure electrical, mechanical and structural sensors and transducers of interest during turbine start-up. Monitor the "wind only" start to 1780 rpm (wye-delta transition speed) at which time the turbine is stopped.

**Results:** The turbine has self started in wind speeds up to 50 mph and free wheeled at between 1/2 and 3/4 speed.

**VIII.4p.** Prototype Turbine Wake Study/Analysis

**Objective:** Measure baseline 19-m and EHD down-wind wake profile.

**Procedure:** Monitor and record turbine performance and both up- and down-wind anemometry. Correlate input wind speed and turbine power to down wind anemometry.

**Results:** A wake deficit and vertical profile study was undertaken at 19-m turbine 111E, Altamont from late July to August 93. Refer to Figure 60 for a time history plot for one of the tests. One meteorological (met) tower was installed two rotor diameters (D) upwind and 3 met towers were installed 8 D downwind in the prevailing direction, and at +/- 10 degrees of prevailing. Anemometers and wind direction vanes were installed at the equator height on all four towers. The turbine was turned on and off every 15 minutes for three 8-hour periods. The 15-minute data were analyzed to determine speed deficits, turbulence increases and wind direction variability increases. The results from the three data sets were combined and compared to the DOE/SERI/FloWind study undertaken in Tehachapi with the 17-m turbines in 1988. Data points from the 19-m Altamont test were superimposed on the 17-m Tehachapi test velocity deficit vs. wind speed plot and found to fall neatly within the main area of scatter. That the results were so similar was remarkable considering i) different size turbines were used, ii) the area has different atmospheric characteristics, and iii) the Altamont test site has much more complex terrain. Further, the very narrow profile of the wake structure was verified by calculating deficits at the met towers on either side of the wake centerline; it was less than 1%. This was also in line with the findings in the SERI/FloWind



study where anemometers 100 ft (~2D) off-axis from the centerline barely showed any wake effects.

A wake study has not yet been performed at the 17-m EHD prototype test site; at the first prototype site, the tower location at 8 D downwind of the turbine would have fallen beyond FloWind's property line. A wake study is planned for the second prototype site which has the advantages that a 19-m turbine is located exactly 8 D downwind so that power deficits can be measured, and the terrain is flat.

**VIII.4q.**     Rain Flow Study/Analysis (fatigue cycles)

**Objective:**    Acquire stress signals in the time domain for later use.

**Procedure:**   Measure and record turbine structural performance using strain gages, accelerometers and transducers to correlate structural response to turbine output and wind input on the rotor.

**Results:**     Modal frequency avoidance has been achieved as predicted by analysis. Dynamic rms levels correlate well with predictions. It is important to note that predictions and test rms results match well even though the predictions do not include stochastic turbulence. This is indicative of the dominance of deterministic aerodynamic forces in the machine response. Observed responses show that the dominant deterministic forcing establishes the cycles of stress, and turbulence only serves to vary the peak levels from cycle to cycle. The crest factors (max amplitude divided by rms level), are greater in the test, as would be expected, and these factors can be used to easily adjust fatigue analysis based on deterministic amplitudes.

Adjustment based on crest factor alone is very conservative, because it assumes all cycles are at maximum level. The available 20 Hz sampled data is also useful for determining the probabilistic distribution of peak level if a more sophisticated adjustment of the fatigue analysis is desired. However, this has not been warranted because fatigue safety factors are very large even with the conservative approach (cumulative damage less than 0.01 for 20 years).

**VIII.r.**     Test Bed Wind Shear Study/Analysis

**Objective:**    To identify characteristic turbulence of the Cameroon Ridge EHD site and correlate input wind speed to rotor equator position for control algorithm considerations.

**Procedure:**   Monitor and record each wind input of the baseline EHD meteorological tower. Analyze and report.

**Results:**     Since the flow of the wind at the test site is being compressed as it accelerates up over the ridge from the canyon upwind, it would be expected that the wind shear be quite low. Indeed an average ratio of wind speeds between 131 ft and 93 ft levels is 1.39 and yields an exponent value of 0.04.

## **IX. DESIGN MODIFICATIONS & PLANNING FOR FLEET DEPLOYMENT**

### **Plan**

1). Using EHD prototype test and operating data; a). review, b). enhance or c). modify component designs to further improve system cost, performance, and reliability, 2). fabricate and test component changes as required and 3). prepare development plans for installation of the EHD VAWT upgrade.

### **Accomplishments**

Using hardware and system test results, changes have been made to further enhance the performance of the EHD VAWT system. EHD testing continues for validation of design modifications. Turbine sites have been identified and preliminary schedules have been prepared for upgrade installation.

### **IX.1. Design Modifications**

#### **IX.1a. "B" Blade**

A new airfoil profile, the "B" blade, has been designed by Dan Somers of Airfoils, Inc. with a conservative pressure distribution for reduced transition drag sensitivity, a leading edge contour having lower roughness sensitivity, and a lower maximum coefficient of lift to restrain peak power.

The blade cross-section has been optimized for cost and ease of manufacture. Off-the-shelf broad good fiberglass materials have been specified to further reduce cost. The structural dynamics of the "B" blade turbine will be nearly identical to the SNLA2150 blade turbine, i.e., the natural vibration modes are very close in frequency. Figure 61 shows the "B" blade turbine Campbell diagram. All modes above the first differ by 7% or less; the first mode differs by 25% but is not an excited mode. Figure 62 illustrates predicted flutter damping coefficients and shows no expected flutter instabilities (indicated by negative damping). These results are a product of the complex modal analysis.

Fabrication tooling has been procured which further reduces manpower requirements.

#### **IX.1b. Root Attachment**

Based on full-scale blade root fatigue testing at Sandia National Laboratories, the blade root mount inside radius has been increased to reduce local stress concentrations. Further detail changes will be implemented as described earlier in section II.3. Rodeman (25) describes the tests.

#### **IX.1c. Brake Assemblies**

In efforts to reduce the largest maintenance item associated with the 19-m baseline machine, the brake system was redesigned. The original 19-m brake system utilized 12 hydraulic calipers and three spring applied hydraulic release calipers. To increase

reliability and improve maintainability, the 12 fixed brake calipers were replaced by six floating brake calipers of equal brake torque capability.

### **IX. 2. Testing of Design Modifications**

Both airfoil and rotor structural performance testing will be performed following AWEA and ASME performance test standards.

### **IX. 3. Fleet Deployment**

Fleet deployment is planned immediately following completion of performance testing. This includes 50 of FloWind's existing 19-m VAWT fleet in Tehachapi, California.

## Final Summary

### Accomplishments

Development of; 1). an "Extended Height to Diameter" (EHD) VAWT geometry, 2). a structurally soft, three bladed VAWT rotor, 3). a continuous span (jointless design) fiberglass blades, 4). pultrusion process and tooling for continuous low cost VAWT blade manufacturing, and 5). improved analytical and design capabilities (models and codes).

### Objectives Achieved

Development of a high energy rotor retrofit for FloWind's existing 19 meter VAWT fleet including; 1). maximize installed capacity and infrastructure, 2). increased energy capture, 3). improved reliability (continuous span fiberglass blade design)

### Constraint Changes

Constraints were not changed. The design was initially constrained to the existing infrastructure with emphasis on maximizing energy delivery and minimizing costs where modifications were required. The design matured to include; 1). three blades rather than two, and 2). lightweight struts to provide structural tuning and transmittal of torque to the drive train (initially struts were going to be eliminated if possible).

### Pultrusion a Viable Process

Low cost VAWT blades require constant chord geometry. The pultrusion process offers a low cost approach in materials (fiberglass and resin) and processing to meet this requirement. A blade manufactured using the pultrusion method routinely yields consistent chordwise and spanwise material properties.

### Project Successes

The successes included 1). a low cost blade manufacturing process, 2). a three bladed soft VAWT geometry, 3). development of material handling procedures for shipping, handling and installing the 160 foot long blade, 4). low cost approach to mast re-use, 5). successful use of a tether and damper system for the EHD guy cable system, 6). successful diagnosis of gear train component vibration (demonstrated on the 60 rpm gearbox), 7). initial testing of alternative brake designs, 8). improved analysis tools, and 9). close correlation of predicted to measured structural performance.

### Project Challenges

FloWind Design and Engineering staff confronted challenges beginning in the preliminary design and continuing through post-project testing. These challenges included; 1). lack of state-of-the-art analysis tools. State-of-the-art tools (principally PC based) were not available at the onset of the project but were developed over time including batch processing of aerodynamic configuration data and development of a VAWT model for dynamic and structural optimization, 2). pultrusion infeed tooling which was improved following initial pultrusion runs, 3). guy cable dynamic response. Predictive methods were unable to quickly establish a solution to the guy cable vibration. A tether and damper arrangement was

ultimately configured to eliminate cable resonance problems, 4). aerodynamic performance of the SNLA2150 blade profile was less than predicted. Several tests were performed to determine the effects of instrumentation wires, dirt, and other aerodynamic properties. The performance was determined to be the characteristic of the profile (testing continues). A new blade has been developed and initial tests performed. Aerodynamic testing is ongoing, 5). Gearbox challenges include retrofit cost and specification. The initial 60 rpm gearbox retrofit resulted in excessive vibration. This "quality" challenge directed attention on the original retrofit requirement. As a result, existing, 52 rpm, gearboxes will be used on the EHD turbine with a slightly larger rotor to achieve peak power requirements, and 6). data acquisition system challenges effecting both the rotating and non-rotating frame components prevented continuous acquisition of turbine system performance data. The DAS is based on a "mini" computer system, interfaced to early technology telemetry equipment for transmittal of rotating frame data. Data dropouts proved problematic and difficult to diagnose.

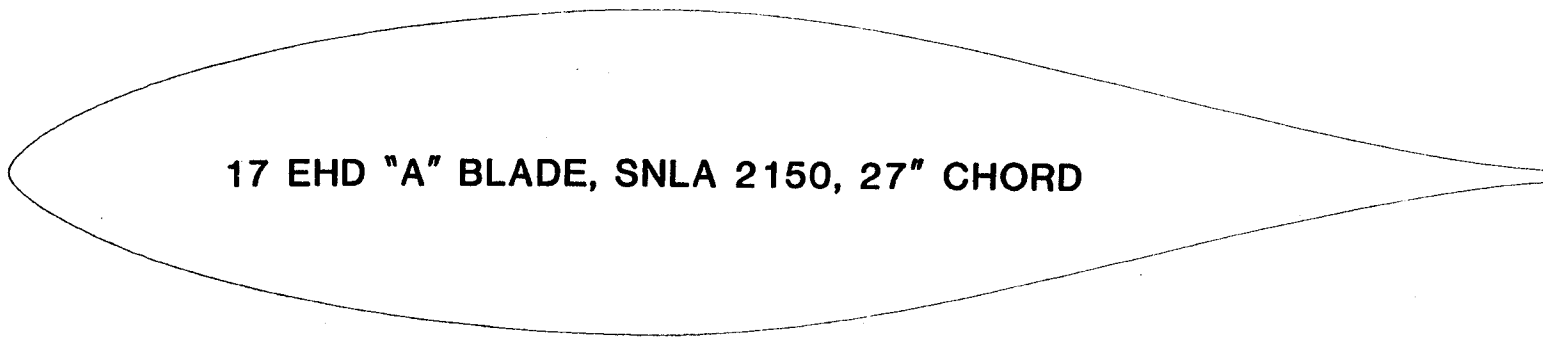
## References

1. T.G. Carne, SANDIA, memo to B. Bell, FloWind, "The Modal Test Of The FloWind 17-EHD VAWT," January 1995.
2. H.-T. Liu, J.W. Buck, A.C. Germain, M.E. Hinchee, T.S. Solt, G.M. LeRoy, R.A. Srnsky, Field Investigation of A Wake Structure Downwind of a VAWT in a Wind Farm Array, SERI/STR-217-3370, DE89000821, September 1988.
3. R. Nierenberg, memo to FloWind, "19-m Wake Test Results in Altamont," August 14, 1993.
4. L.L. Wendell, J.C. Barnard, and V.R. Morris, "New Parameters For Characterizing Turbulence At A Potential Wind Site, Pacific Northwest Laboratory," Presented at AWEA Windpower '93, June 12-16, 1993.
5. L.L. Wendell, J.C. Barnard and V.R. Morris, "Turbulence Characterization," Pacific Northwest Laboratory, Presented May 9, 1994, Windpower '94.
6. J.R. Connell (Colorado State University), V.R. Morris (Pacific Northwest Laboratory), Turbulent Wind At The Equatorial Segment Of An Operating Darrieus Wind Turbine Blade, DE-AC06-76RLO 1830.
8. Eppler, Richard. Airfoil Design and Data. Springer Verlag (Berlin), 1990.
9. Eppler, R. Airfoil Program System. User's Guide. R. Eppler, c.1993.
10. Convergence Engineering, Vertical Axis Wind Turbine Analysis System, March 15, 1993.
11. Performance Test Codes, Wind Turbines, ASME/ANSI. PTC 42-1988.
12. Standard Performance Testing Of Wind Energy Conversion Systems, AWEA Standard, AWEA 1.1-1988.
13. Anemometer Control and Data Line, Conduit Layout, Cameroon Ridge, Lower Wuerth Property, FloWind Drawing # 0201-E-07, R2.
14. W.F. Rahhal. Memo to FloWind Corporation, "Structural Analysis of FloWind Turbine Blade, Finite Element Modeling & Analysis of Composite Blade, Fiber Concepts," October 15, 1992.
15. W. F. Rahhal memo to FloWind Corporation, "Structural Analysis Of FloWind Turbine Blade, Stress Analysis, Fiber Concepts," January 20, 1993.

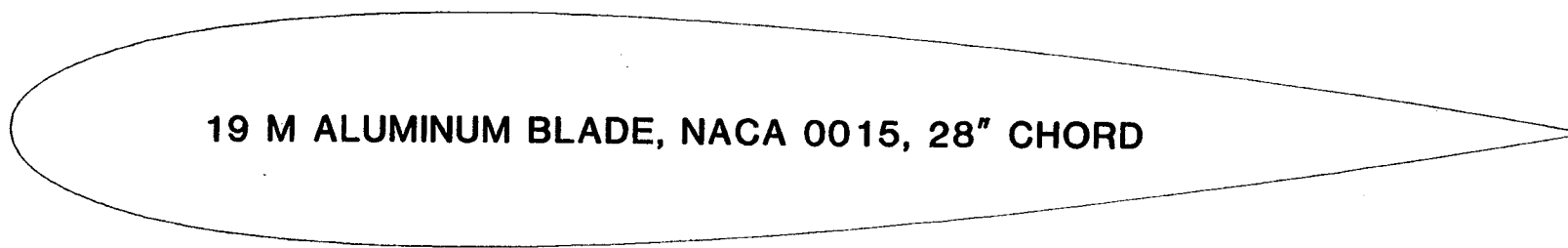
16. W. F. Rahhal. Memo to V. Wallace, FloWind, "27-in Blade Laminate Potential For Patent," July 9, 1993.
17. Tsai Stephen, W., Composite Design, Third Edition, p. 17-19.
18. J. Rodgers. Memo to FloWind, "ALGOR Finite Element Stress Analysis Results," Upper Bearing Cone - Drawings 501292 & 501293, October 5, 1993.
19. R. D'Amato. Report to FloWind Corporation, Structural Evaluation of Existing Foundations For FloWind 17-III VAWT, September 7, 1993.
20. R. Malhotra-Bush, FloWind, VG Program Final Report, 28 July 1993.
21. R. Malhotra-Bush, FloWind, Interim Memo On Blade Cleaning Results, November 19, 1992.
22. V. Wallace. Brake System Analysis, Spreadsheet and Backup Timeseries Data.
23. FloWind, F17 EHD B-Blade, 18-Nov-93, B Blade Design Analysis.
24. FloWind Corporation, October 6, 1994, EHD VAWT Upgrade Program Presentation.
25. R. Rodeman and D. Gregory, Sandia National Labs. Memo to P. Veers, "Wind Turbine Blade Joint Fatigue Test," September 14, 1994.
26. W.F. Rahhal, "Structural Analysis of FloWind Turbine Blade- Ply Schedule", Fiber Concepts, December 12, 1992. Data for parallel-laminated 181 E-Glass fabric (satin weave, 6 over/1 under)/polyester resin, parallel to warp, 73 F.
27. Dean, M.W., "Fatigue Behavior of Flat Leaf Composite Springs", GlasForms Report #GF-002B, May 18, 1987. Data for XK325-113.1 E-Glas uni/proprietary resin system, approx. 70% fiber weight.
28. Mandell, J.F., Reed, R.M., and Samborsky, D.D., "Fatigue of Fiberglass Wind Turbine Blade Materials", Sandia Labs Contractor Report #SAND92-7005, August, 1992. Data for Vinyl Ester Uni, fiber volume of 30%.
29. Kensche, C.W., "High Cycle Fatigue of Glass Fibre Reinforced Epoxy Materials for Wind Turbines", Deutsche Forschungsanstalt fur Luft- und Raumfahrt (DLR) report #DLR-FB92-17, April, 1992. Data for 2C=60/40 Uni/bias, 2A=67/33 Uni/bias, 1A=Uni.
30. Goldsworthy, W.B., "Continuous Manufacturing Processes", Chapter 17 of Handbook of Composites, Van Nostrand Reinhold, 1982. Data for HTS-904/826 resin Uni.

31. Branwell, R. ed. "Natural Laminar Flow and Laminar Flow Control", Springer - Verlag, 1992.





17 EHD "A" BLADE, SNLA 2150, 27" CHORD



19 M ALUMINUM BLADE, NACA 0015, 28" CHORD

SNLA 2150 27" Airfoil vs NACA0015 28" Airfoil

Figure 1

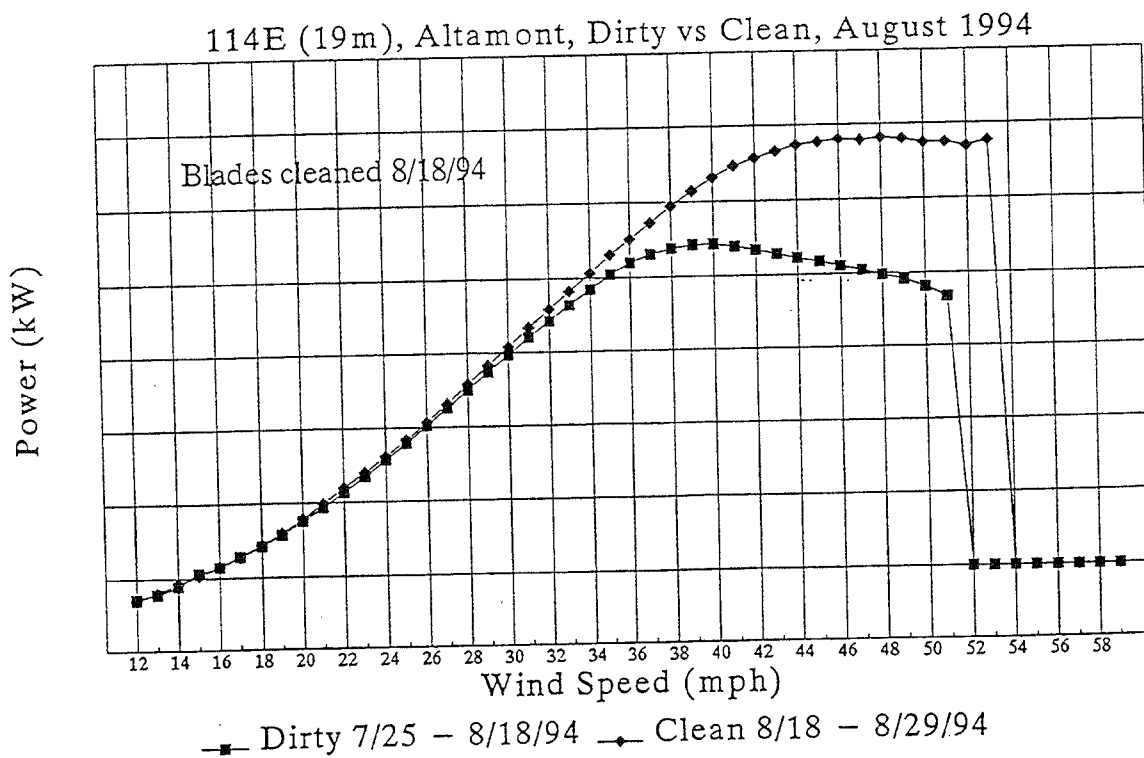
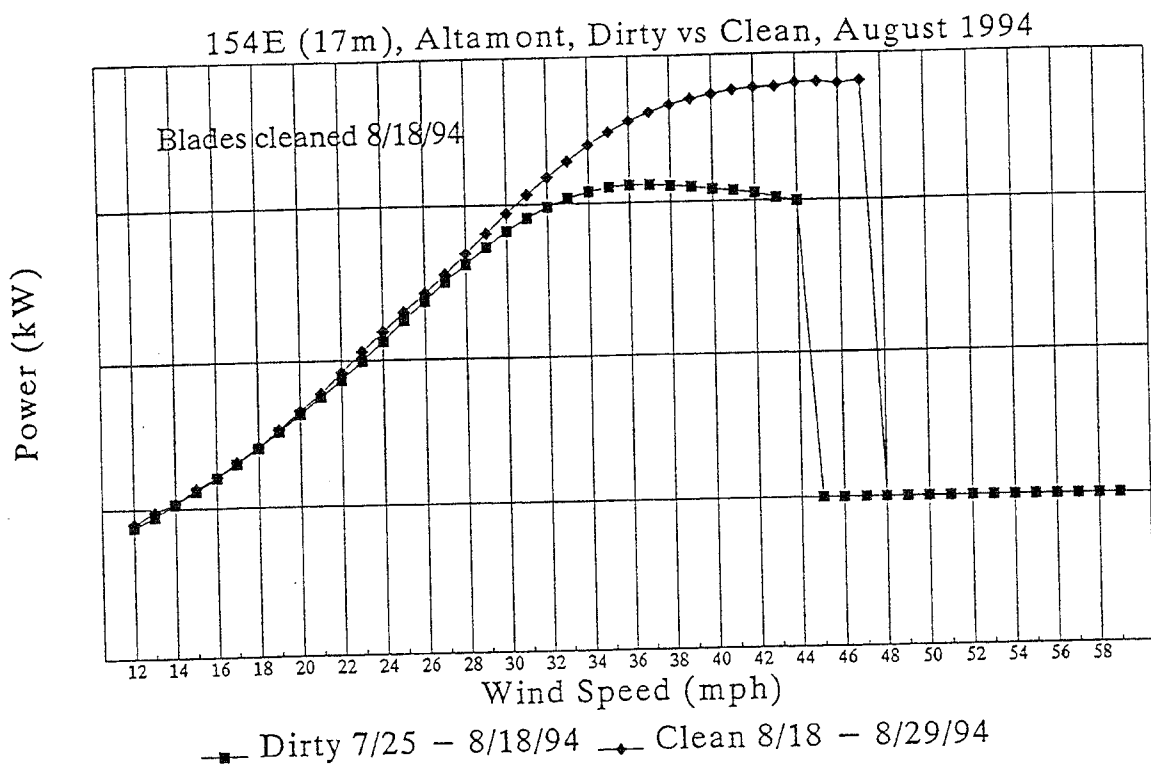
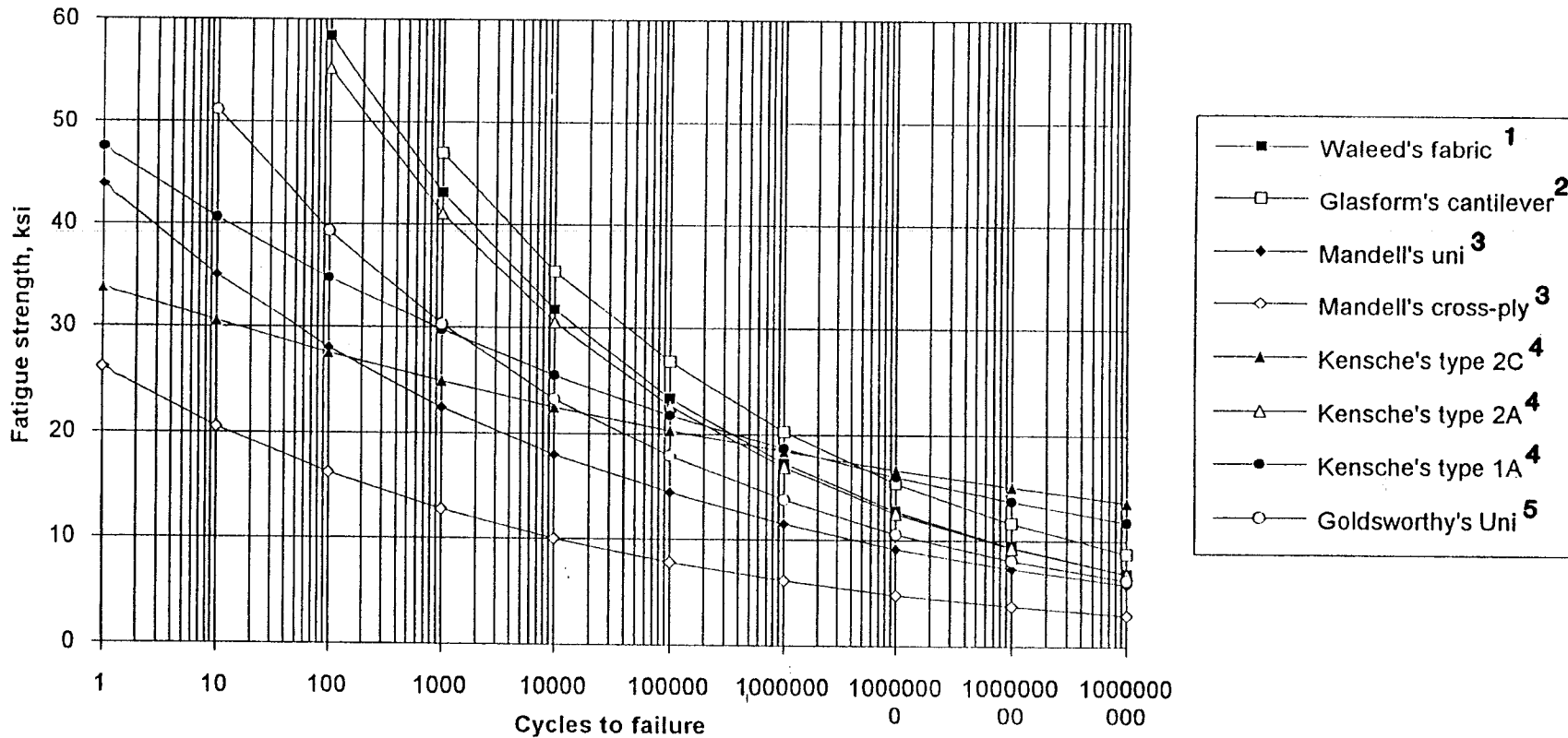


Figure 2

**S-N Curves**  
**R=-1, referenced to Su=57.4 ksi**



**NOTES:**

- 1 See reference 26
- 2 See reference 26
- 3 See reference 27
- 4 See reference 28
- 5 See reference 29
- See reference 30

Figure 3

# WELD FATIGUE ALLOWABLES

Category "C", case 24 from AISC

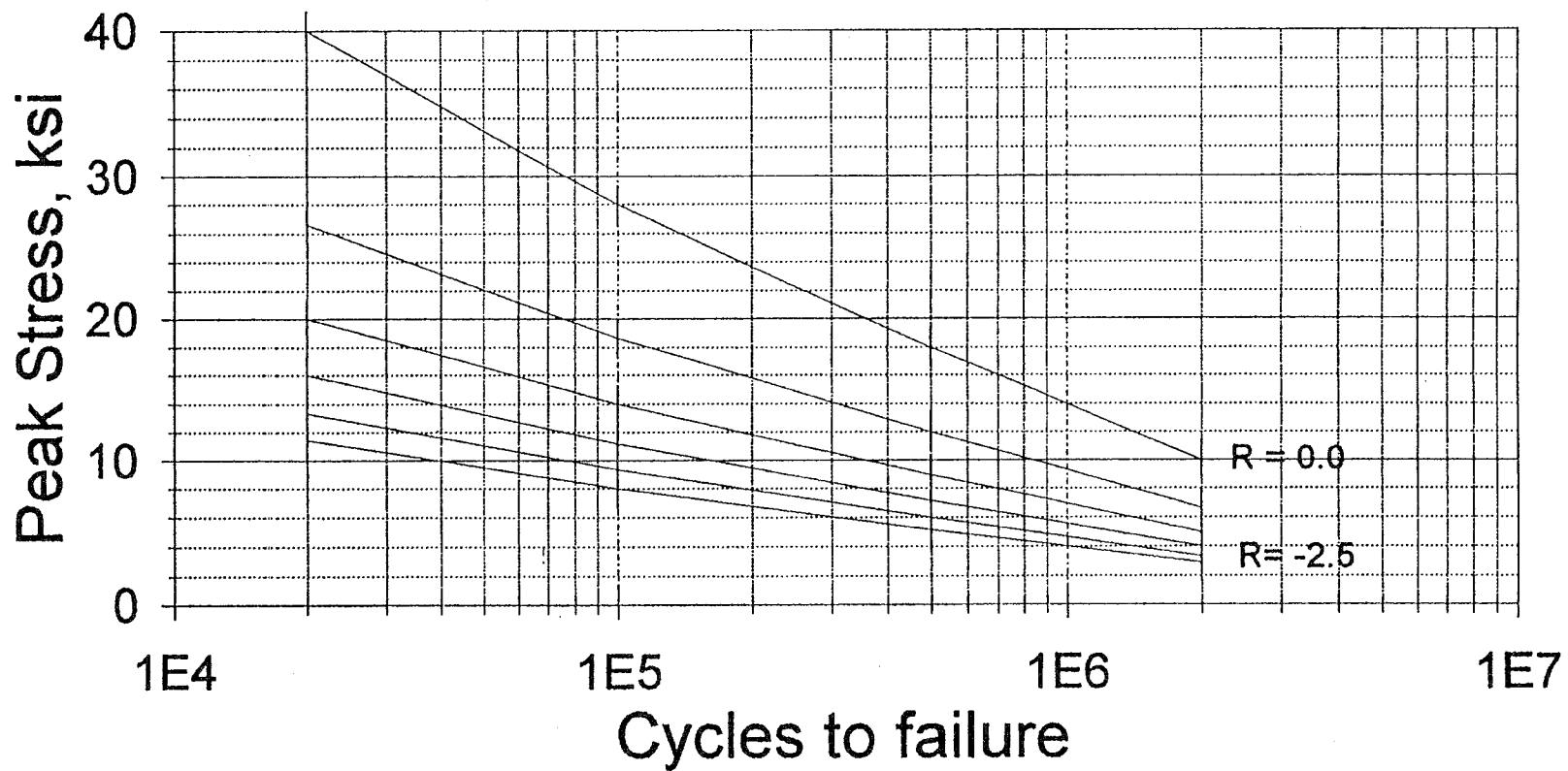
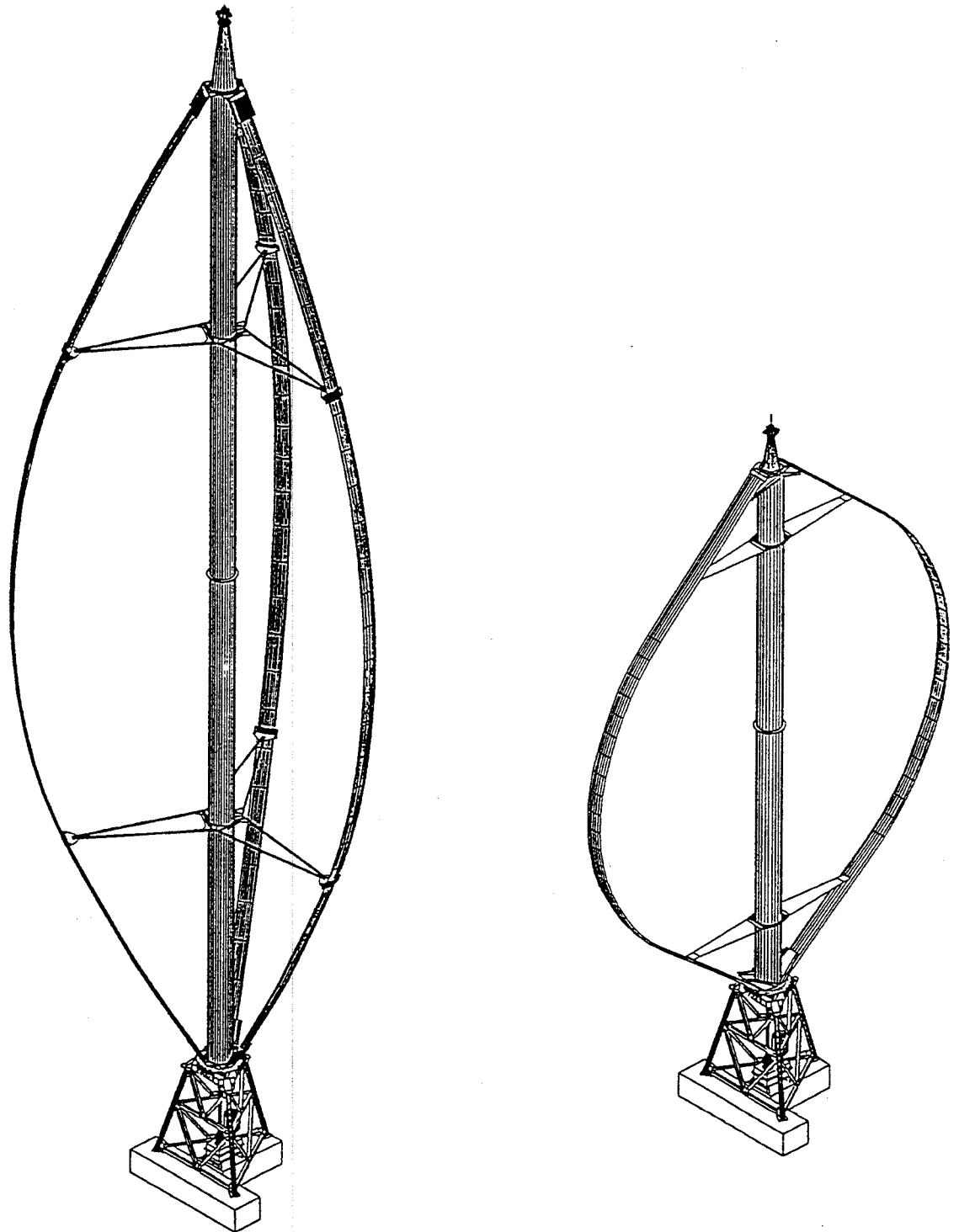


Figure 4

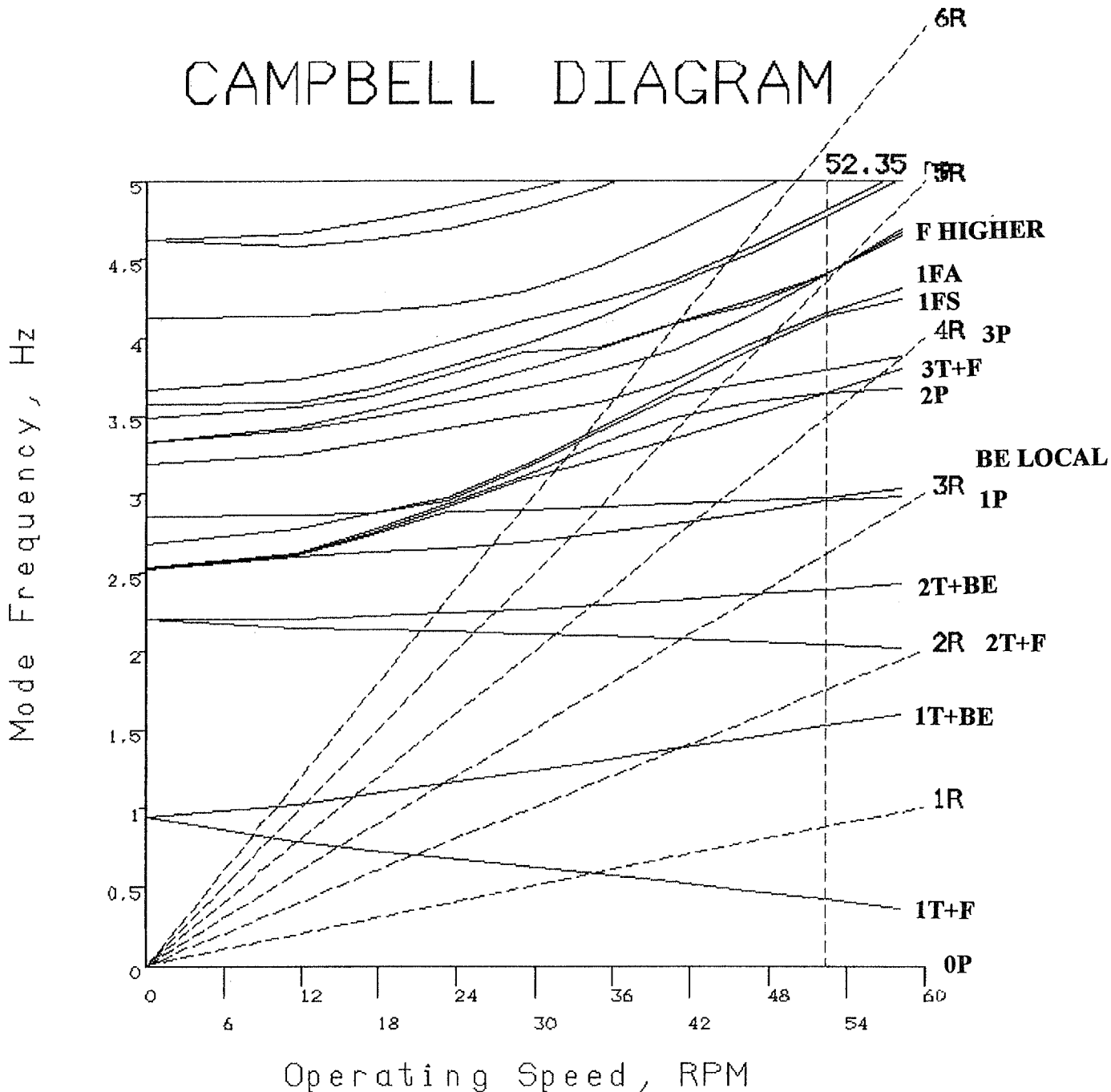
John Rodgers  
9/11/93



3D 17 EHD and 19-meter VAWTs

Figure 5

# CAMPBELL DIAGRAM



ANSYS 5.0 18  
 APR 21 1995  
 16:10:57  
 PLOT NO. 1  
 POST26

ZV =1  
 DIST=0.75  
 XF =0.5  
 YF =0.5  
 ZF =0.5  
 CENTROID HIDDEN

POST26

ZV =1  
 DIST=0.75  
 XF =0.5  
 YF =0.5  
 ZF =0.5  
 CENTROID HIDDEN

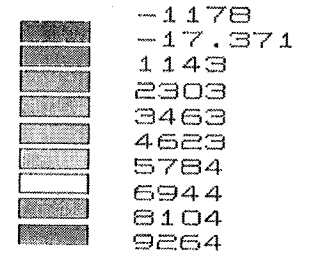
POST26

ZV =1  
 DIST=0.75  
 XF =0.5  
 YF =0.5  
 ZF =0.5  
 CENTROID HIDDEN

Figure 6  
 52

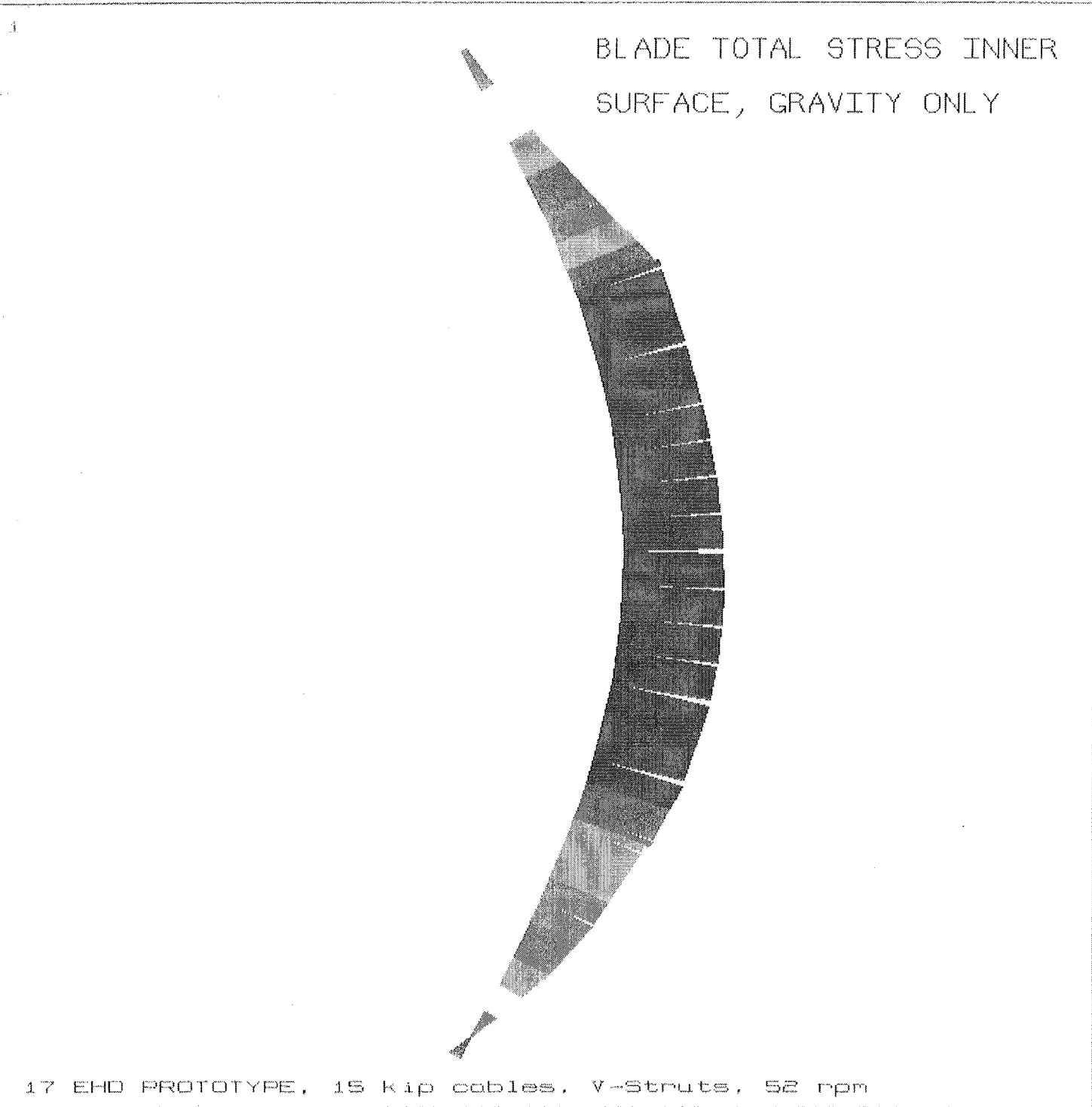
ANSYS 5.0 18  
MAY 15 1995  
05:40:31  
PLOT NO. 7  
LINE STRESS  
STEP=2  
SUB =1  
FREQ=2  
BFTI\_G BFTJ\_G  
MAX =9264  
ELEM=40

BLADE TOTAL STRESS OUTER  
SURFACE, GRAVITY ONLY



17 EHD PROTOTYPE, 15 kip cables, V-Struts, 52 rpm

Figure 7



ANSYS 5.0 18  
MAY 15 1995  
05:40:32  
PLOT NO. 8  
LINE STRESS  
STEP=2  
SUB =1  
FREQ=2  
BFBI\_G BFBJ\_G  
MAX =1013  
ELEM=1

■	-9310
■	-8163
■	-7016
■	-5869
■	-4722
■	-3575
■	-2428
■	-1281
■	-134.11
■	1013

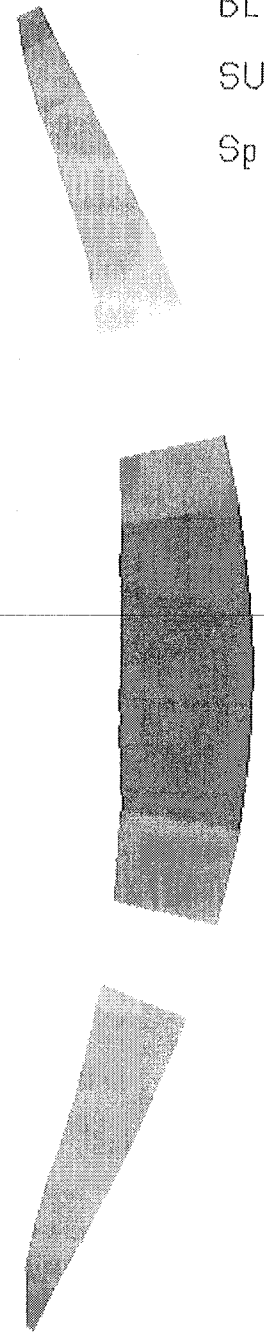
Figure 8



BLADE TOTAL STRESS OUTER  
SURFACE, GRAVITY & OMEGA  
Speed=52.35 rpm

ANSYS 5.0 18  
MAY 15 1995  
05:40:33  
PLOT NO. 13  
LINE STRESS  
STEP=2  
SUB =1  
FREQ=2  
BFTI\_06 BFTJ\_06  
MAX =11411  
ELEM=49

531.987
1741
2950
4158
5367
6576
7785
8993
10202
11411



17 EHD PROTOTYPE, 15 kip cables, V-Struts, 52 rpm

Figure 9

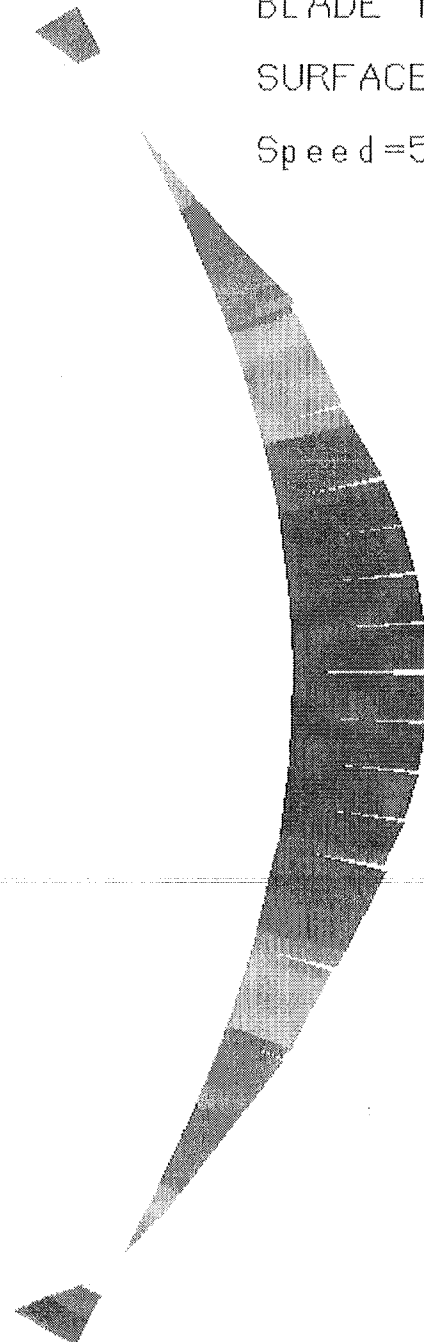
1

BLADE TOTAL STRESS INNER  
SURFACE, GRAVITY & OMEGA

Speed=52.35 rpm

ANSYS 5.0 18  
MAY 15 1995  
05:40:33  
PLOT NO. 14  
LINE STRESS  
STEP=2  
SUB =1  
FREQ=2  
BFBI\_0G BFBJ\_0G  
MAX =3826  
ELEM=1

█	-7490
█	-6233
█	-4975
█	-3718
█	-2461
█	-1203
█	54.059
█	1311
█	2569
█	3826



17 EHD PROTOTYPE, 15 kip cables, V-Struts, 52 rpm

Figure 10

Flatwise Dynamic RMS Stress  
(from bottom to top blade, 60.89 rpm, 63 mph wind)

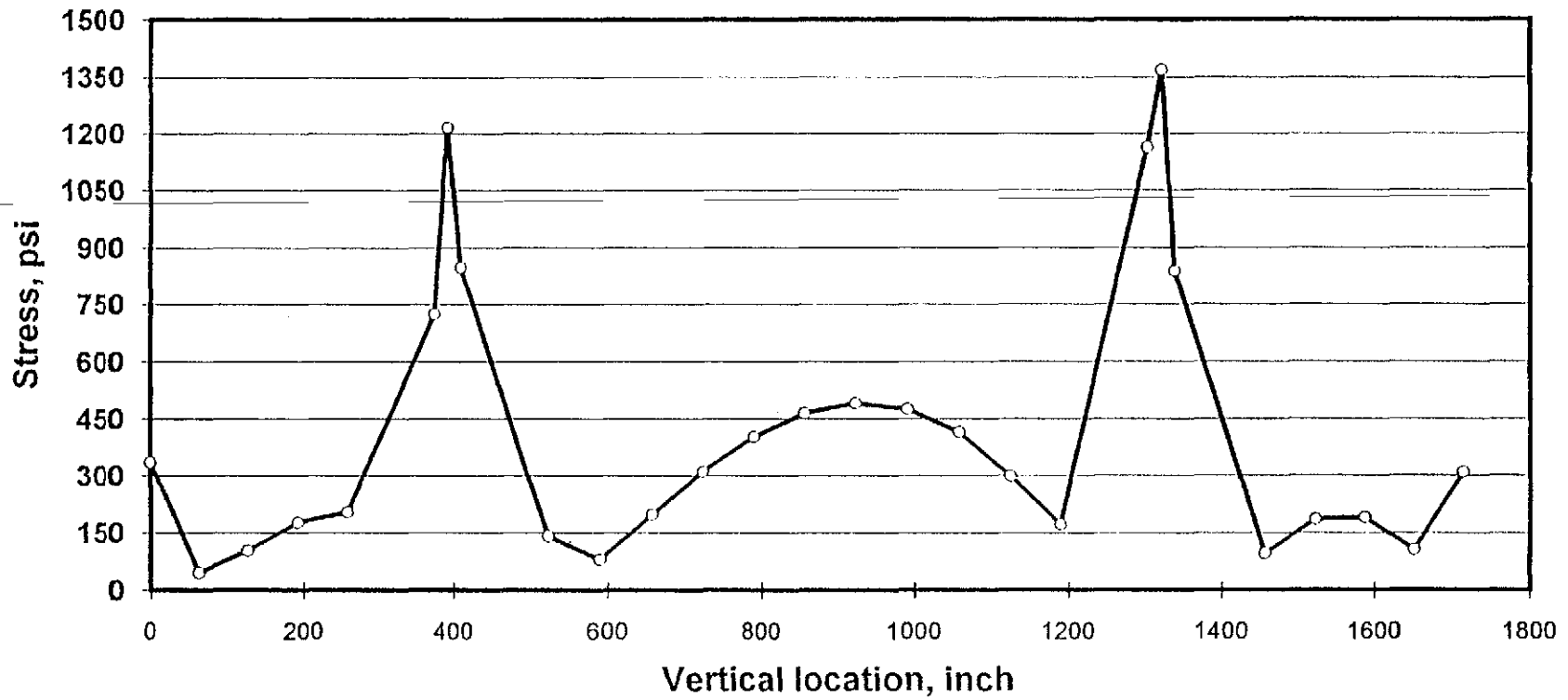


Figure 11

Edgewise Dynamic RMS Stress  
(from bottom to top blade, 60.89 rpm, 63 mph wind)

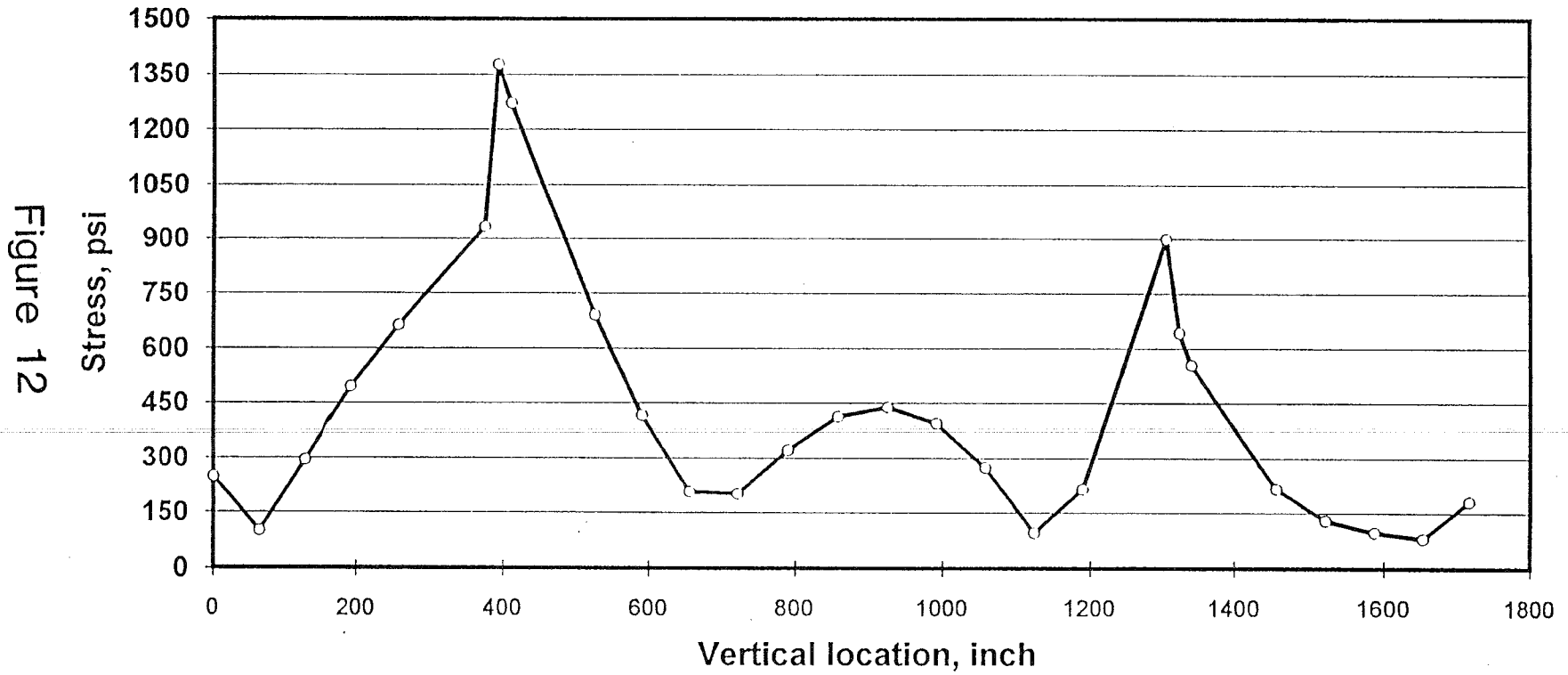
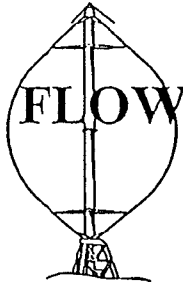


Figure 12



**FLOWIND CORPORATION'S ADVANCED EHD SERIES VAWT  
EHD AIRFOIL**

"A" BLADE

SNLA 2150

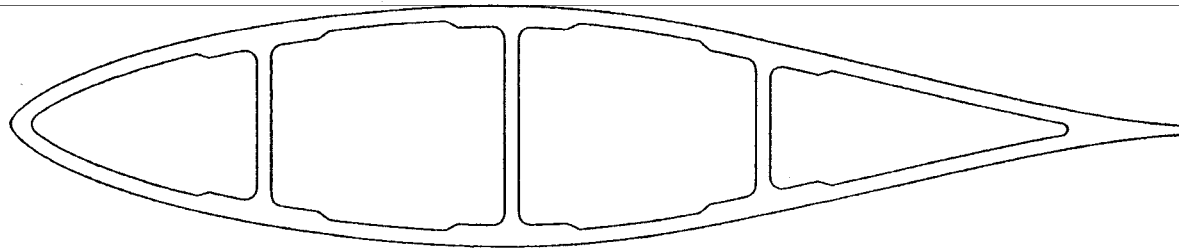


**Figure 13**

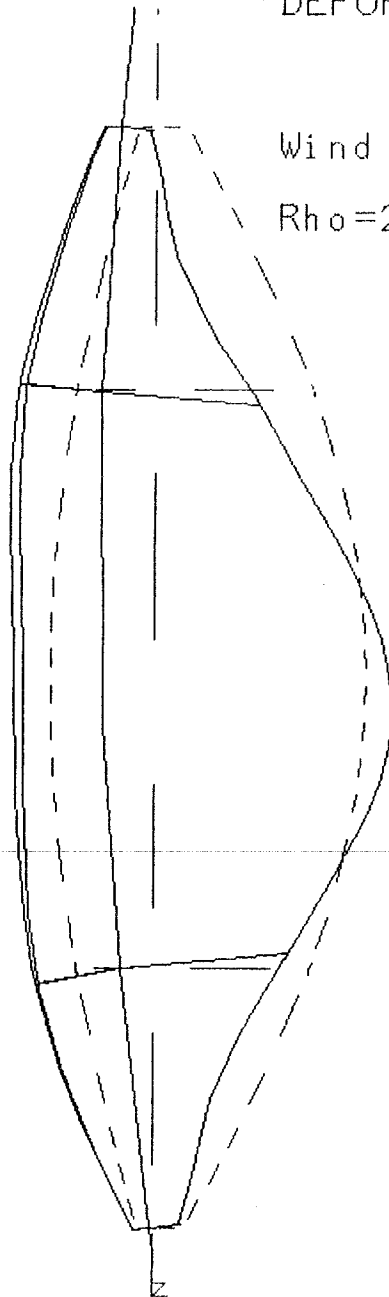
ANSYS 5.0 18  
MAY 15 1995  
05:40:11  
PLOT NO. 3  
DISPLACEMENT  
STEP=3  
SUB =5  
TIME=3  
RSYS=1  
DMX =14.222  
  
OSCA=7.894  
YV =-1  
DIST=1123  
XF =82.876  
YF =-0.688E-04  
ZF =1113  
VUP =Z  
CENTROID HIDDEN

DEFORMATION,

GRAVITY+HIGH WIND

Wind Velocity=130.0 mph

Rho=2.04508E-03 slug/ft^3

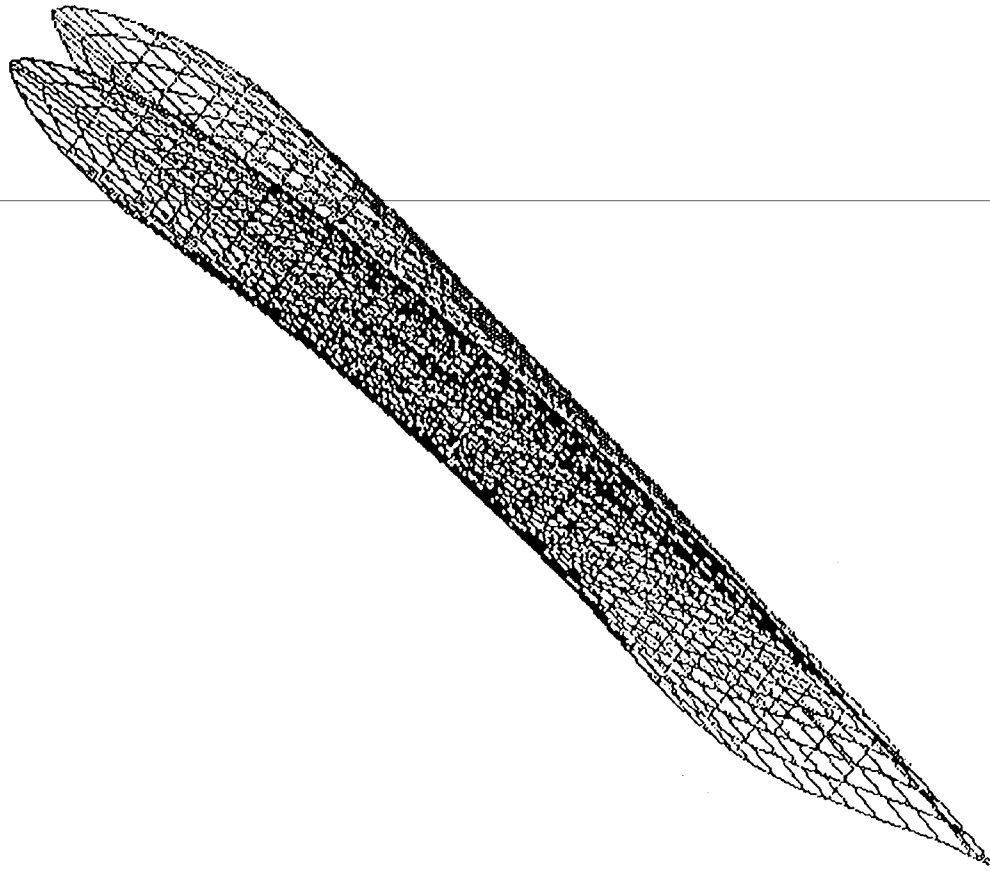


17 EHD PROTOTYPE. 15 kip cablesx V-Struts. 52 rpm

Figure 14

DISPLAY .II - GEOMETRY MODELING SYSTEM (92.0) PRE/POST MODULE

DISPLACED-SHAPE  
MX DEF= 1.98E+00  
NODE NO.= 1248  
SCALE = 1.0  
(MAPPED SCALING)



GRAVITY + CENTRIFUGAL  
FloWind 27 inch Blade

WIND SPEED = 45 MPH

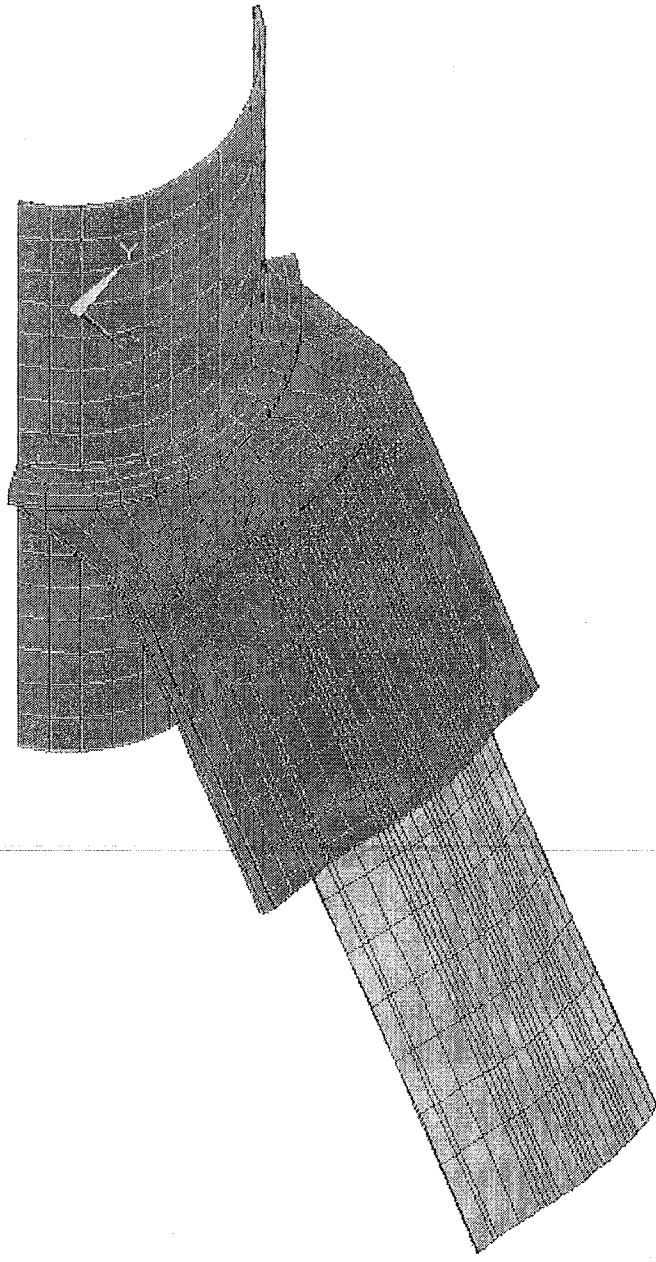
EMRC-NISA/DISPLAY  
MAR/04/93 01:08:41

Z	ROT X
Y	-45.0
	ROT Y
	0.0
X	ROT Z
	-45.0

Figure 15

ANSYS 5.0 18  
JUN 7 1994  
12:17:44  
PLOT NO. 1  
ELEMENTS  
REAL NUM

XV =1  
YV =-1  
ZV =2  
DIST =77.395  
XF =43.976  
ZF =-18.989  
VUP =Z  
PRECISE HIDDEN



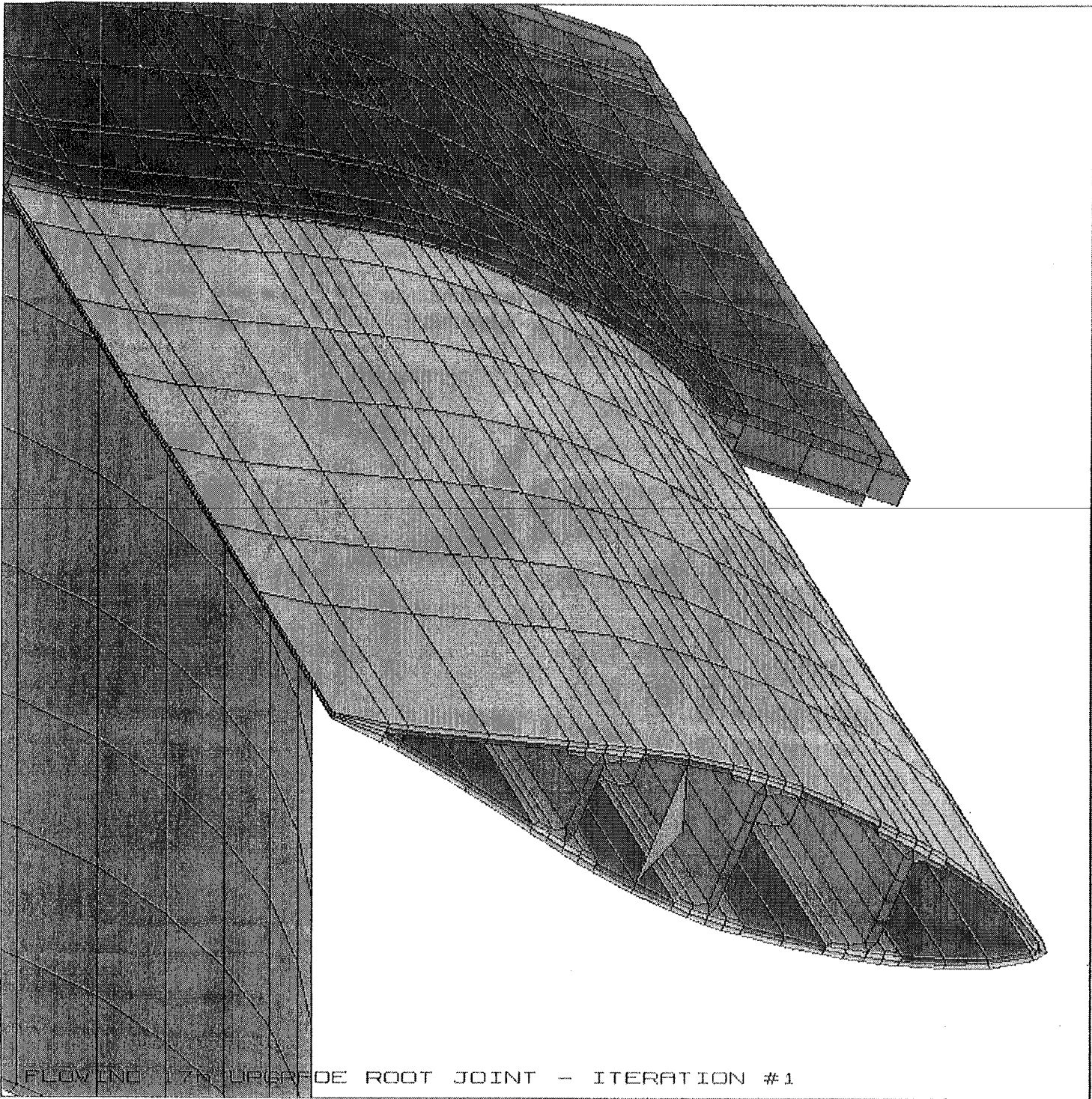
FLOWIND 17m UPGRADE ROOT JOINT - ITERATION #1

Figure 16

1

69





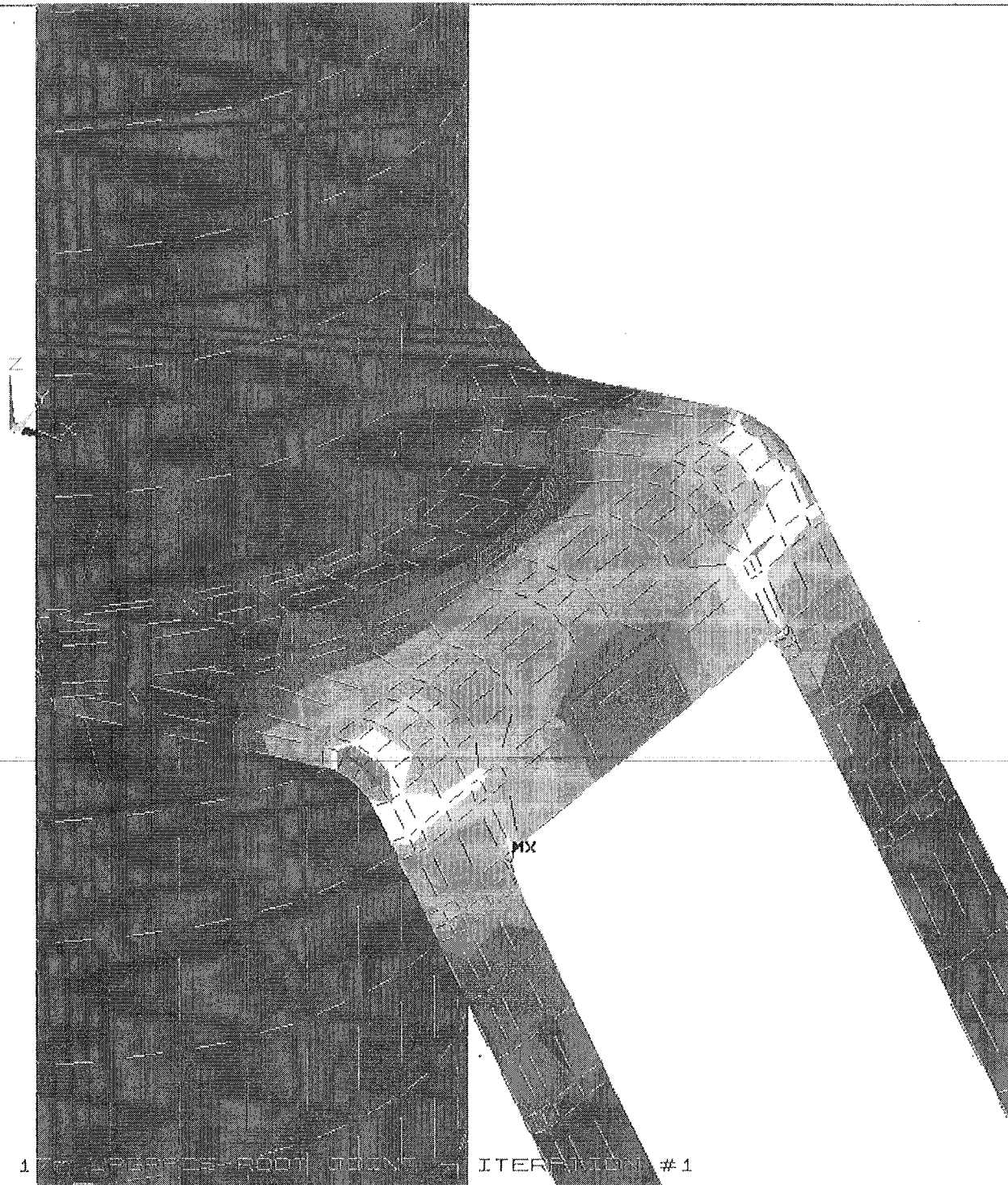
ANSYS 5.0 18  
JUN 7 1994  
12:18:59  
PLOT NO. 2  
ELEMENTS  
REAL NUM

XV =1  
YV =-0.5  
ZV =-1  
\*DIST=18.447  
\*XF =35.807  
\*YF =14.208  
\*ZF =-34.262  
VUP =Z  
PRECISE HIDDEN

Figure 17

FLOWING IN TURBINE UPGRADE ROOT JOINT - ITERATION #1

ANSYS 5.0 18  
 DEC 8 1993  
 07:50:45  
 PLOT NO. 1  
 NODAL SOLUTION  
 STEP=2  
 SUB =1  
 TIME=2  
 SEQV (AVG)  
 TOP  
 DMX =0.010558  
 SMN =0.210E-10  
 SMX =123.646  
 SMXB=244.782  
 0.210E-10  
 13.738  
 27.477  
 41.215  
 54.954  
 68.692  
 82.431  
 96.169  
 109.908  
 123.646



FLOWIND 1 UPGRADE ROOT JOINT ITERATION #1

Upgrade Root Joint -  
 Flatwise Moment Stress

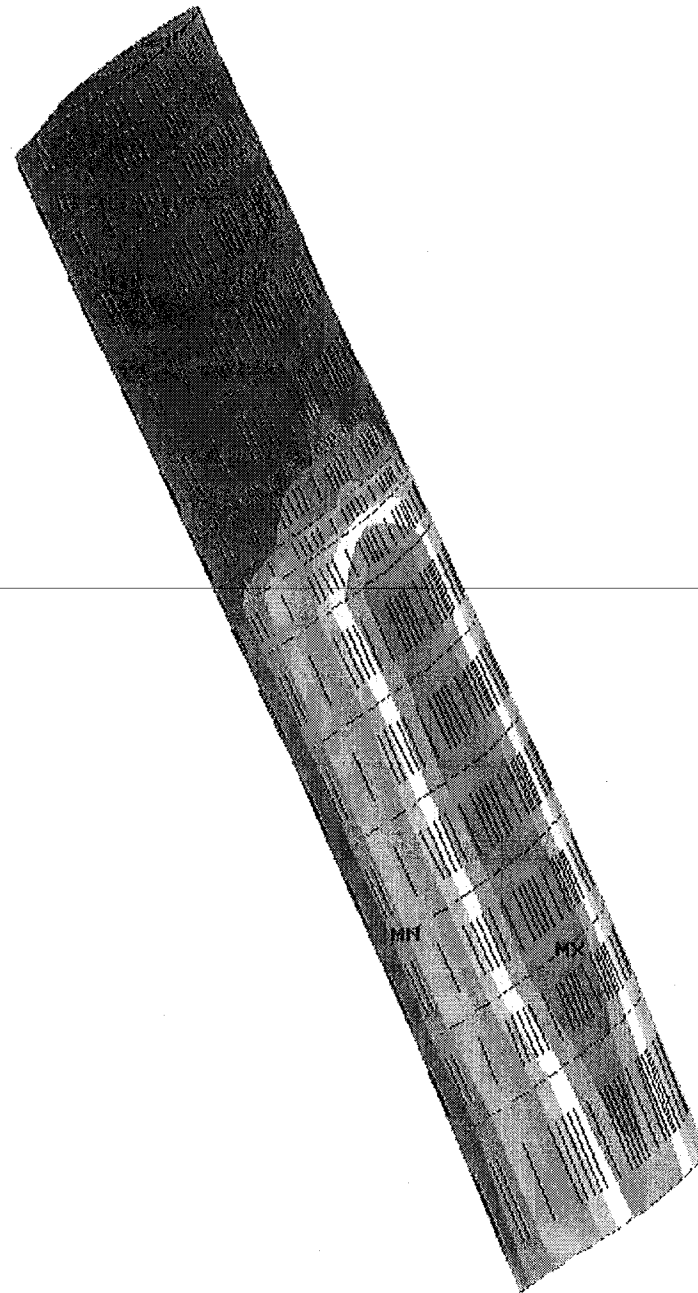
Figure 18

```

ANSYS 5.0      18
DEC  7 1993
16:22:27
PLOT NO.      1
NODAL SOLUTION
STEP=2
SUB  =1
TIME=2
SEQV          (AVG)
TOP
LAYR=2
DMX  =0.010566
SMN  =0.082584
SMNB=0.082584
SMX  =41.024
SMXB=41.024

```

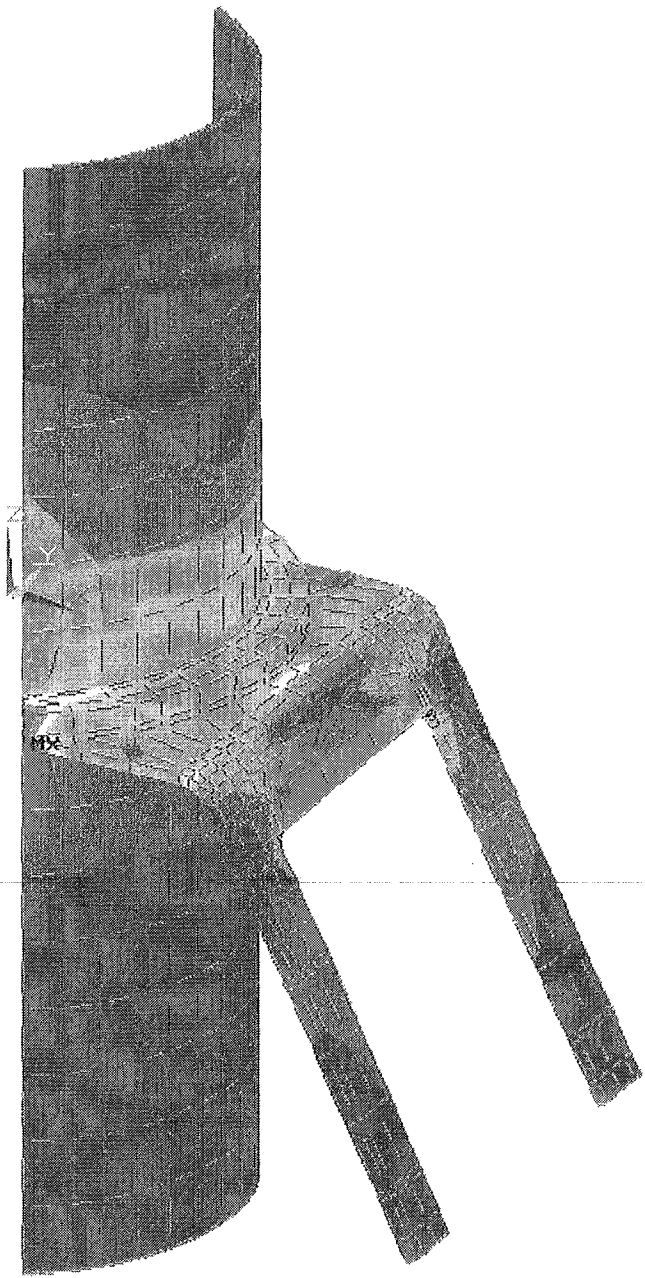
█	0.082584
█	4.632
█	9.181
█	13.73
█	18.279
█	22.828
█	27.377
█	31.926
█	36.475
█	41.024



Upgrade Root Joint -  
Flatwise Moment Stress

FLOWIND 17m UPGRADE ROOT JOINT - ITERATION #1

Figure 19



```

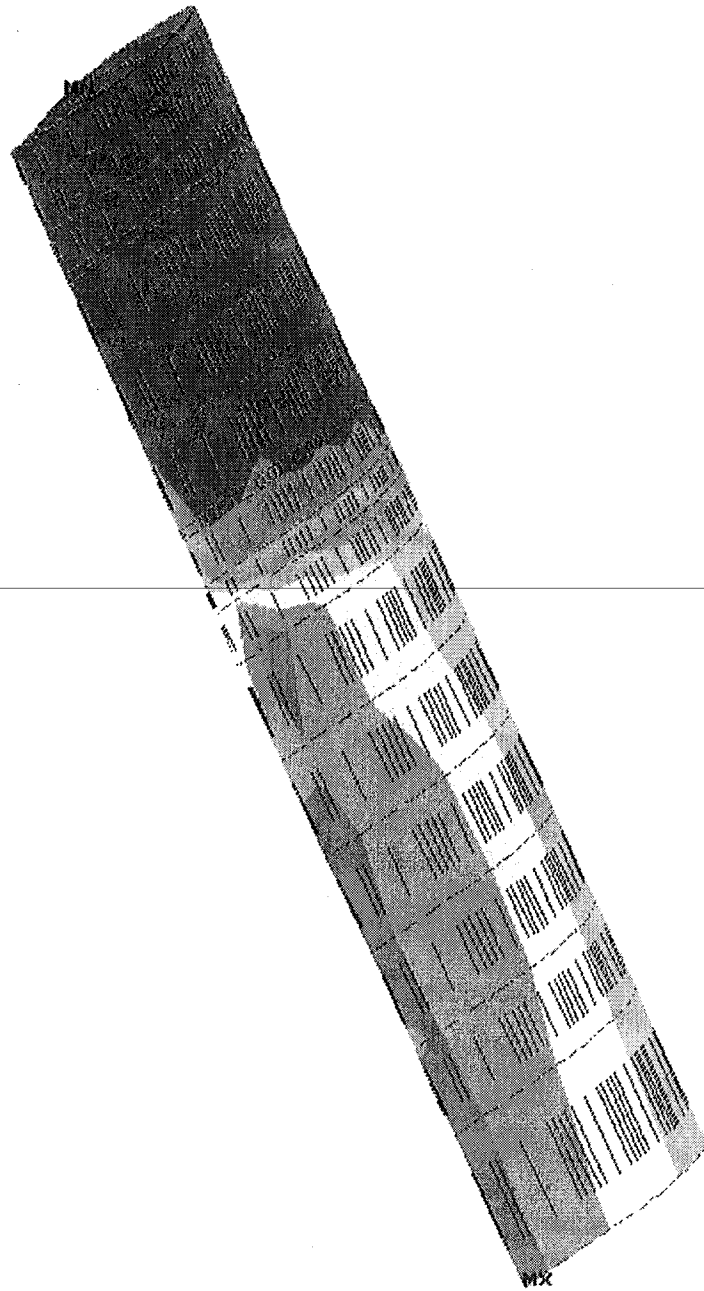
ANSYS 5.0      18
DEC  7 1993
15:42:44
PLOT NO.      2
NODAL SOLUTION
STEP=1
SUB  =1
TIME=1
SEQV          (AVG)
TOP
DMX  =0.006863
SMN  =0.906E-11
SMX  =172.961
SMXB=481.873
          0.906E-11
          19.218
          38.436
          57.654
          76.872
          96.09
          115.307
          134.525
          153.743
          172.961
  
```

Figure 20

Upgrade Root Joint -  
Axial Moment Stress

FLOWIND 17m UPGRADE ROOT JOINT - ITERATION #1

1



```

ANSYS 5.0      18
DEC  7 1993
13:48:53
PLOT NO.      1
NODAL SOLUTION
STEP=1
SUB  =1
TIME=1
SEQV          (AVG)
TOP
LAYR=2
DMX  =0.006874
SMN  =0.545659
SMNB=0.545659
SMX  =72.339
SMXB=72.339
          0.545659
          8.523
          16.5
          24.477
          32.454
          40.431
          48.408
          56.385
          64.362
          72.339

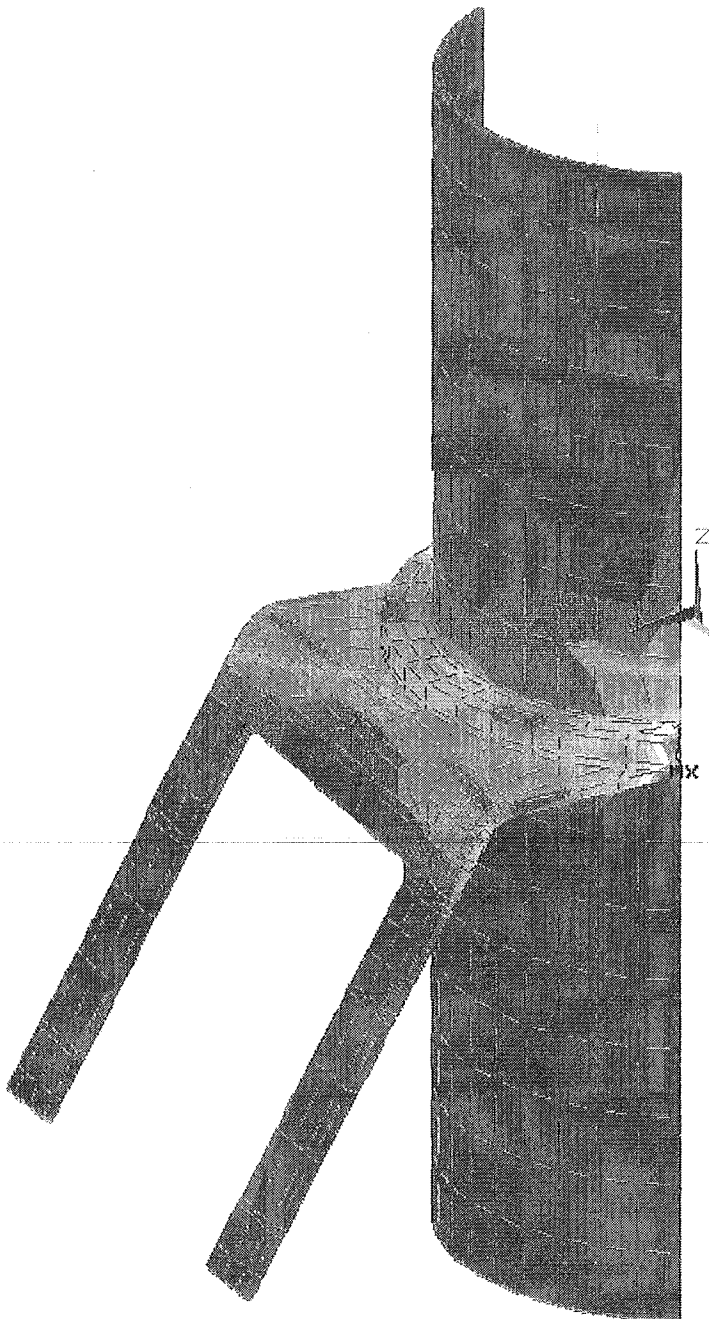
```

Figure 21

FLOWIND 17m UPGRADE ROOT JOINT - ITERATION #1

Upgrade Root Joint -  
Axial Moment Stress

1



```
ANSYS 5.0      18  
DEC  7 1993  
17:22:37  
PLOT NO.      2  
NODAL SOLUTION  
STEP=3  
SUB  =1  
TIME=3  
SEQV          (AVG)  
TOP  
DMX  =0.490E-03  
SMN  =0.169E-11  
SMX  =19.433  
SMXB=44.922  
0.169E-11  
2.159  
4.318  
6.478  
8.637  
10.796  
12.955  
15.115  
17.274  
19.433
```

Figure 22

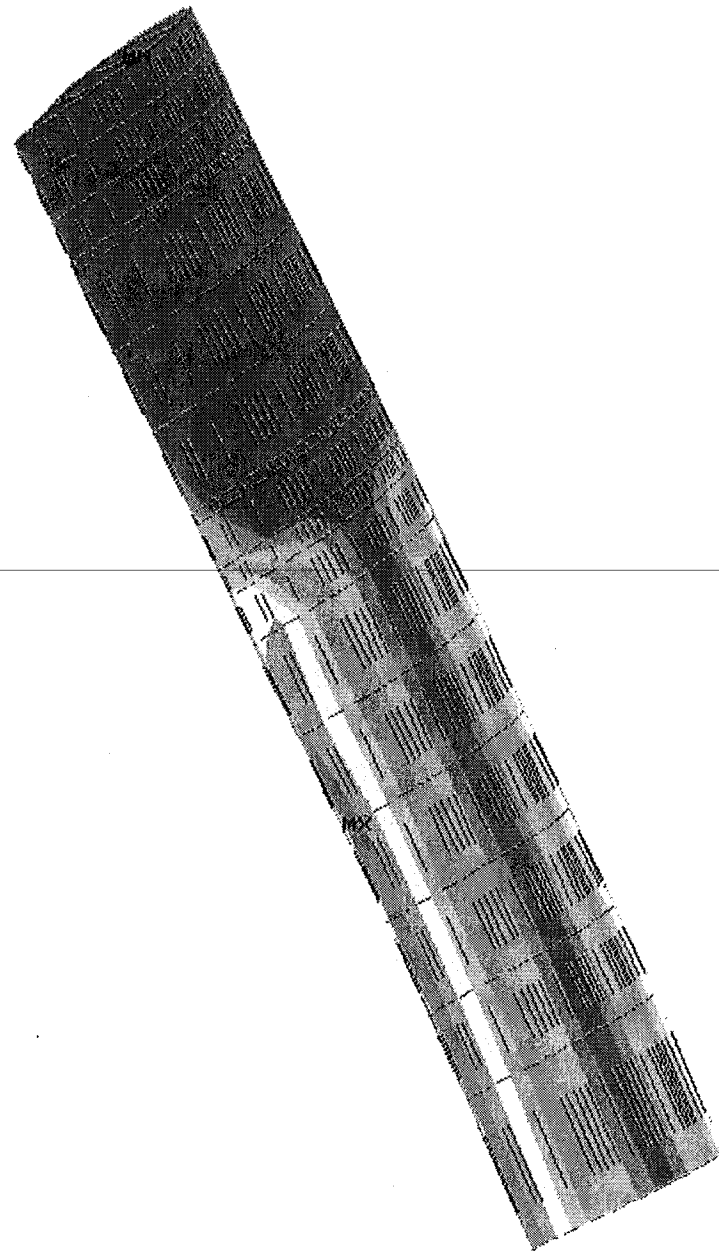
FLOWIND 17m UPGRADE ROOT JOINT - ITERATION #1

Upgrade Root Joint -  
Edgewise Moment Stress

```

ANSYS 5.0      18
DEC  7 1993
16:52:06
PLOT NO.      4
NODAL SOLUTION
STEP=3
SUB  =1
TIME=3
SEQV          (AVG)
TOP
LAYR=2
DMX  =0.512E-03
SMN  =0.007265
SMNB=0.007265
SMX  =15.224
SMXB=15.224
0.007265
1.698
3.389
5.08
6.77
8.461
10.152
11.843
13.534
15.224

```

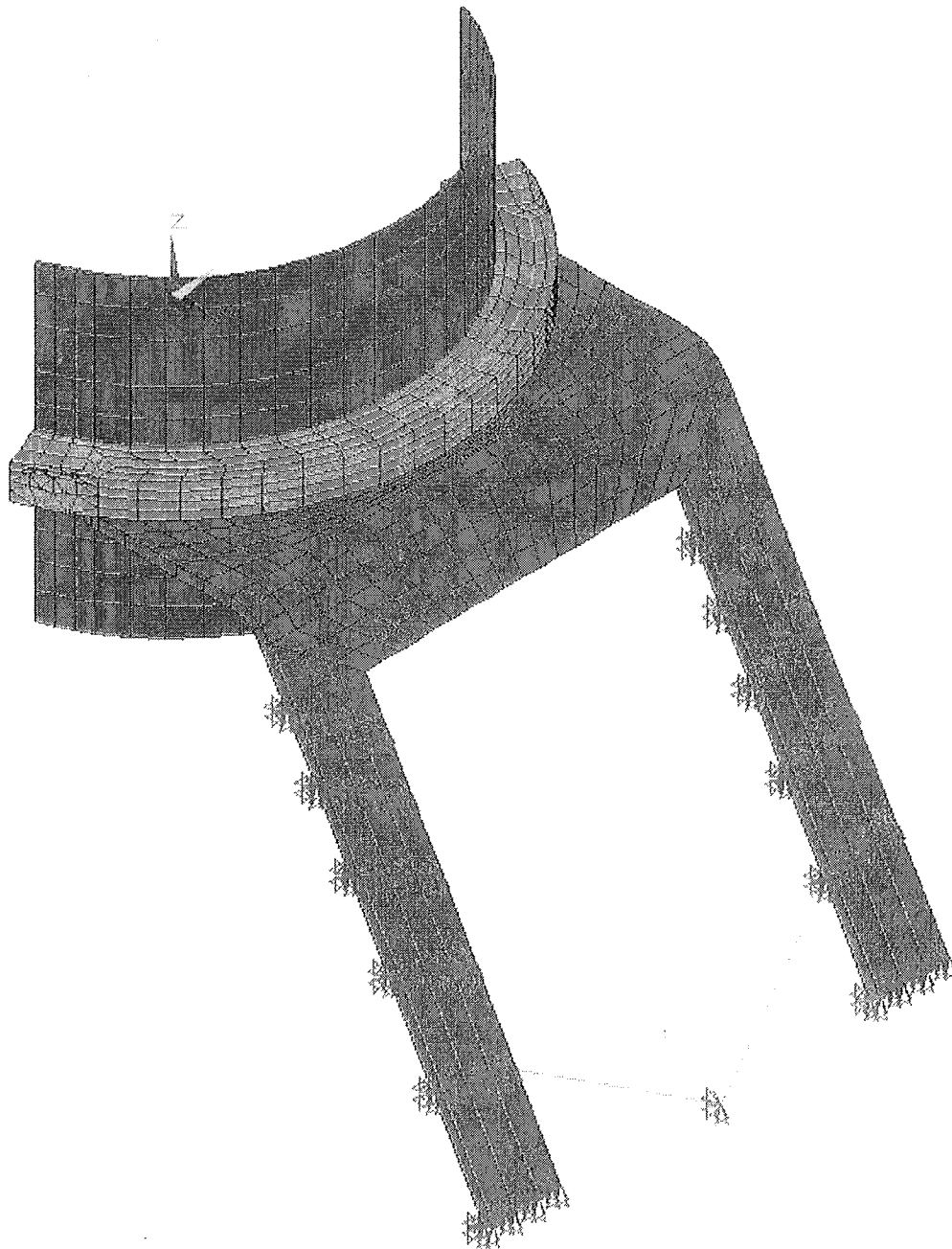


Upgrade Root Joint -  
Edgewise Moment Stress

FLOWIND 17m UPGRADE ROOT JOINT - ITERATION #1

Figure 23

ANSYS 5.0 A  
NOV 16 1994  
17:16:44  
ELEMENTS  
REAL\_NUM  
CE  
  
XV =1  
YV =-1  
ZV =1  
DIST=44.662  
XF =28.322  
ZF =-11.111  
VUP =Z  
CENTROID HIDDEN



Root Joint Bolt Interface Model, Iteration #0

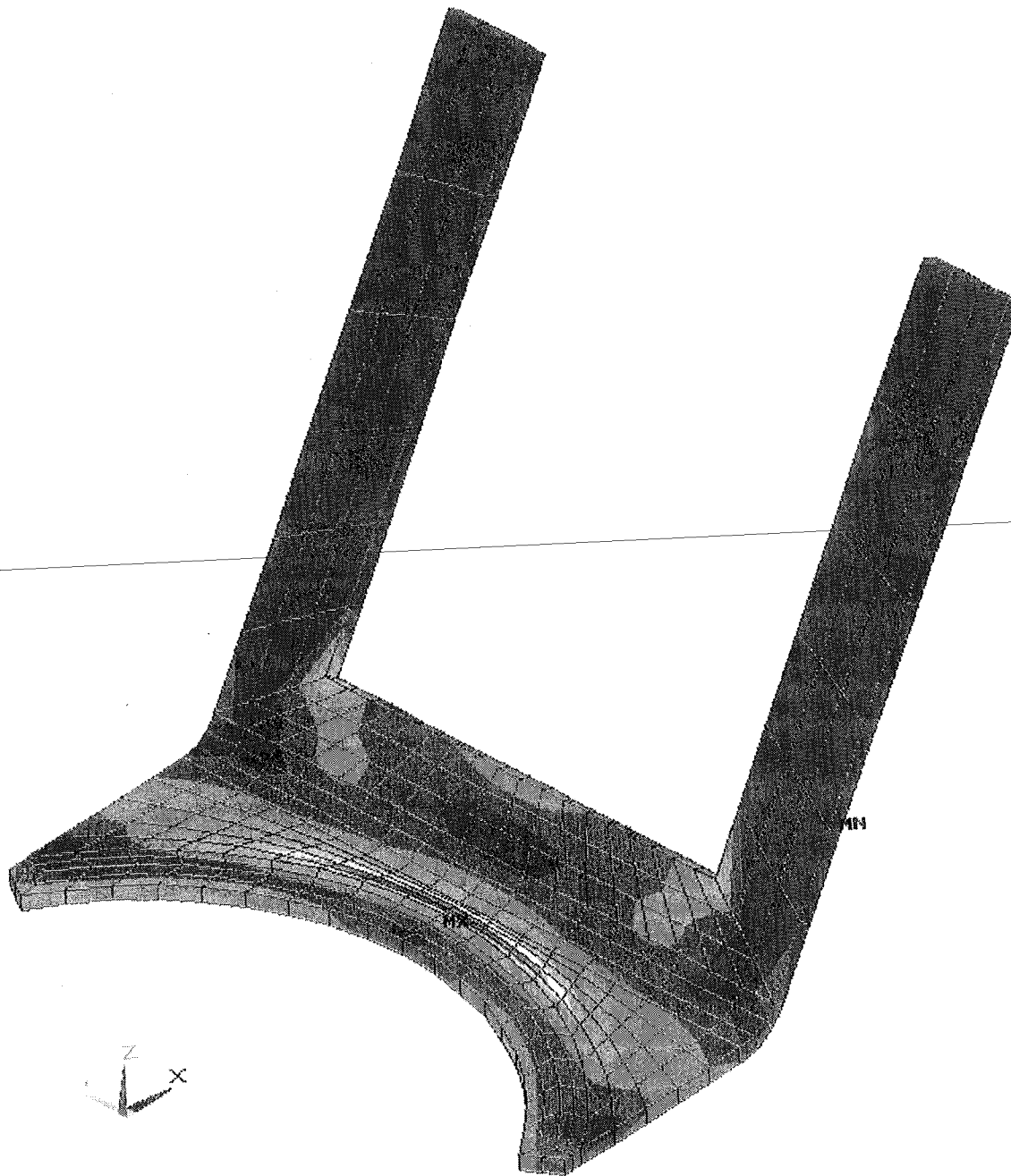
Figure 24



```

ANSYS 5.0 A
NOV 15 1994
16:50:26
PLOT NO. 2
NODAL SOLUTION
STEP=1
SUB =1
TIME=1
SEQV (AVG)
DMX =0.008272
SMN =0.503E-11
SMX =719.97
SMXB=965.774
0.503E-11
79.997
159.993
239.99
319.987
399.983
479.98
559.977
639.973
719.97

```



Root Bolt Model, Iteration #1, opposite side of flange

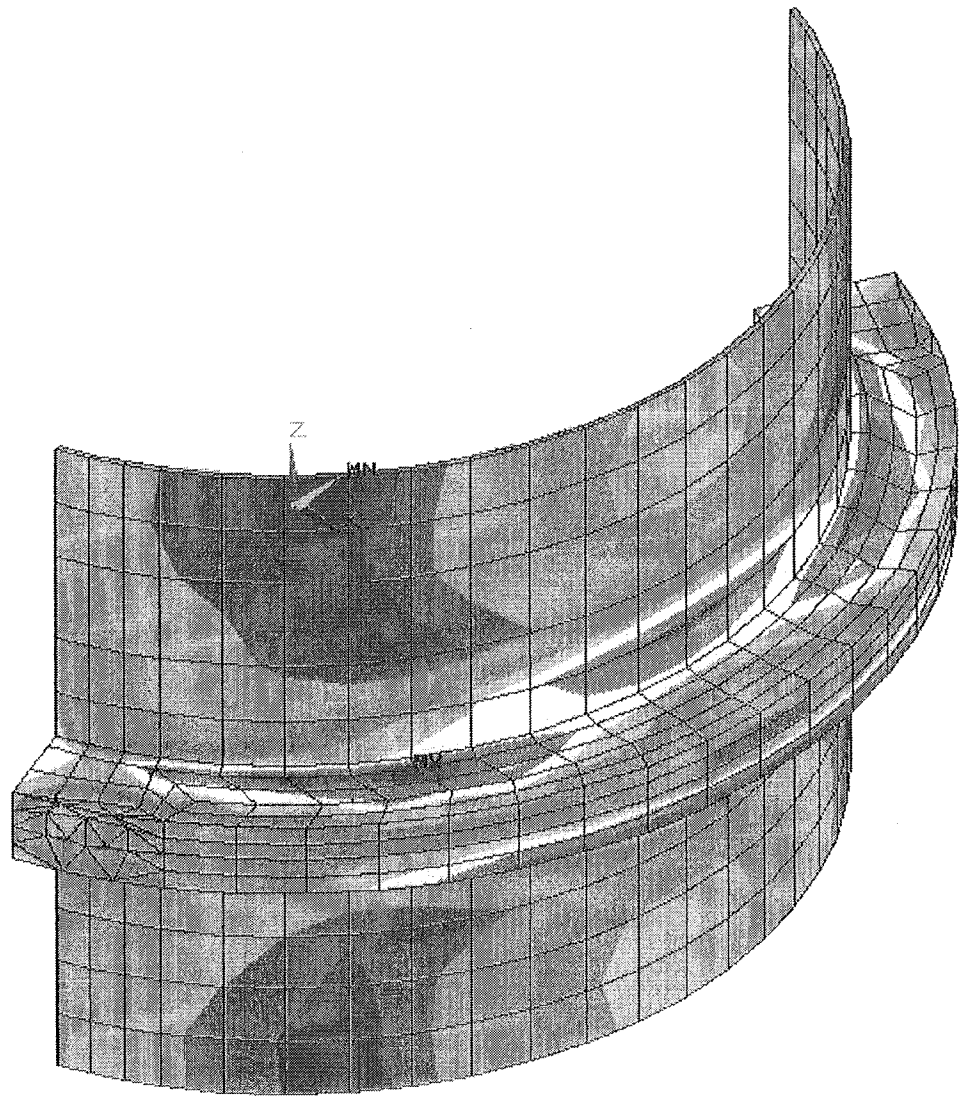
Root Bolt Model, Iteration  
Number 1, Flatwise Response

Figure 25

```

ANSYS 5.0 A
NOV 15 1994
16:49:32
PLOT NO. 1
NODAL SOLUTION
STEP=1
SUB =1
TIME=1
SEQV (AVG)
DMX =0.440E-03
SMN =4.379
SMX =260.705
SMXB=468.26
4.379
32.86
61.34
89.821
118.302
146.782
175.263
203.743
232.224
260.705

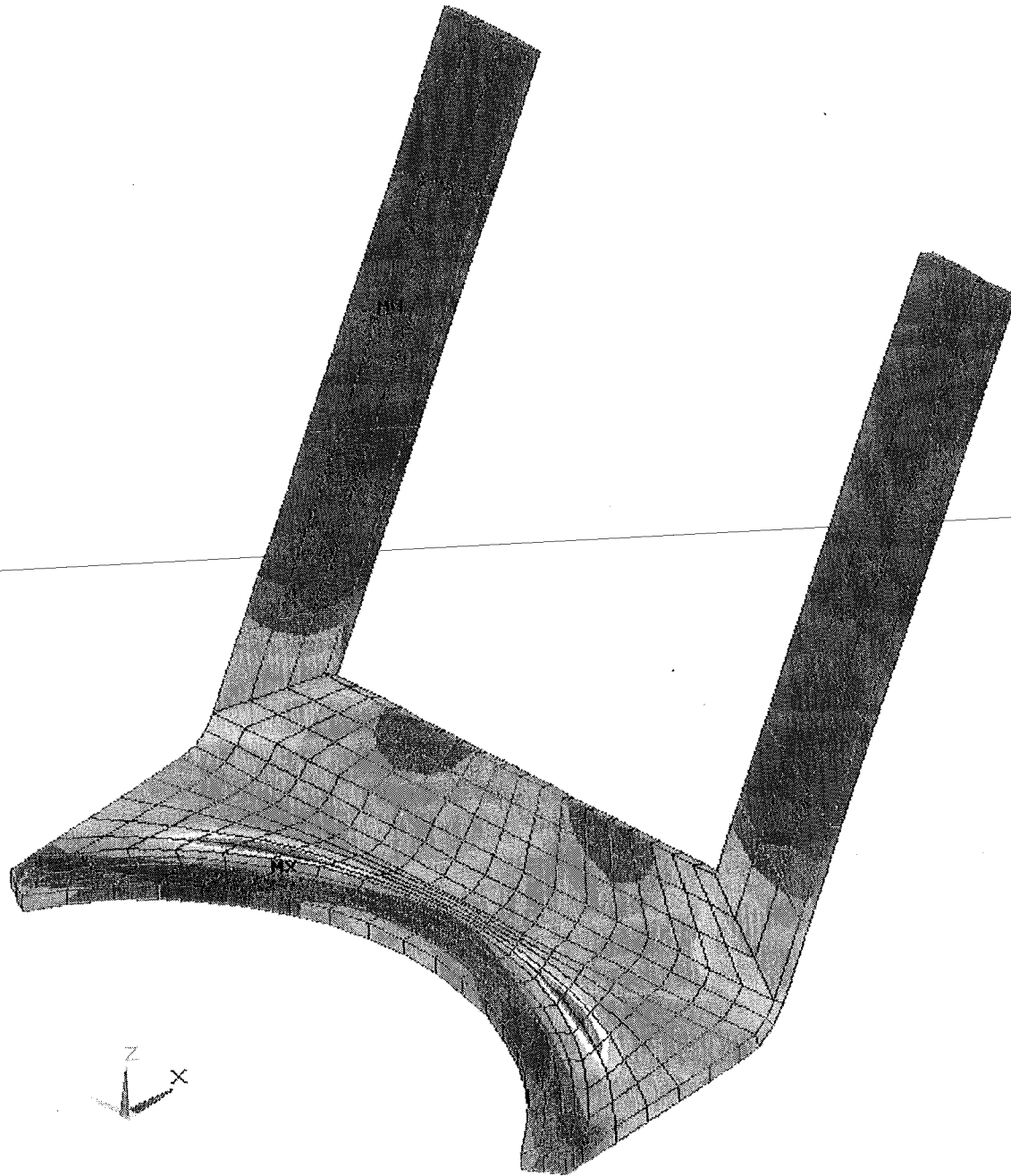
```



Root Bolt Model, Iteration #1, opposite side of flange

Figure 26

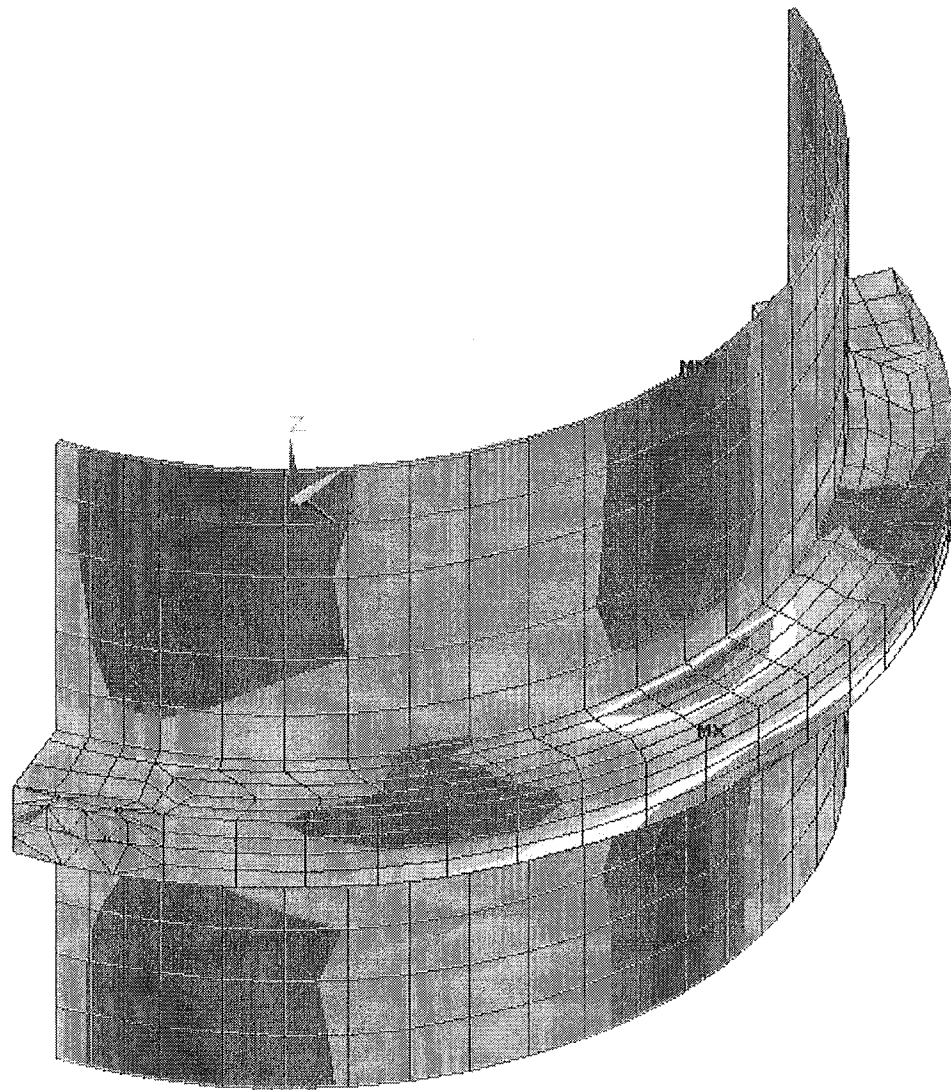
ANSYS 5.0 A  
 NOV 15 1994  
 16:51:30  
 PLOT NO. 3  
 NODAL SOLUTION  
 STEP=2  
 SUB =1  
 TIME=2  
 SEQV (AVG)  
 DMX =0.011884  
 SMN =0.593E-11  
 SMX =2018  
 SMXB=2670  
 0.593E-11  
 224.237  
 448.474  
 672.711  
 896.948  
 1121  
 1345  
 1570  
 1794  
 2018



Root Bolt Model, Iteration #1, opposite side of flange

Root Bolt Model, Iteration Number 1, Edgewise Response

Figure 27



```

ANSYS 5.0 A
NOV 15 1994
16:54:08
PLOT NO. 4
NODAL SOLUTION
STEP=2
SUB =1
TIME=2
SEQV (AVG)
OMX =0.646E-03
SMN =1.817
SMX =948.031
SMXB=1264
1.817
106.952
212.087
317.222
422.357
527.492
632.627
737.761
842.896
948.031

```

Figure 28

Root Bolt Model, Iteration #1, opposite side of flange

Root Bolt Model, Iteration Number 1, Edgewise Response

ANSYS 5.0 A  
NOV 16 1994  
16:39:10  
ELEMENTS  
REAL NUM

XV =0.57735  
YV =-0.57735  
ZV =0.57735  
DIST=116.815  
XF =130.159  
ZF =-0.003641  
VUP =Z  
PRECISE HIDDEN

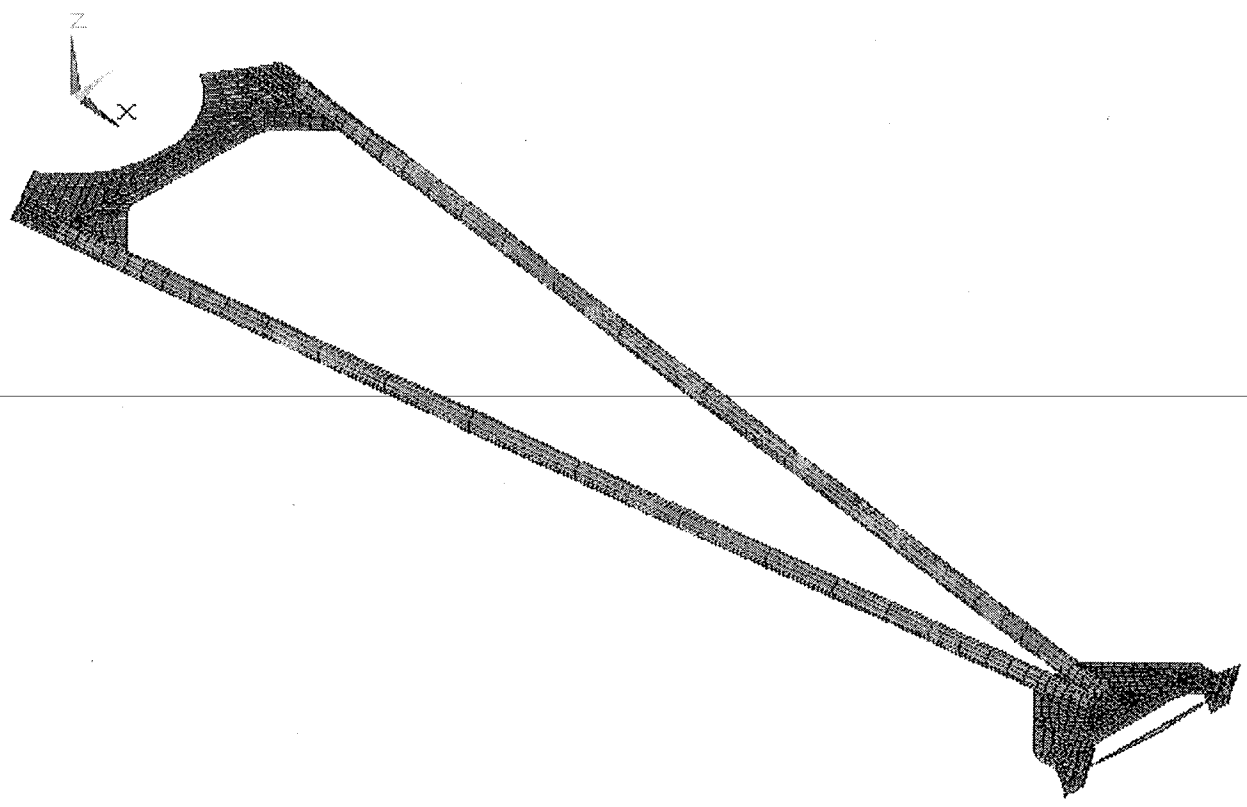
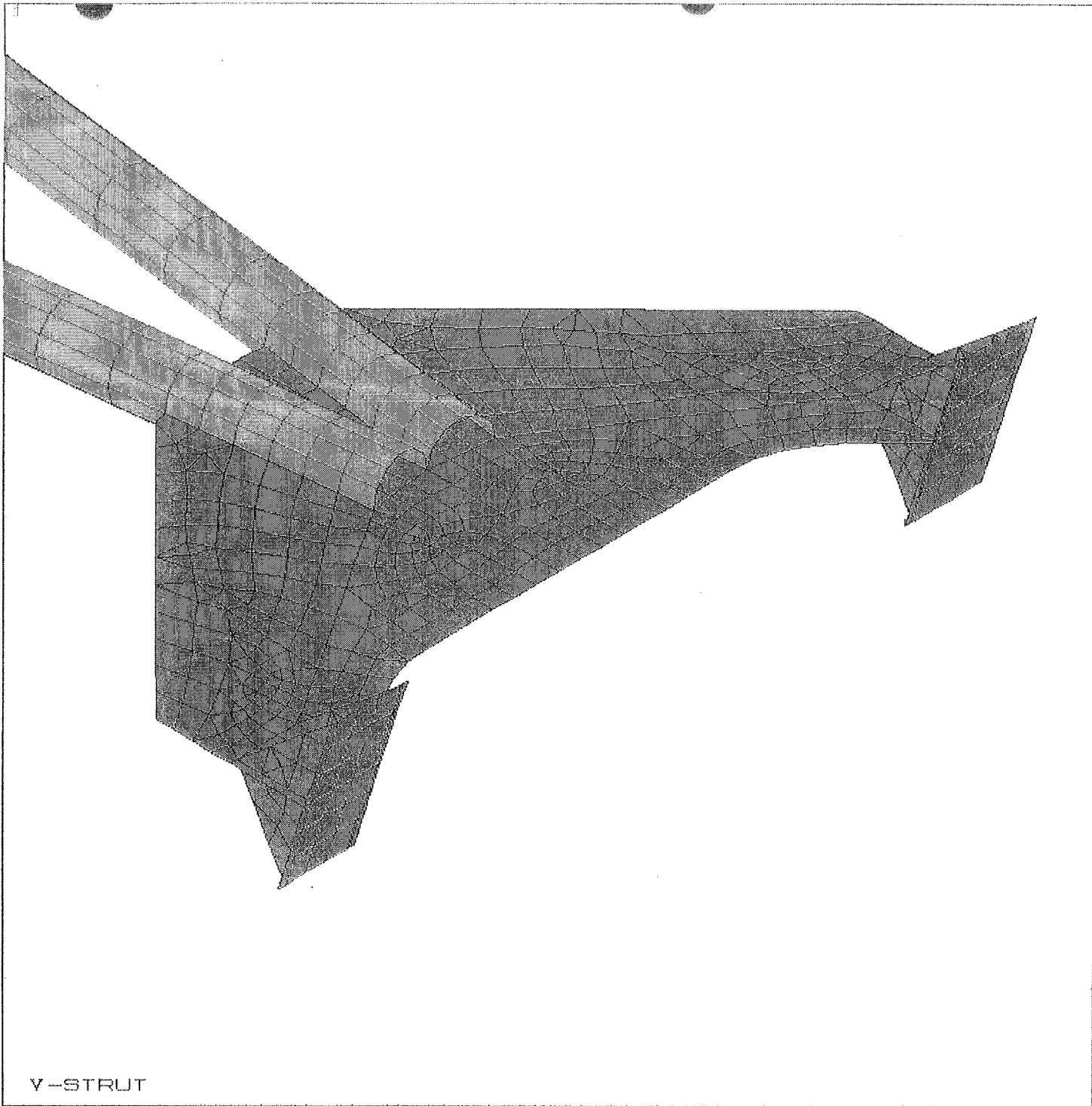


Figure 29

V-Strut Model




```
ANSYS 5.0   
JUN 16 1994  
18:10:49  
ELEMENTS  
REAL NUM  
  
XV =0.57735  
YV =-0.57735  
ZV =0.57735  
*DIST=20.361  
*XF =206.04  
*YF =37.07  
*ZF =-37.816  
YUP =Z  
PRECISE HIDDEN
```

Figure 30

V-STRUT

```

ANSYS 5.0
JUN 16 1994
19:43:24
PLOT NO. 3
NODAL SOLUTION
STEP=2
SUB =1
TIME=2
SEQV (AVG)
TOP
DMX =0.089389
SMN =0.547E-10
SMX =2225
SMXB=3186
0.547E-10
247.182
494.364
741.546
988.728
1236
1483
1730
1977
2225

```

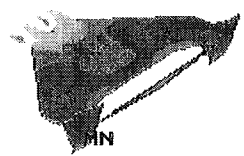
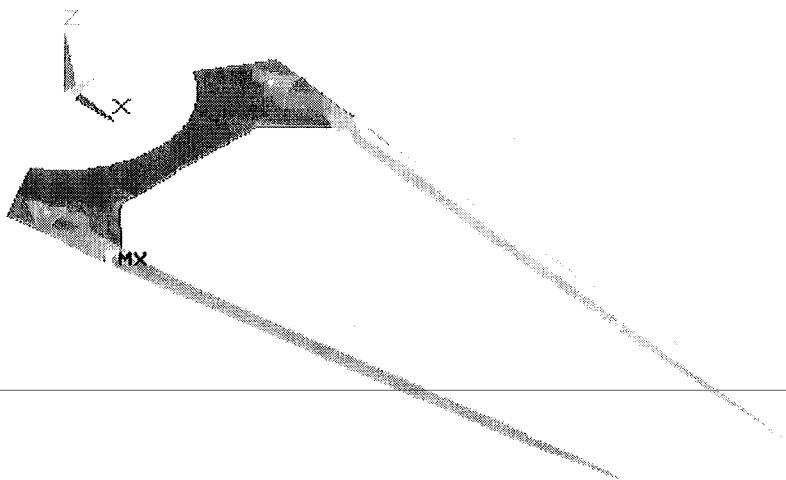


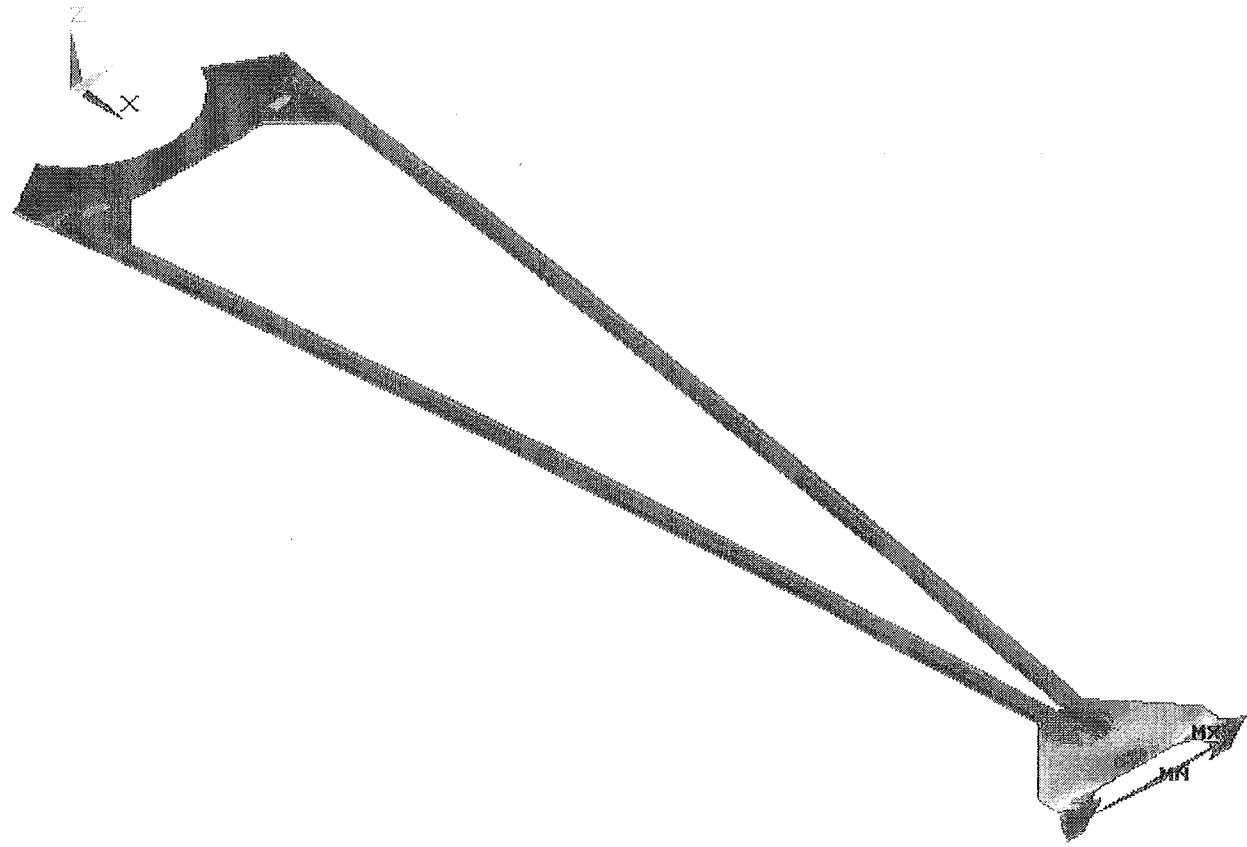
Figure 31

V-Strut - FY=1000, Edgewise force at blade

```

ANSYS 5.0.11,
JUN 16 1994
19:46:11
PLOT NO. 3
NODAL SOLUTION
STEP=5
SUB =1
TIME=5
SEQV (AVG)
TOP
DMX =1.625
SMN =0.213E-10
SMX =12346
SMXB=18171
0.213E-10
1372
2743
4115
5487
6859
8230
9602
10974
12346

```

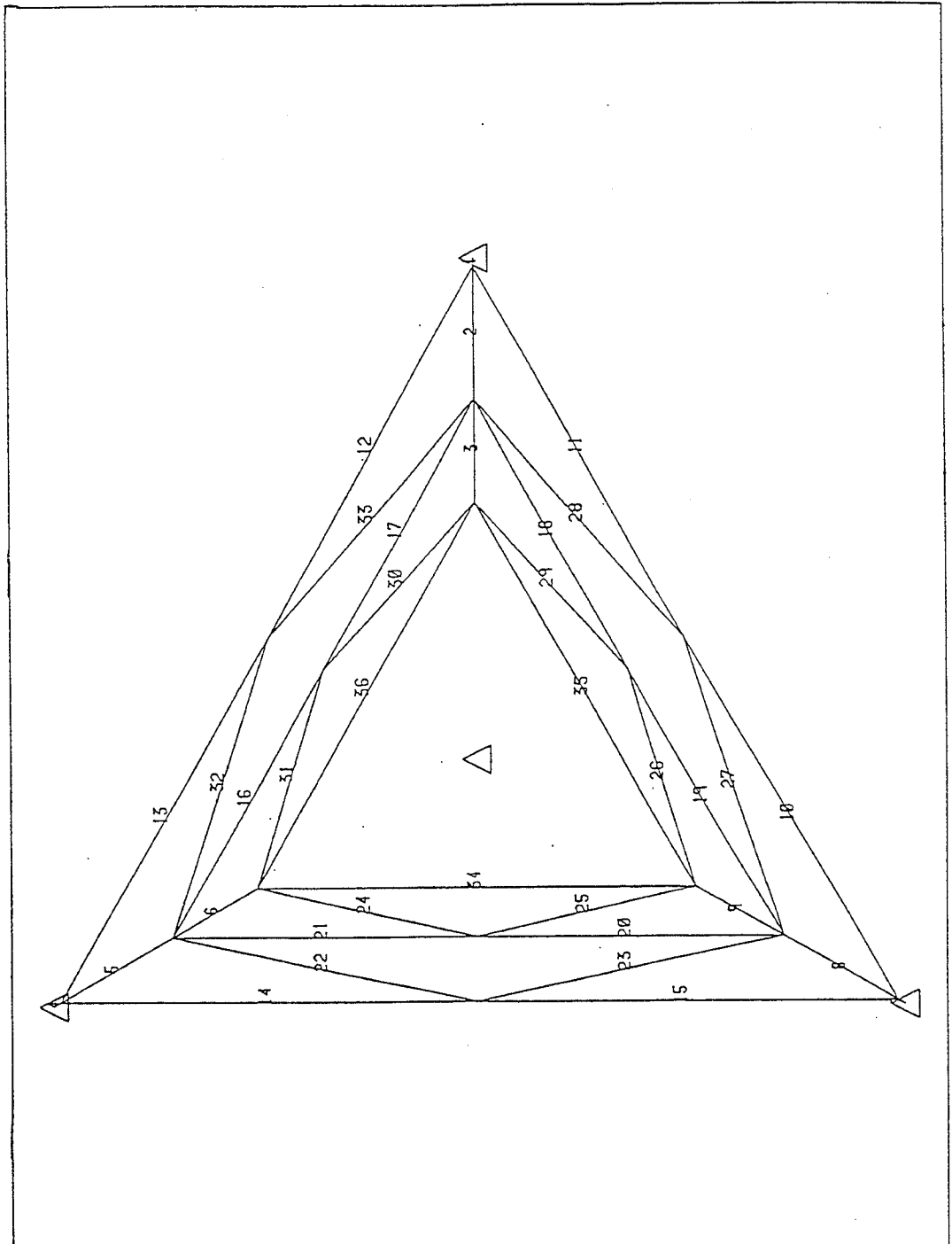


V-Strut - MY=10000, Flatwise moment at blade

Figure 32







Base Structure (pedestal model).

Figure 34

Guy Anchor Foundation.

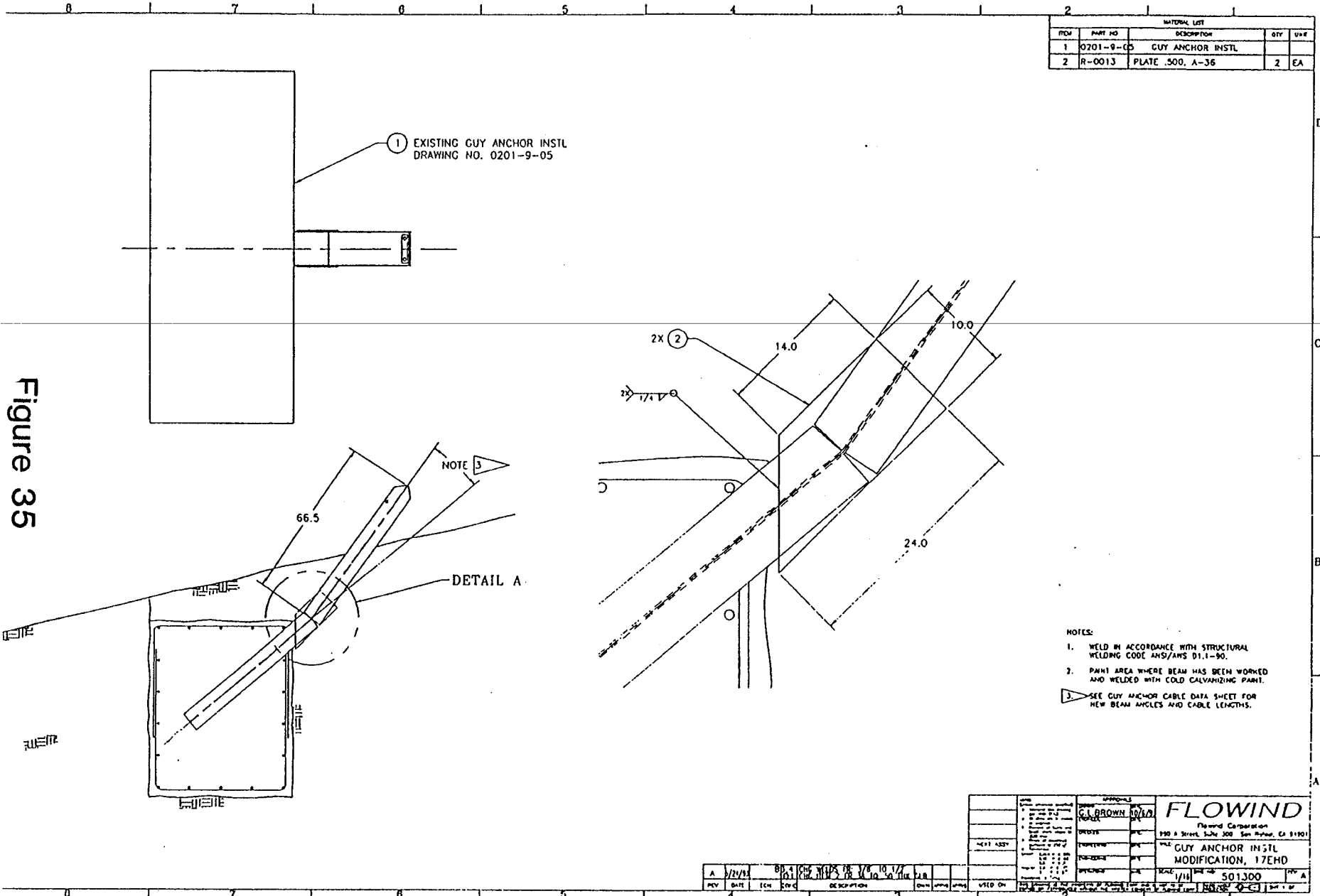
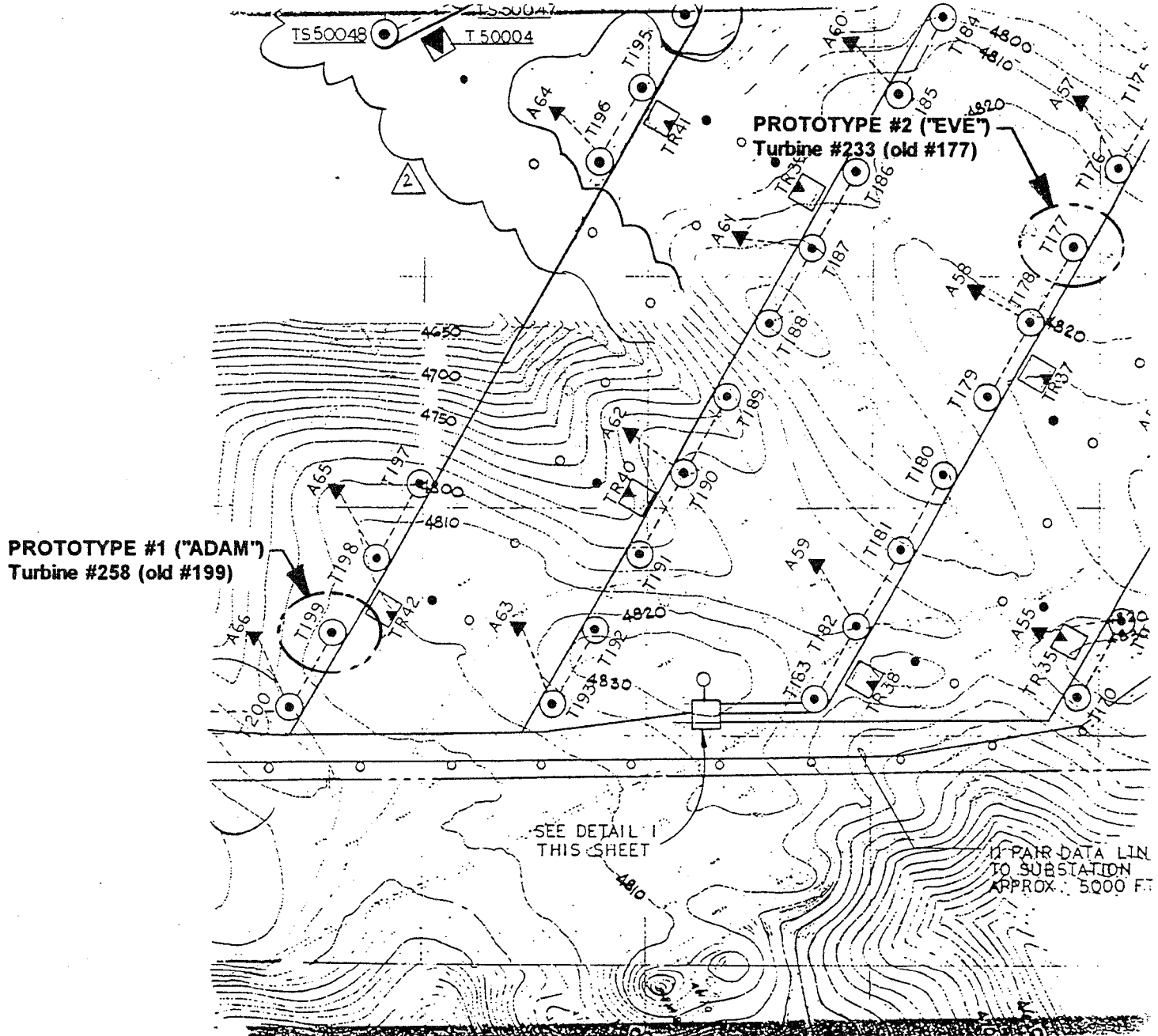


Figure 35

R1

"OLD" NUMBER TURBINES, TEHACHAPI



Test Site Layout.

Figure 36



BLADE #1				
URF1	Upper	blade @ root	flatwise bending	blade #1
URE1	Upper	blade @ root	edgewise bending	blade #1
USF1	Upper	blade @ strut	flatwise bending	blade #1
USE1	Upper	blade @ strut	edgewise bending	blade #1
EQF1	Equator	Blade @ equator	flatwise bending	blade #1
EQE1	Equator	Blade @ equator	edgewise bending	blade #1
LSF1	Lower	blade @ strut	flatwise bending	blade #1
LSE1	Lower	blade @ strut	edgewise bending	blade #1
LRF1	Lower	blade @ root	flatwise bending	blade #1
LRE1	Lower	blade @ root	edgewise bending	blade #1
LRA1	Lower	blade @ root	axial (tension)	blade #1

BLADE #2				
URF2	Upper	blade @ root	flatwise bending	blade #2
URE2	Upper	blade @ root	edgewise bending	blade #2
USF2	Upper	blade @ strut	flatwise bending	blade #2
USE2	Upper	blade @ strut	edgewise bending	blade #2
EQF2	Equator	Blade @ equator	flatwise bending	blade #2
EQE2	Equator	Blade @ equator	edgewise bending	blade #2
LSF2	Lower	blade @ strut	flatwise bending	blade #2
LSE2	Lower	blade @ strut	edgewise bending	blade #2
LRF2	Lower	blade @ root	flatwise bending	blade #2
LRE2	Lower	blade @ root	edgewise bending	blade #2
LRA2	Lower	blade @ root	axial (tension)	blade #2

BLADE #3				
LRA3	Lower	blade @ root	axial (tension)	blade #3
LSF3	Lower	blade @ strut	flatwise bending	blade #2

BLADE #1 MOUNTS (TUNING FORK)				
UMFW	Upper	blade mount	flatwise bending	
UMEW	Upper	blade mount	edgewise bending	
LMFW	Lower	blade mount	flatwise bending	
LMEW	Lower	blade mount	edgewise bending	
LMCB	Lower	blade mount	plate center @ inboard	bend
TERA	Trailing	edge of lower blade	mount @ inboard bending radius	
TEFI	Trailing	edge tuning fork	@ fillet of lower blade mount	
LEFI	Leading	edge tuning fork	@ fillet of lower blade mount	

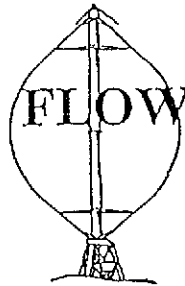
BLADE #1 MOUNTING "CLAM SHELL" - LOWER ONLY				
TEJO	Trailing	edge outboard plate	(lower ) @ root end joggle in plate	
LEJO	Leading	edge outboard plate	(lower ) @ root end joggle in plate	

TOWER				
TB00	Tower	bending 0 degrees	relative blade #1 (near eq node)	
TB90	Tower	bending 90 degrees	relative blade #1 (near eq node)	
TAX	Tower	axial stress	near lower root end	

Figure 38

STRUTS				
UAEW	Upper	arm (strut tube)	local	edgewise bending blade #1
UALE	Upper	strut arm leading edge		edgewise bending
UATE	Upper	strut arm trailing edge		edgewise bending
UAAX	Upper	arm (strut tube)	local	axial blade #1
USFW	Upper	strut: (both tubes)		avg flatwise bending blade #1
UALF	Upper	strut arm leading edge		flatwise bending
UATF	Upper	strut arm trailing edge		flatwise bending
URLA	Upper	tie rod @ leading edge		axial blade #1
URTA	Upper	tie rod @ trailing edge		axial blade #1
LAEW	Lower	arm (strut tube)	local	edgewise bending blade #1
LALE	Lower	strut arm leading edge		edgewise bending
LATE	Lower	strut arm trailing edge		edgewise bending
LAAX	Lower	arm (strut tube)	local	axial blade #1
LSFW	Lower	strut (both tubes)		avg flatwise bending blade #1
LALF	Lower	strut arm leading edge		flatwise bending
LATF	Lower	strut arm trailing edge		flatwise bending
LRLA	Lower	tie rod @ leading edge		axial blade #1
LRTA	Lower	tie rod @ trailing edge		axial blade #1
GUY CABLES				
G11A	Guy	cable lower turnbuckle #1		left cable of pair axial
G11B	Guy	cable lower turnbuckle #1		right cable of pair axial
G22A	Guy	cable lower turnbuckle #2		left cable of pair axial
G22B	Guy	cable lower turnbuckle #2		right cable of pair axial
G33A	Guy	cable lower turnbuckle #3		left cable of pair axial
G33B	Guy	cable lower turnbuckle #3		right cable of pair axial
DRIVE TRAIN				
LSTQ	Low	speed		shaft torque
HSTQ	High	speed		shaft torque
UPPER BEARING				
UBAX	Upper	bearing		acceleration x direction
UBAY	Upper	bearing		acceleration y direction
UBAZ	Upper	bearing		acceleration z direction
BASE STRUCTURE				
BSTQ	Base	structure		torque
GENERATOR				
GEN1		Generator temperature		phase 1
GEN2		Generator temperature		phase 2
GEN3		Generator temperature		phase 3
GEARBOX				
GBOX	Gearbox	lube		temp

Figure 39



# FLOWIND CORPORATION'S ADVANCED EHD SERIES VAWT

## 17 EHD TEST MATRIX

	Target Wind Speed														Test Priority	% Complete
	0	10	20	30	40	50	60	70	80	90	100	110	120			
Blade Bend Into Place only (assembly stress)	█														1	100%
Blade Bend Into Place + Gravity (assembly)	█														2	100%
Guy Cable & Mast Stresses (assembly)	█														3	100%
Turbine Modal Testing (Sandia)	█														4	100%
Turbine Baseline Losses	█														5	100%
Turbine Starting Transients	█	█	█	█	█	█	█	█	█	█					6	75%
Turbine Stopping Transients	█	█	█	█	█	█	█	█	█	█					7	75%
Turbine Brake System Performance	█	█	█	█	█	█	█	█	█	█					8	75%
Turbine Dynamic Response (uniced)	█	█	█	█	█	█	█	█	█	█					9	75%
Coast Down Tests			█	█	█	█	█	█	█	█					10	95%
Turbine Electrical Performance (clean)	█	█	█	█	█	█	█	█	█	█					11	75%
Turbine Electrical Performance (dirty)	█	█	█	█	█	█	█	█	█	█					12	75%
Turbine Electrical Performance (vg'd)	█	█	█	█	█	█	█	█	█	█					13	75%
Parked Stress (multiple orientation)	█	█	█	█	█	█	█	█	█	█	█	█	█	█	14	60%
Dynamically Balance Turbine	█	█	█	█	█	█	█	█	█	█					15	80%
Turbine Dynamic Response (iced)	█	█	█	█	█	█	█	█	█	█					16	0%
Wind Only Start From 0 rpm	█	█	█	█	█	█	█	█	█	█					17	80%
Prototype Turbine Wake Study/Analysis	█	█	█	█	█	█	█	█	█	█					18	0%
Rain Flow Study/Analysis (fatigue cycles)	█	█	█	█	█	█	█	█	█	█	█	█	█	█	19	40%
Test Bed Wind Shear Study/Analysis	█	█	█	█	█	█	█	█	█	█					20	50%
Two Speed Start to Operation (Low Speed)	█	█	█	█	█	█	█	█	█	█					21	0%
Two Speed Transition to High Speed	█	█	█	█	█	█	█	█	█	█					22	0%

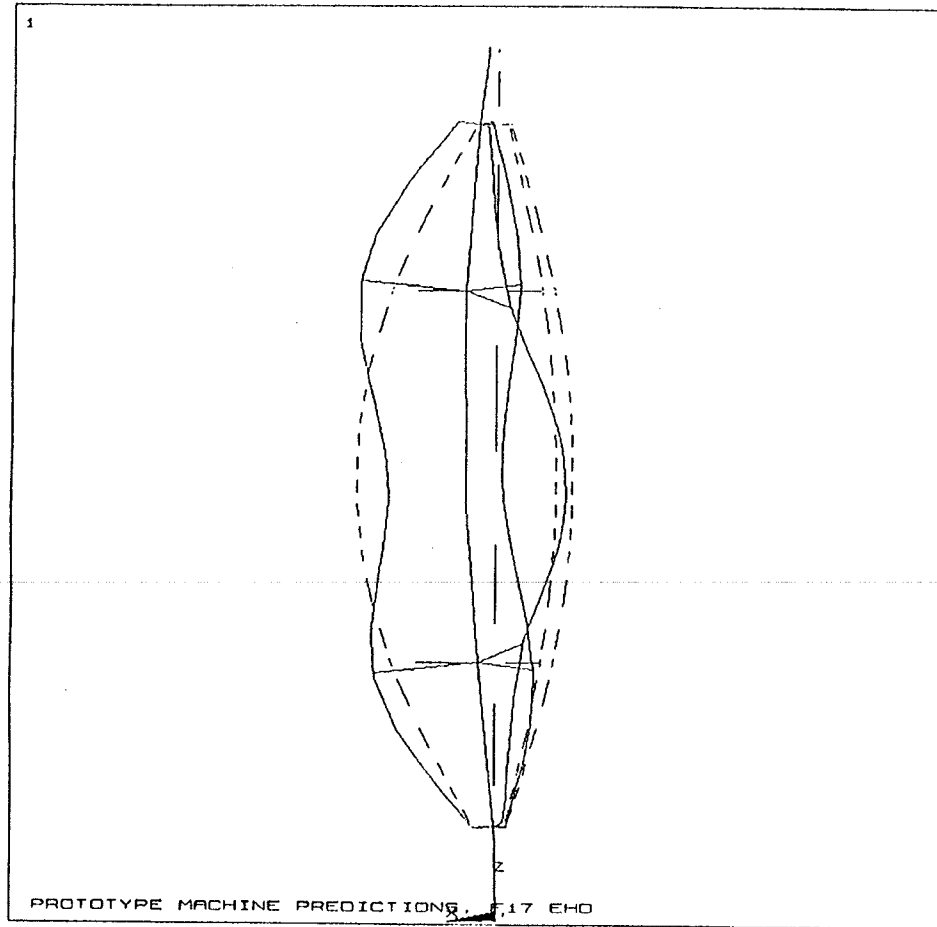
Figure 40

Data for analytical rainflow count is being accumulated as time series data.



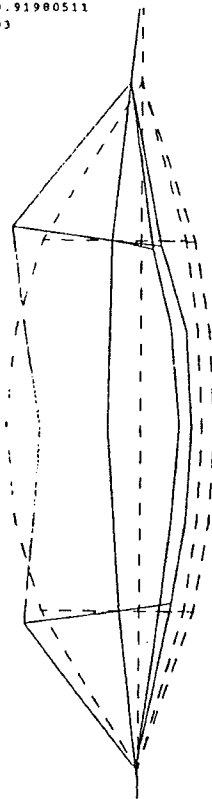
ANSYS 5.0 18  
JUN 7 1994  
12:04:16  
PLOT NO. 1  
DISPLACEMENT

FREQUENCY 1.09 Hz



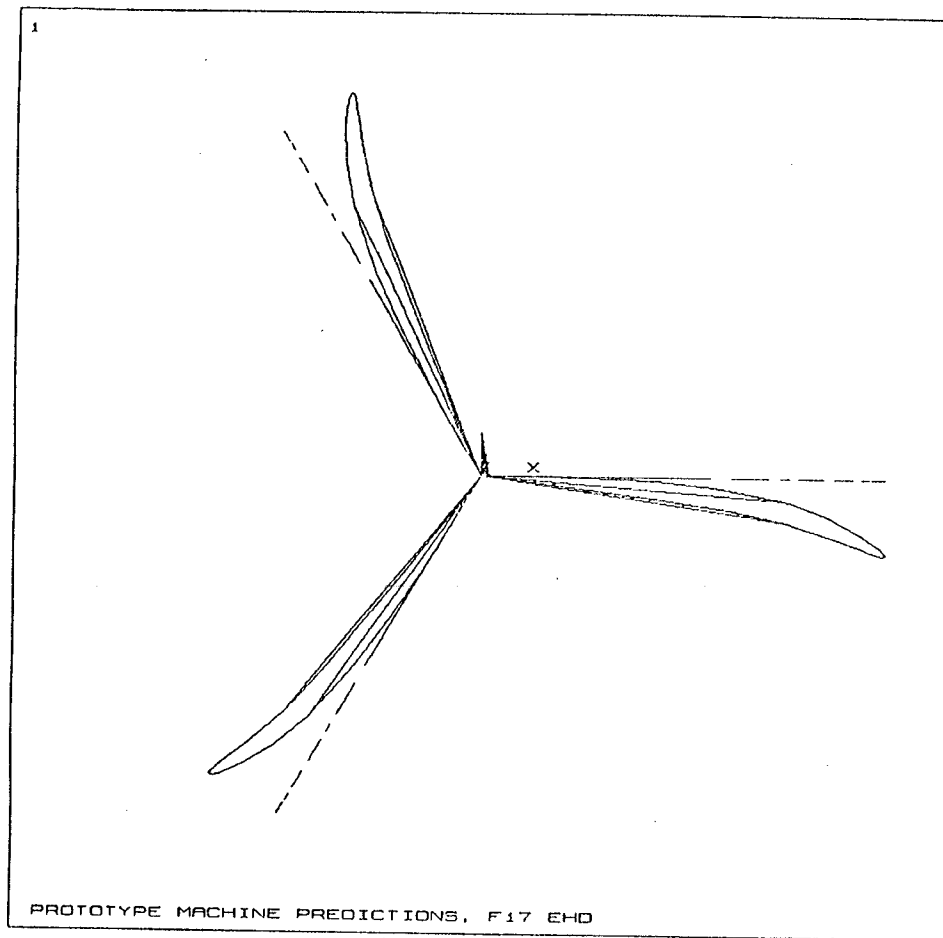
Predicted mode shape and frequency, 1st tower bending.

DEFORMATION: 28-1: STEPTOWER/1.07314  
MODE: 28      FREQ: 1.073143      DAMP: 0.91980511  
ACCELERATION - MAX MIN: 0.00E+00 MAX: 1.64E-03  
FRAME OF REF: PART



Measured mode shape and frequency, 1st tower bending.

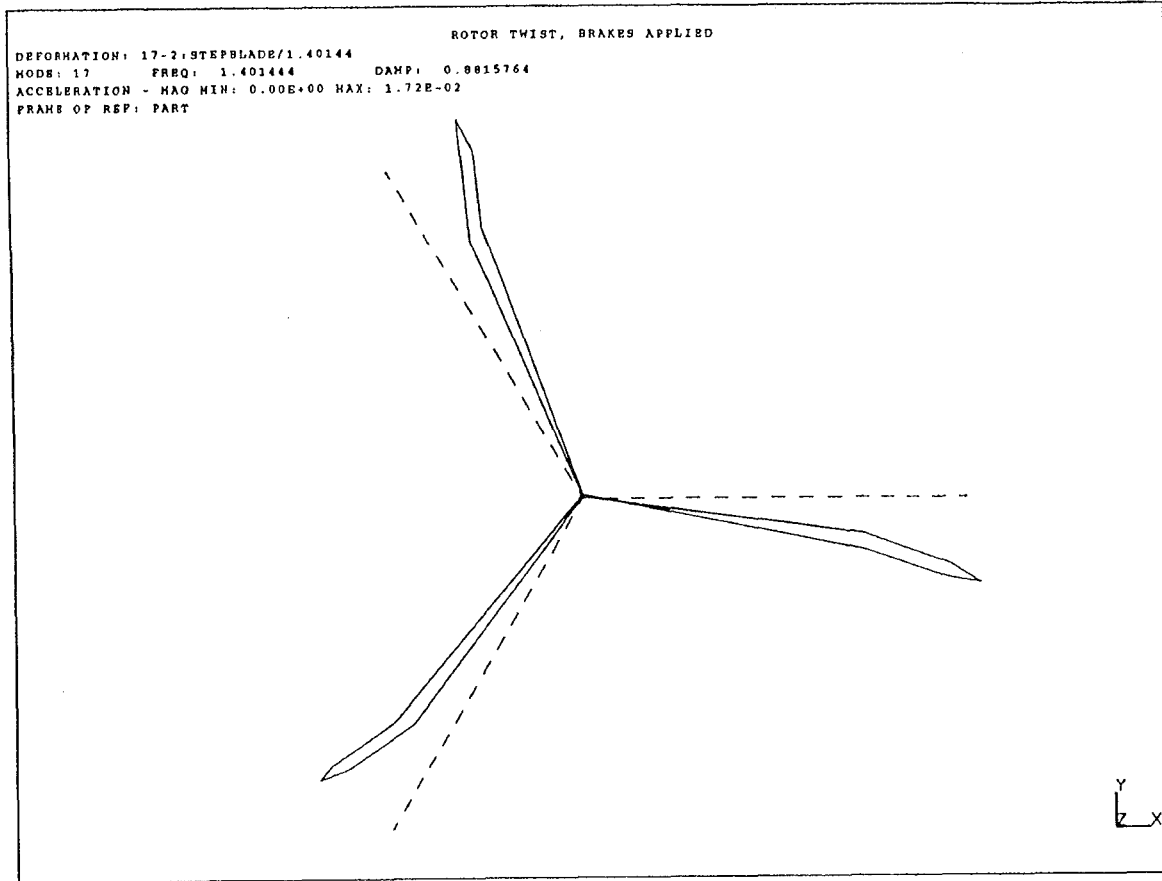
Figure 43



ANSYS 5.0 18  
JUN 7 1994  
11:56:08  
PLOT NO. 1  
DISPLACEMENT

FREQUENCY 1.47 Hz

Predicted mode shape and frequency, 1st propeller, brakes applied.

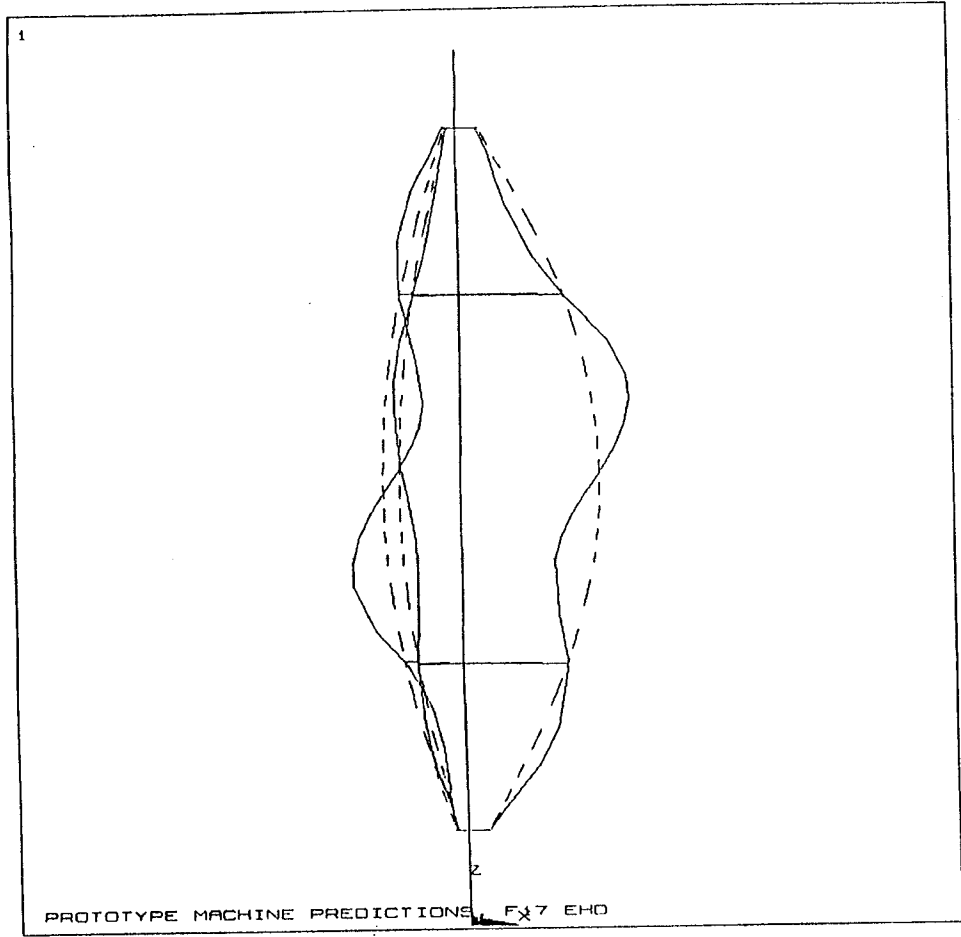


Measured mode shape and frequency, 1st propeller, brakes applied.

Figure 44

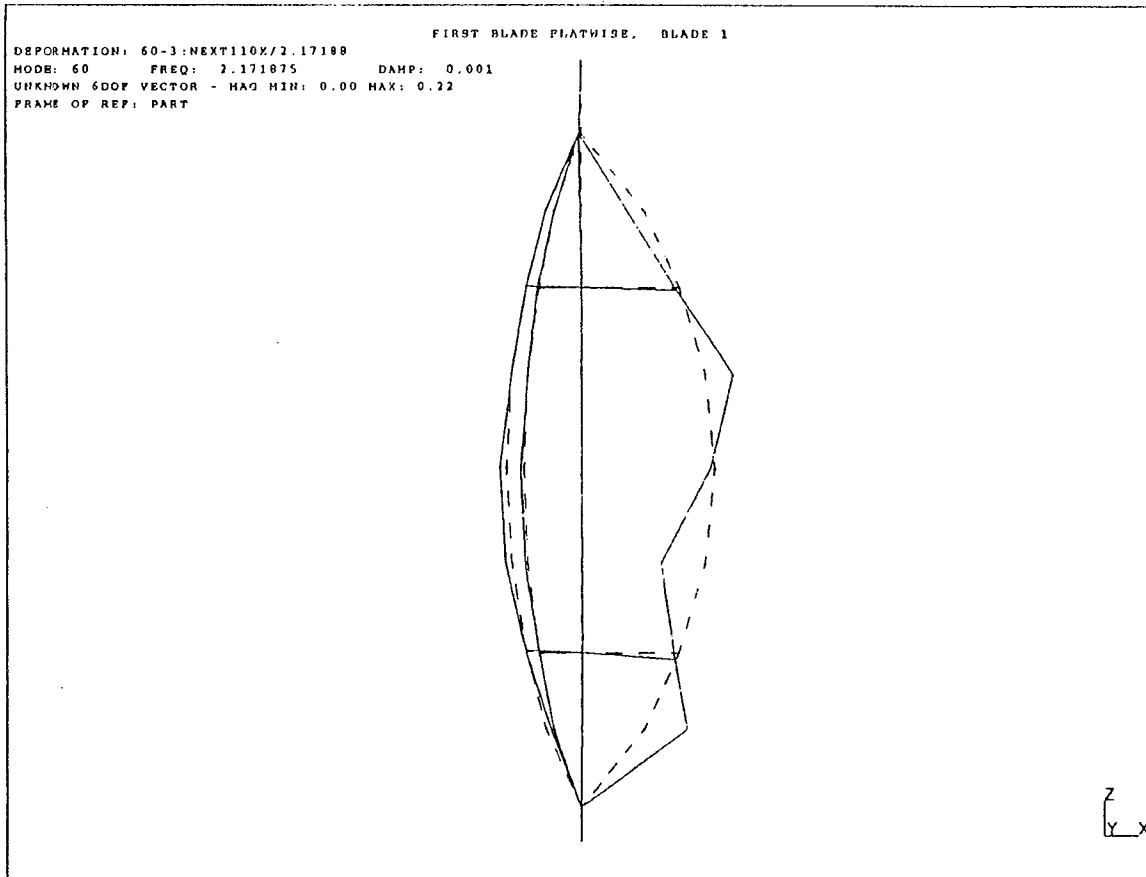
ANSYS 5.0 16  
JUN 7 1994  
12:01:04  
PLOT NO. 1  
DISPLACEMENT

**FREQUENCY 2.40 Hz**



Predicted mode shape and frequency, 1st flatwise blade asymmetric.

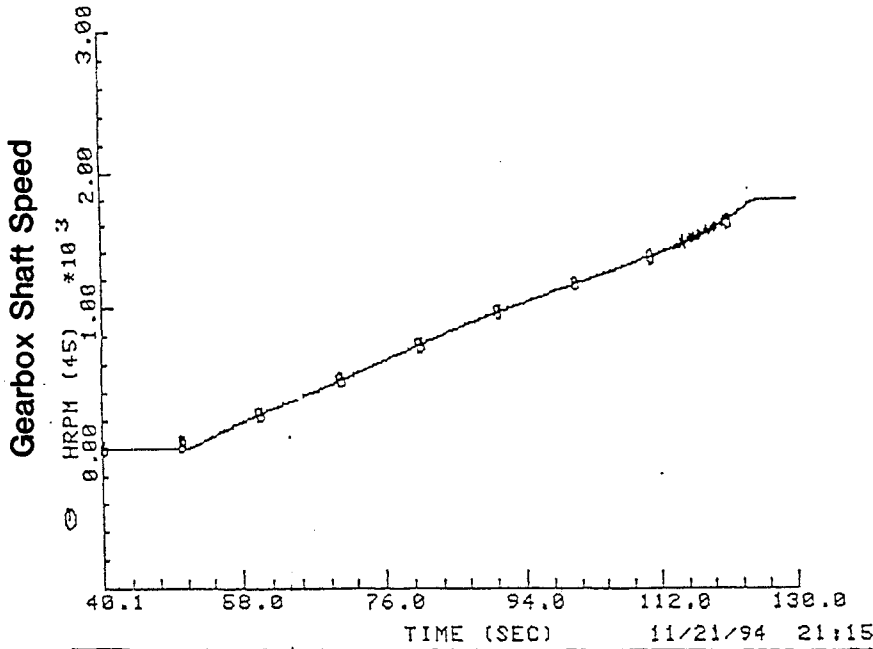
Figure 45



Measured mode shape and frequency, 1st flatwise blade, asymmetric.

Figure 46

FW1121942058 11/21/94 FW 20:59 Sample Rate = 59.999 Hz  
 45(HRPM) avg=881.984 std=577.1  
 STARTUP SMALL DRY SHAFT SMPH



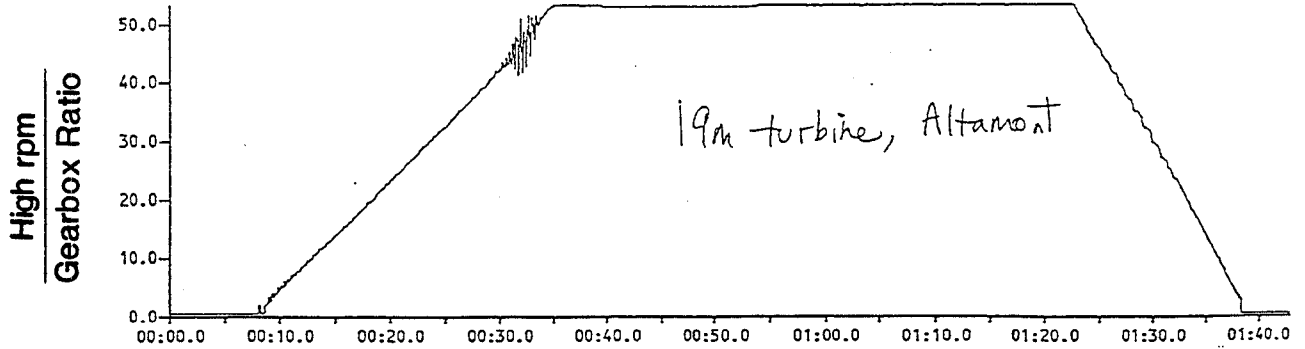
Note different time scales but similar y-axis scale

17m EHD  
 with small drive shaft.

*NORMAL SINGLE BRAKE STOP (POWER X DUCER*

FWT02 Fri May 21, 1993 14:13:50 no ctrlr power pickup  
 T1 Fast Tach - Fwind; From: 00:00.0, To: 01:43.2; Min: 0.0 at 00:00.1; Max: 53.3 at 00:35.0

*CONNECTED)*

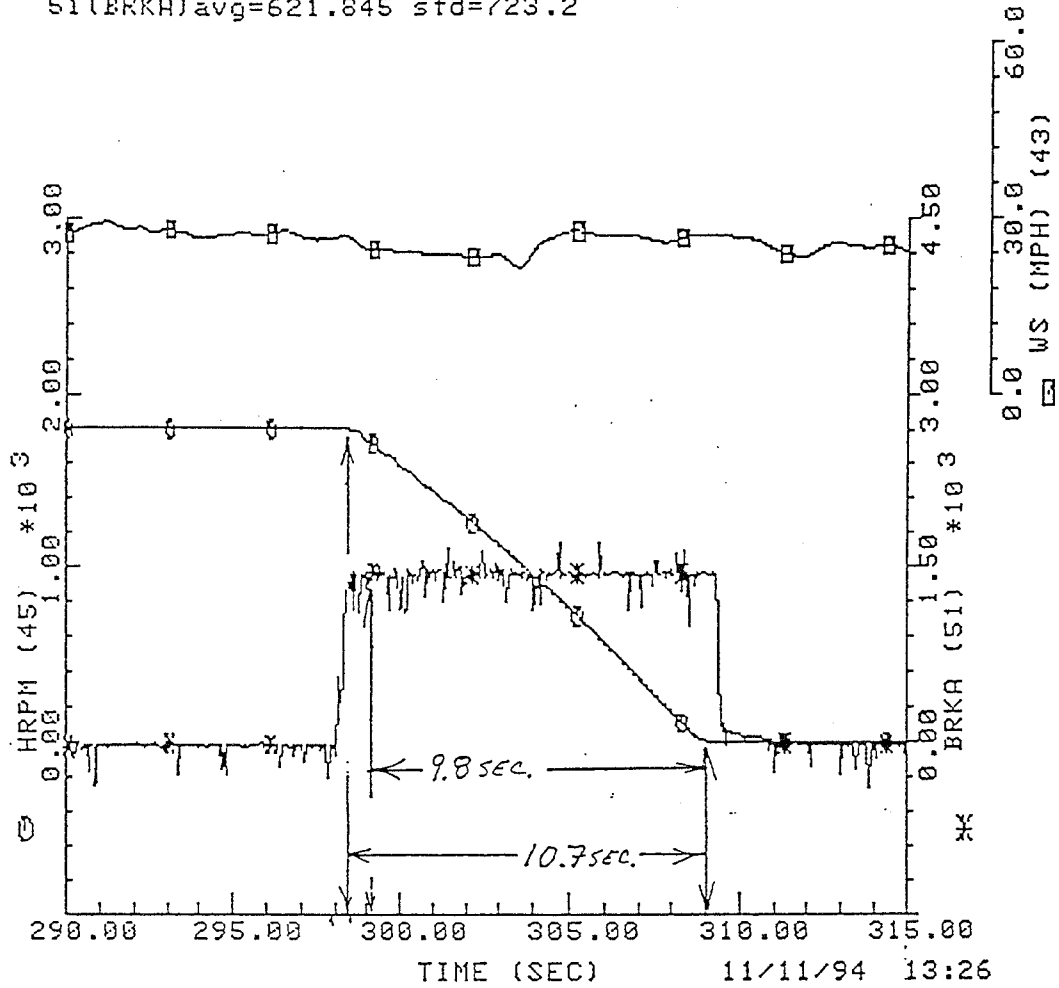


19m turbine, Altamont

Time Series, FW1121942058, Start Up Small Drive Shaft vs 19m Start Up.

Figure 47

FW0617941434 06/17/94 FW 14:34 Sample Rate = 20.000 Hz  
 43(WSEQ)avg=26.0580 std=1.650 45(HRPM)avg=1016.60 std=760.8  
 51(BRKA)avg=621.845 std=723.2



PRESS RISE .6 SEC.

Time Series, FW0617941423 (stope record).

Figure 48





# FLOWIND CORPORATION'S ADVANCED EHD SERIES VAWT MEASURED LOADS

Steady State Response Summary						
Test: 0902 1901						
Condition: 40 mph wind, V-struts; 58.5 rpm ( 0 - 500 sec )						
CHANNEL	UNITS	Q rpm offset	Operating			
			mean level	RMS level	min	max
WSEQ	mph	0	40.25	2.17	34.02	46.26
KW	kw	0	277	12.4	224.6	311.9
HRPM	rpm	0	1822.1	1.33	1817	1828
ACCX	g	0	0	0.422	-1.29	1.51
ACCY	g	0	0	0.404	-1.08	1.2
G11A	lbf	-943	-541	1956	-5710	4214
G22A	lbf	-4508	-2085	1776	-6902	3184
G33A	lbf	-1305	2871	1690	-1910	7940
TEJO	psi	-1084	6338	793	3649	8307
TEFI	psi	-443	-16476	1064	-18392	-14097
TB00	psi	610	-475	2062	-5574	4321
TB90	psi	322	270	1975	-5196	4633
URF1	psi	287	637	142	225	1010
LRF1	psi	165	36	100.1	-308	334
URE1	psi	-1325	-556	213	-1072	18
LRE1	psi	2683	-1057	190	-1574	-498
LSTF	psi	-6869	3447	640	1869	4974
LSTA	psi	-12444	-3092	690	-5025	-1076
LSSM	psi	20770	-2090	839	-4271	229
LSLE	psi	8954	-2962	967	-5911	40
USSM	psi	14469	2353	556	541	4021
USTF	psi	3853	-2080	606	-4349	-384
USTA	psi	1871	-1936	1261	-5693	2099
USLE	psi	-9261	-2578	1067	-5889	1248

Figure 49



# FLOWIND CORPORATION'S ADVANCED EHD SERIES VAWT

## Time History, TB00 (Mast Midspan Bending)

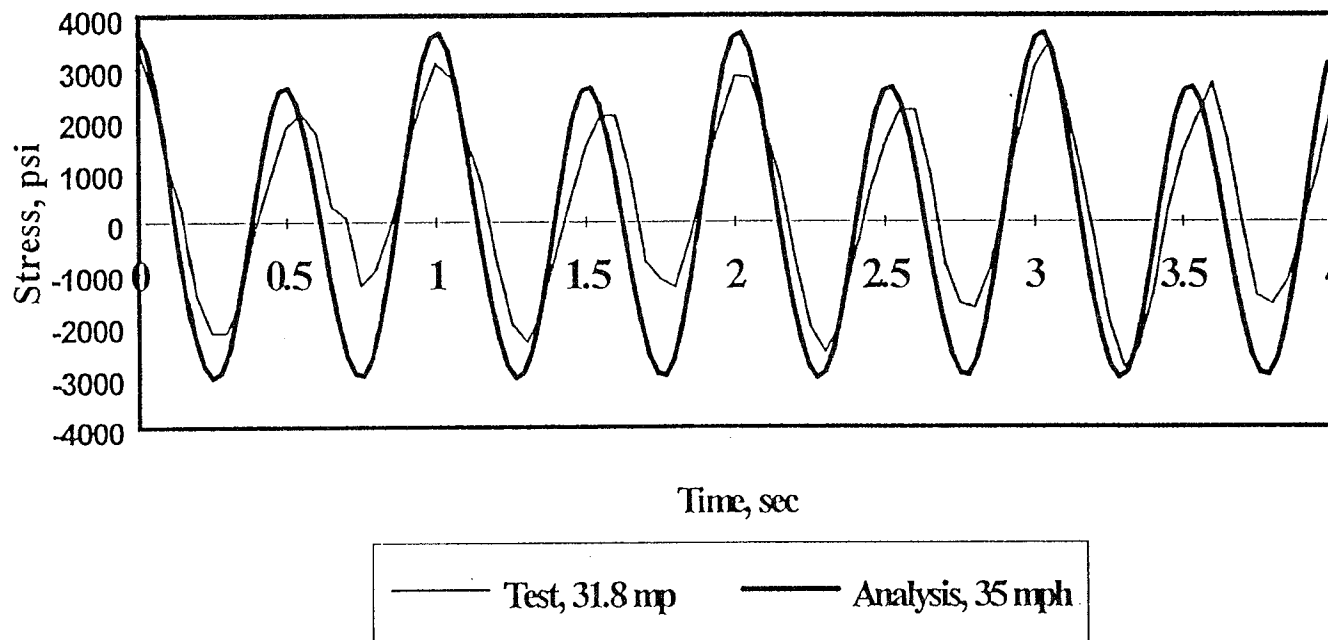
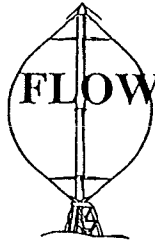


Figure 50



# FLOWIND CORPORATION'S ADVANCED EHD SERIES VAWT

Frequency Spectrum, TB00

(Mast Midspan Bending)

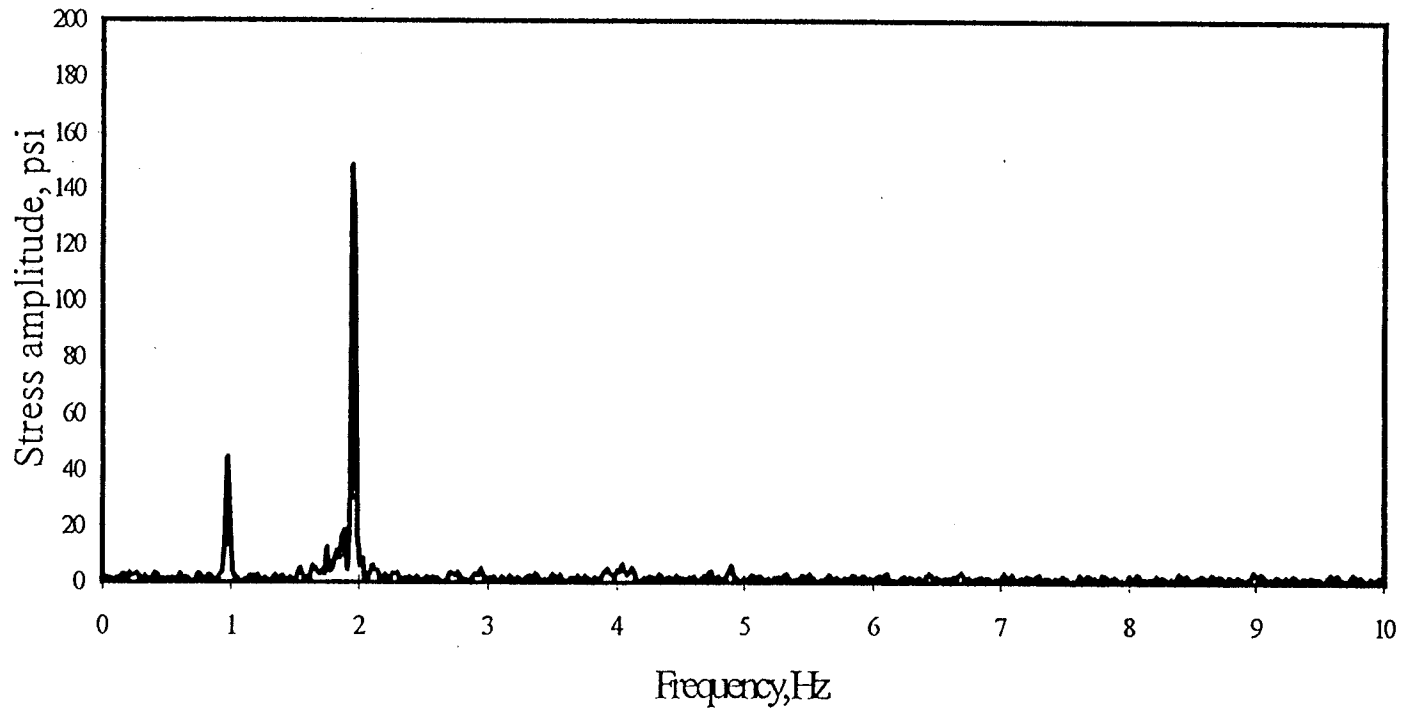


Figure 51



# FLOWIND CORPORATION'S ADVANCED EHD SERIES VAWT

## LOADS CORRELATION

### PRE-TENSIONED STRUTS, 40 mph wind speed

● ROD TENSION	TEST	ANALYSIS
Dynamic RMS	9.30ksi	9.66 ksi
Dynamic Amplitude	16.50	17.20
Crest Factor	1.77	1.78

● FLATWISE BENDING		
Dynamic RMS	1.16 ksi	0.85 ksi
Dynamic Amplitude	2.50	2.11
Crest Factor	2.16	2.48

Figure 52



# FLOWIND CORPORATION'S ADVANCED EHD SERIES VAWT

## LOADS CORRELATION

### ● BLADE STRESS NEAR STRUT, 28 mph wind speed \*

	TEST	ANALYSIS
Flatwise RMS	0.21 ksi	0.32 ksi
Edgewise RMS	0.40	0.29

### ● MAST STRESS, 28 mph wind speed \*\*

	TEST	ANALYSIS
Dynamic RMS	1.11 ksi	1.73 ksi

\* Data comparison is rough – levels are too low for good test resolution

\*\* Analysis response is substantially higher, indicating more damping in actual operation than expected.



# FLOWIND CORPORATION'S ADVANCED EHD SERIES VAWT

Dynamic RMS value, LSTA  
(Lower Strut Trailing Tube Axial)

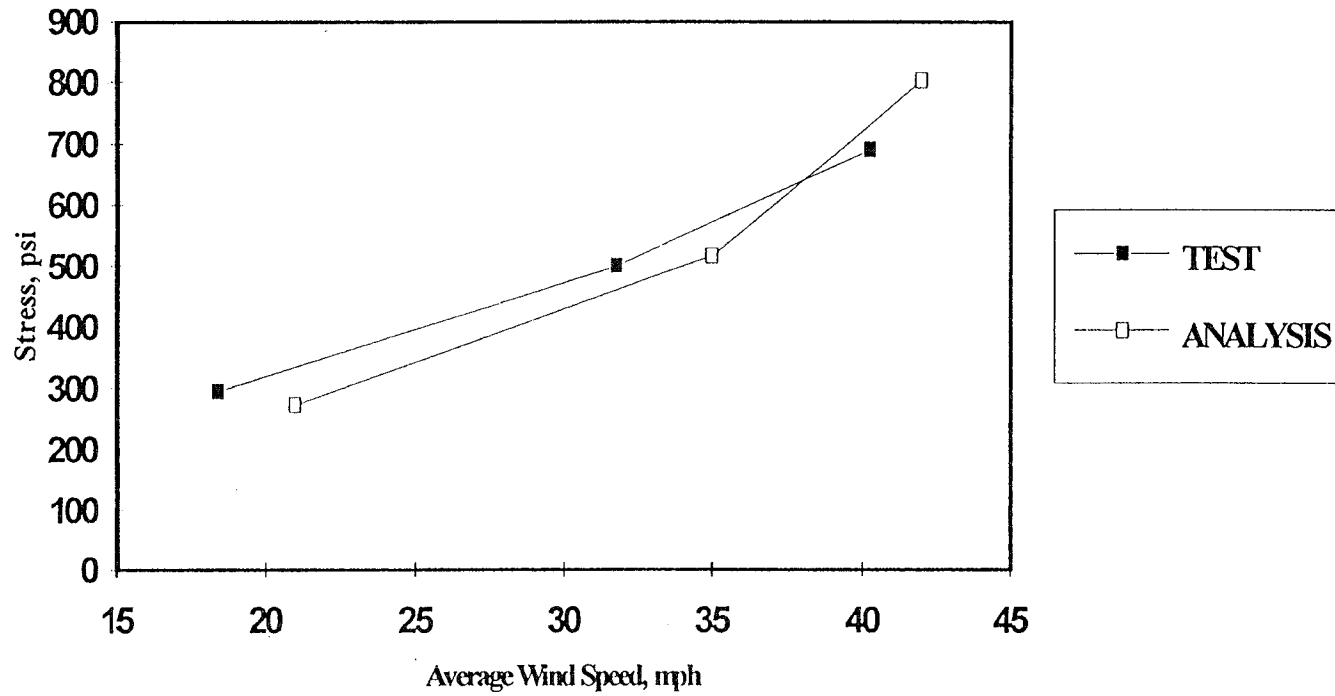
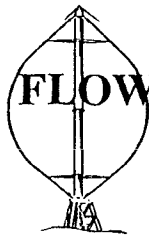


Figure 54



# FLOWIND CORPORATION'S ADVANCED EHD SERIES VAWT

Dynamic RMS value, LRE1  
(Lower Root Blade Edgewise Bending)

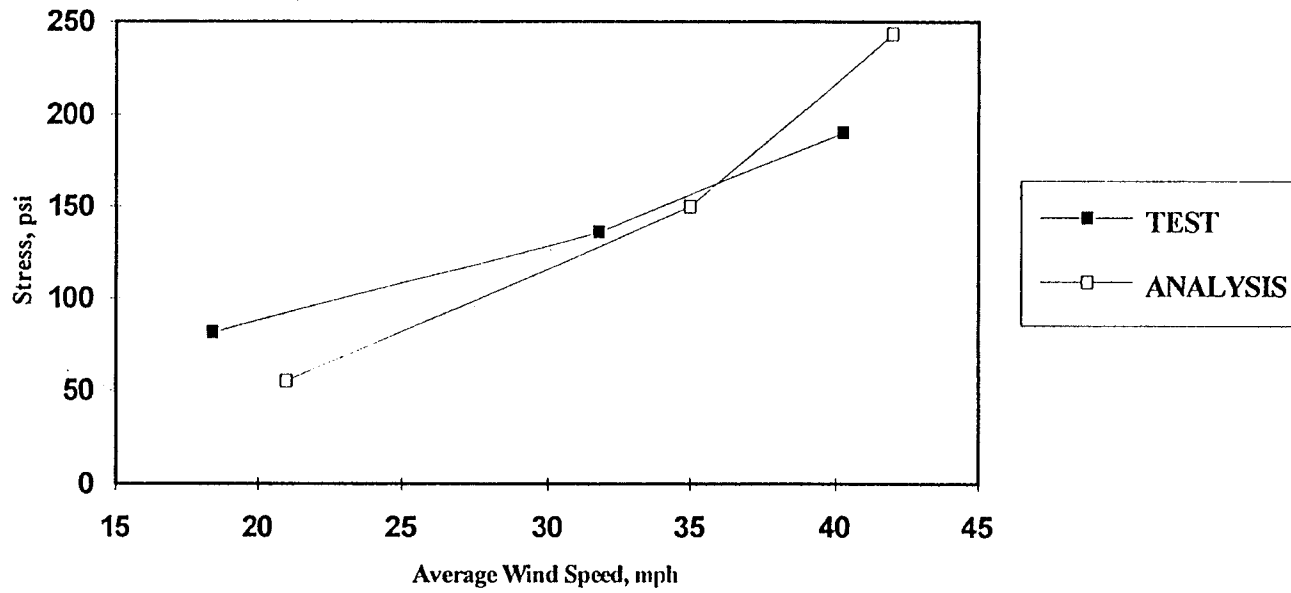
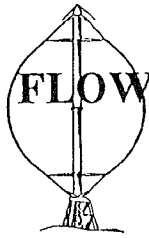


Figure 55



# FLOWIND CORPORATION'S ADVANCED EHD SERIES VAWT

Dynamic RMS value, URF1  
(Upper Root Blade Flatwise Bending)

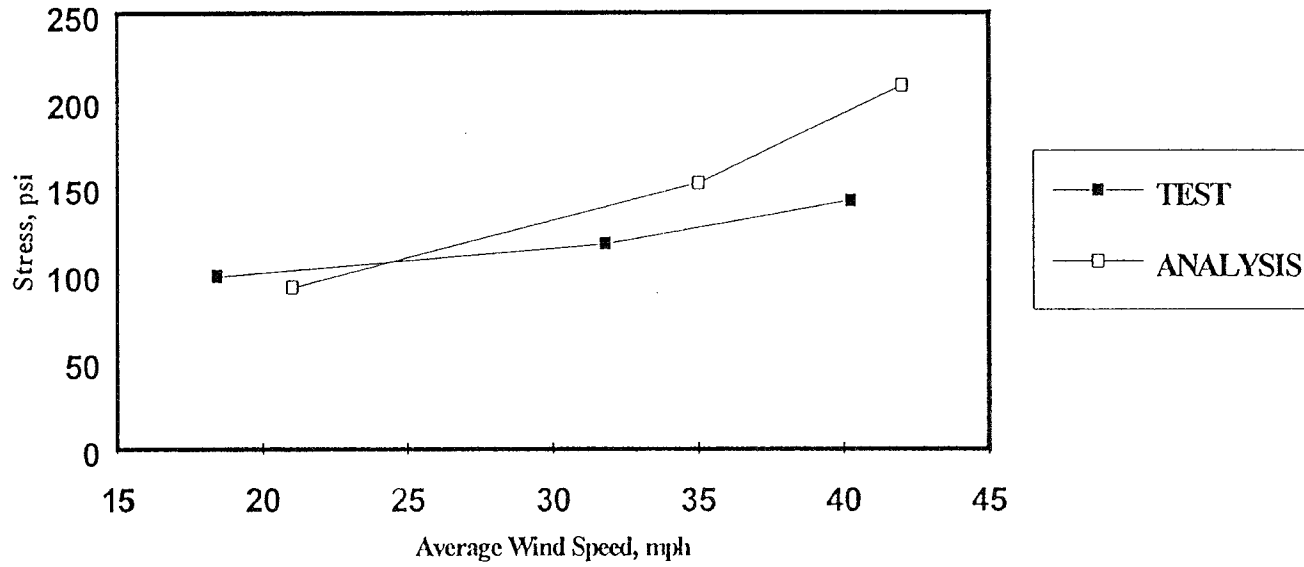
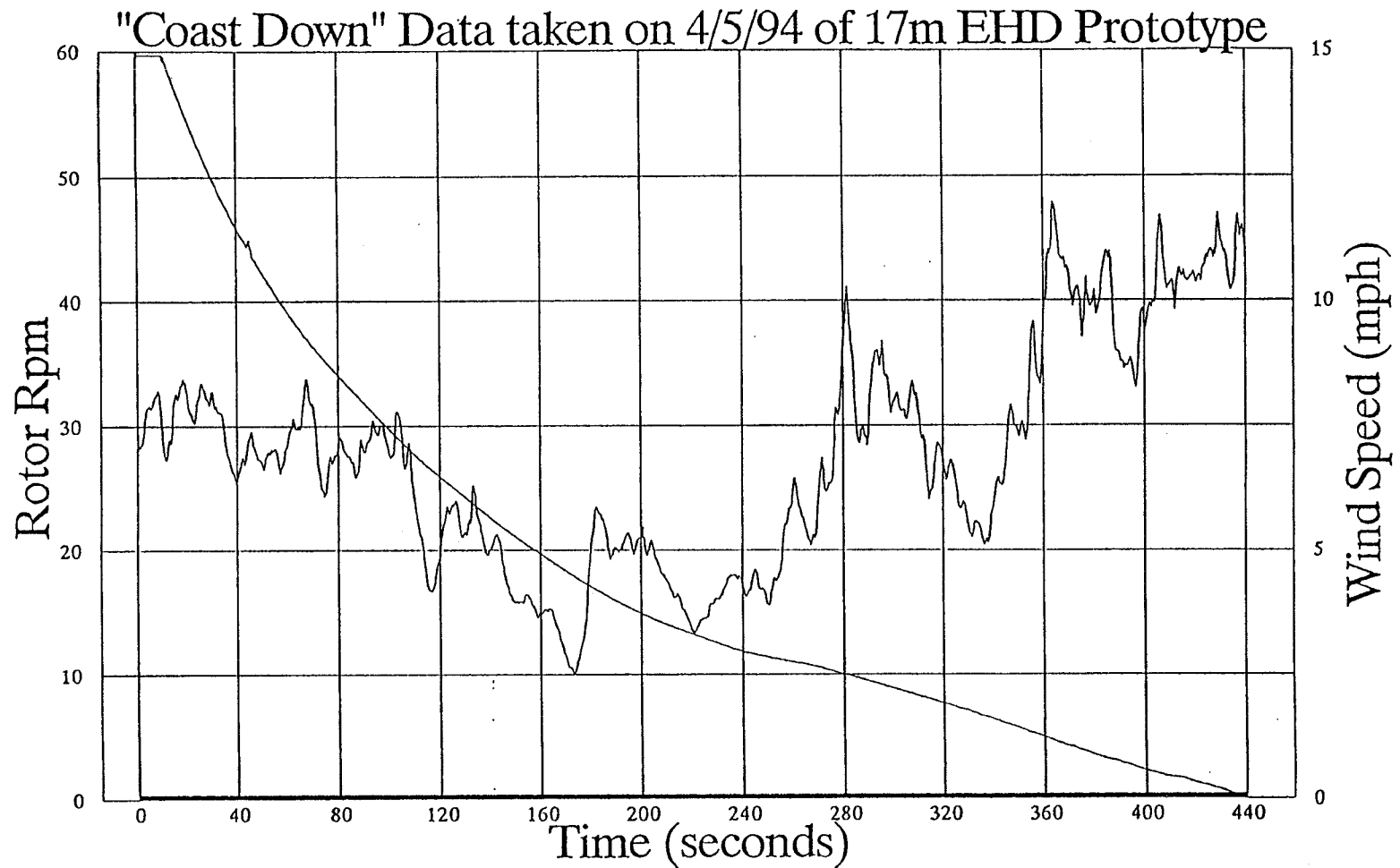


Figure 56

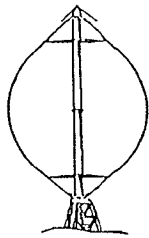


Figure 57

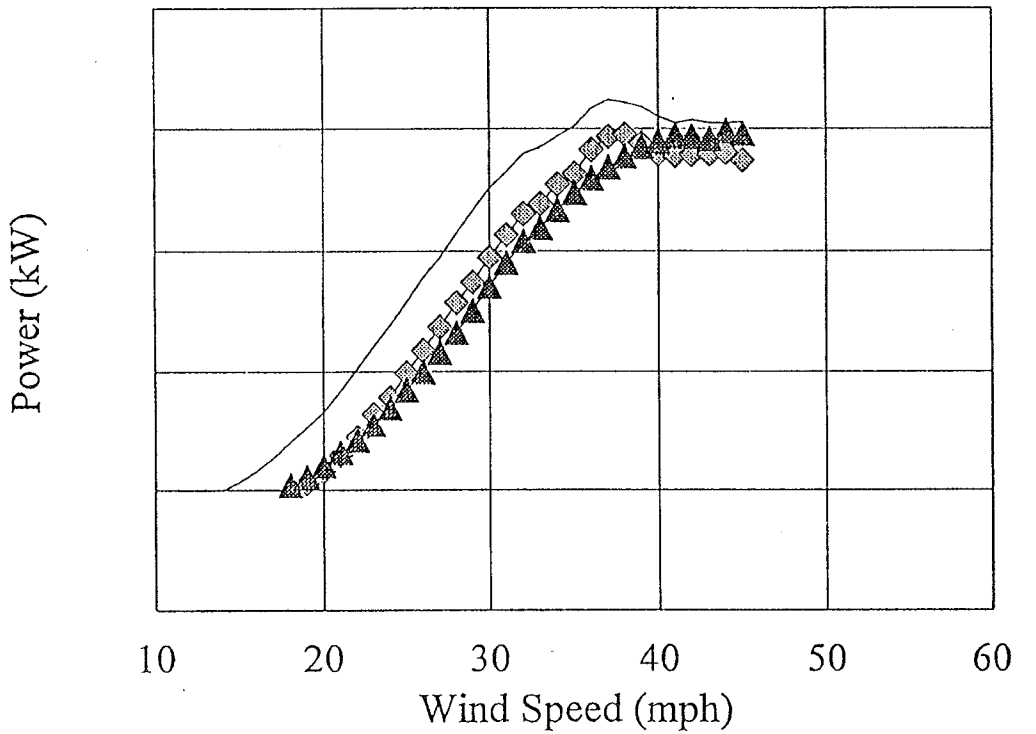


Note that there was some rubbing between brake disk and service brakes.

# FLOWIND CORPORATION'S ADVANCED EHD SERIES VAWT



## FloWind 17 EHD (SNLA 2150 Airfoil)

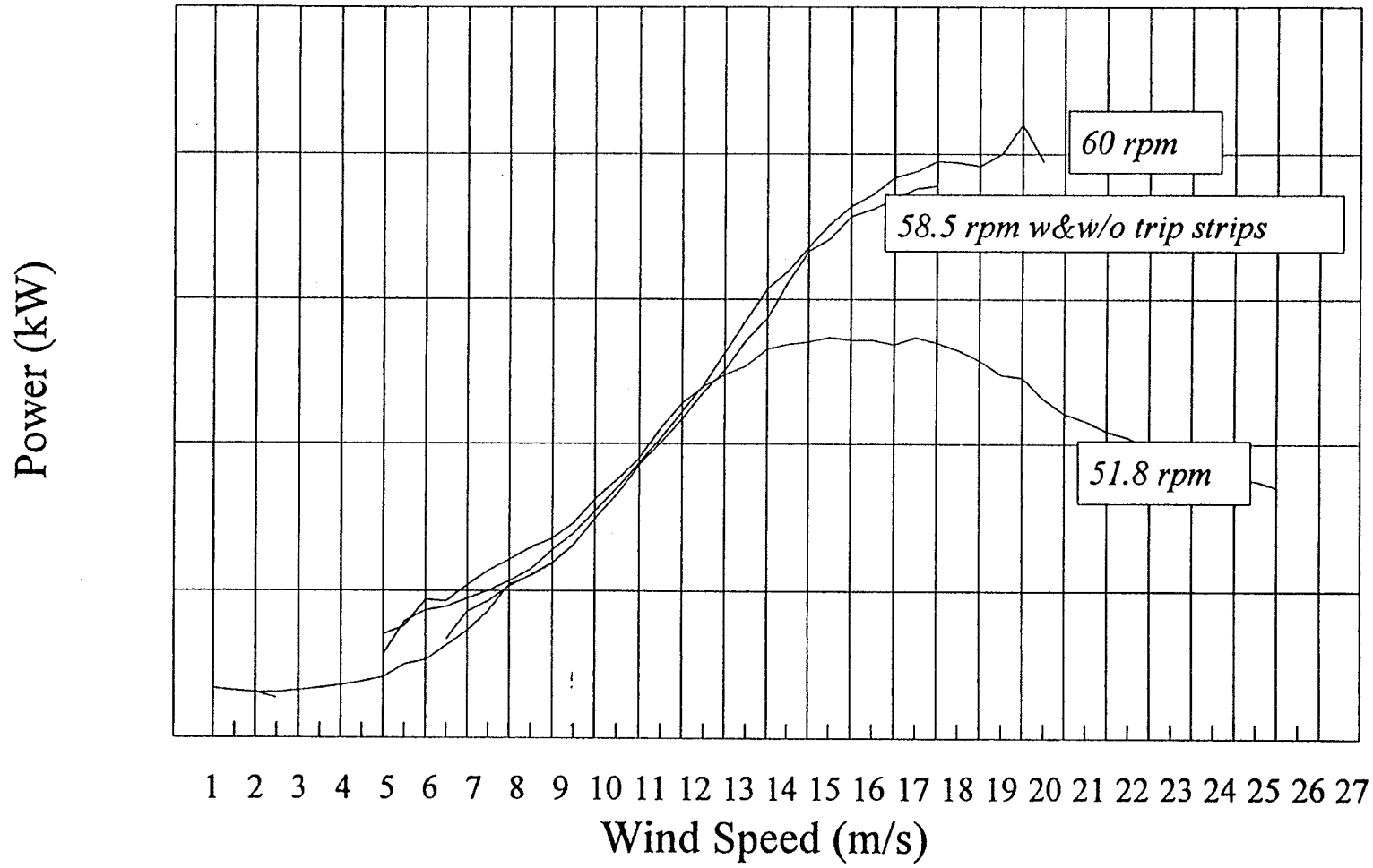


— Predicted SNLA 2150 Performance      ◆ SNLA 2150 with Predicted Laminar Bubble Drag  
 ▲ SNLA 2150 Measured Power Curve

Tehachapi Air Density, 92.5' Equator Height

Figure 58

# FloWind 17 EHD Measured Performance



— Power (11/3/94-51.8rpm)      — Power (8/30/94-58.5rpm)  
 — Power (8/29/94-58.5rpm ttu)      — Power (3/23/94-60rpm)

Figure 59

# Altamont Pass 19m Wake Test #1

Turbine on at 00, 30 minutes past each hour, off at 15, 45 minutes past each hour

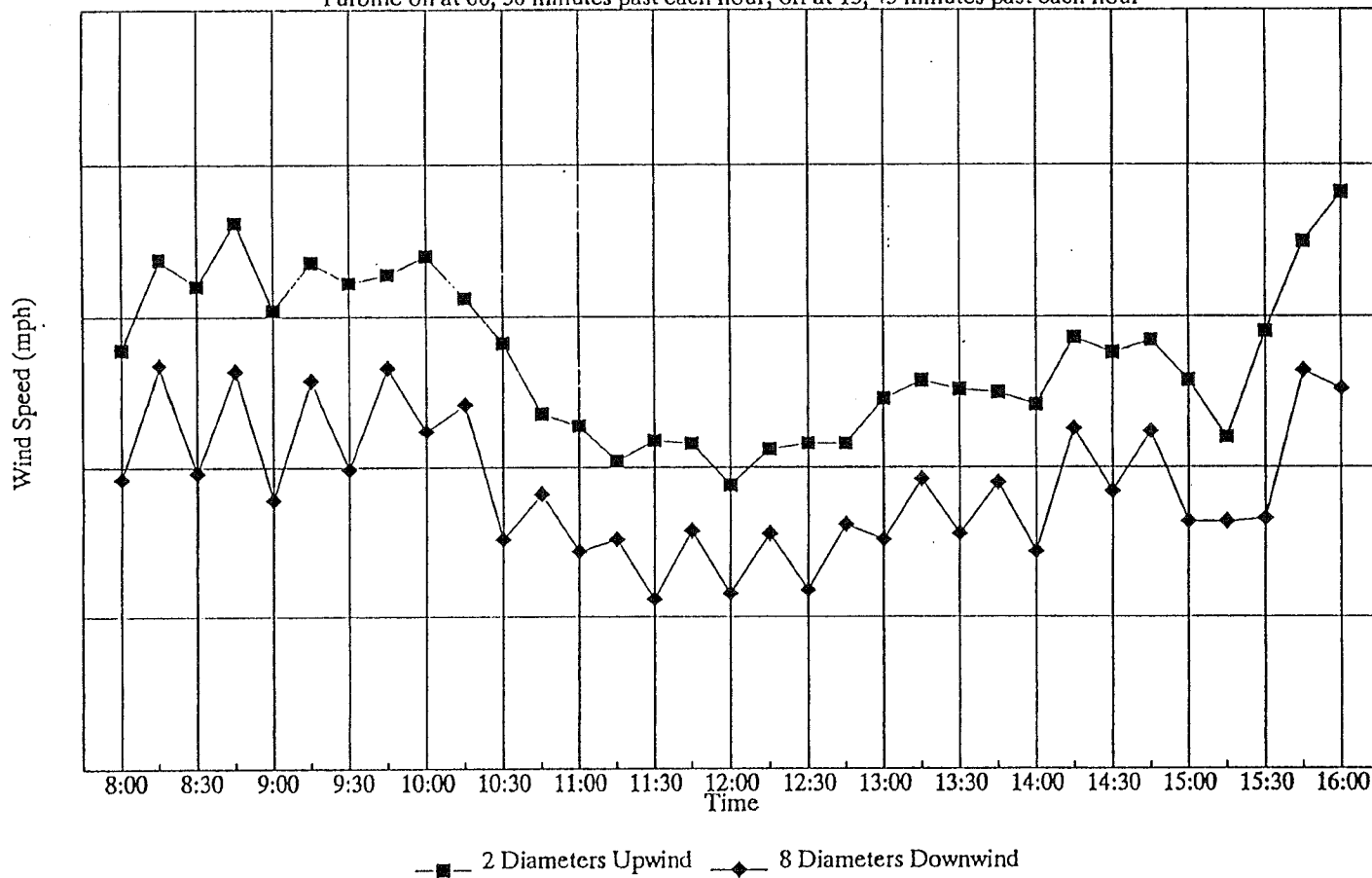


Figure 60

ANSYS 5.0 18  
 APR 20 1995  
 20:30:21  
 PLOT NO. 1  
 POST26

ZV = 1  
 DIST = 0.75  
 XF = 0.5  
 YF = 0.5  
 ZF = 0.5  
 CENTROID HIDDEN

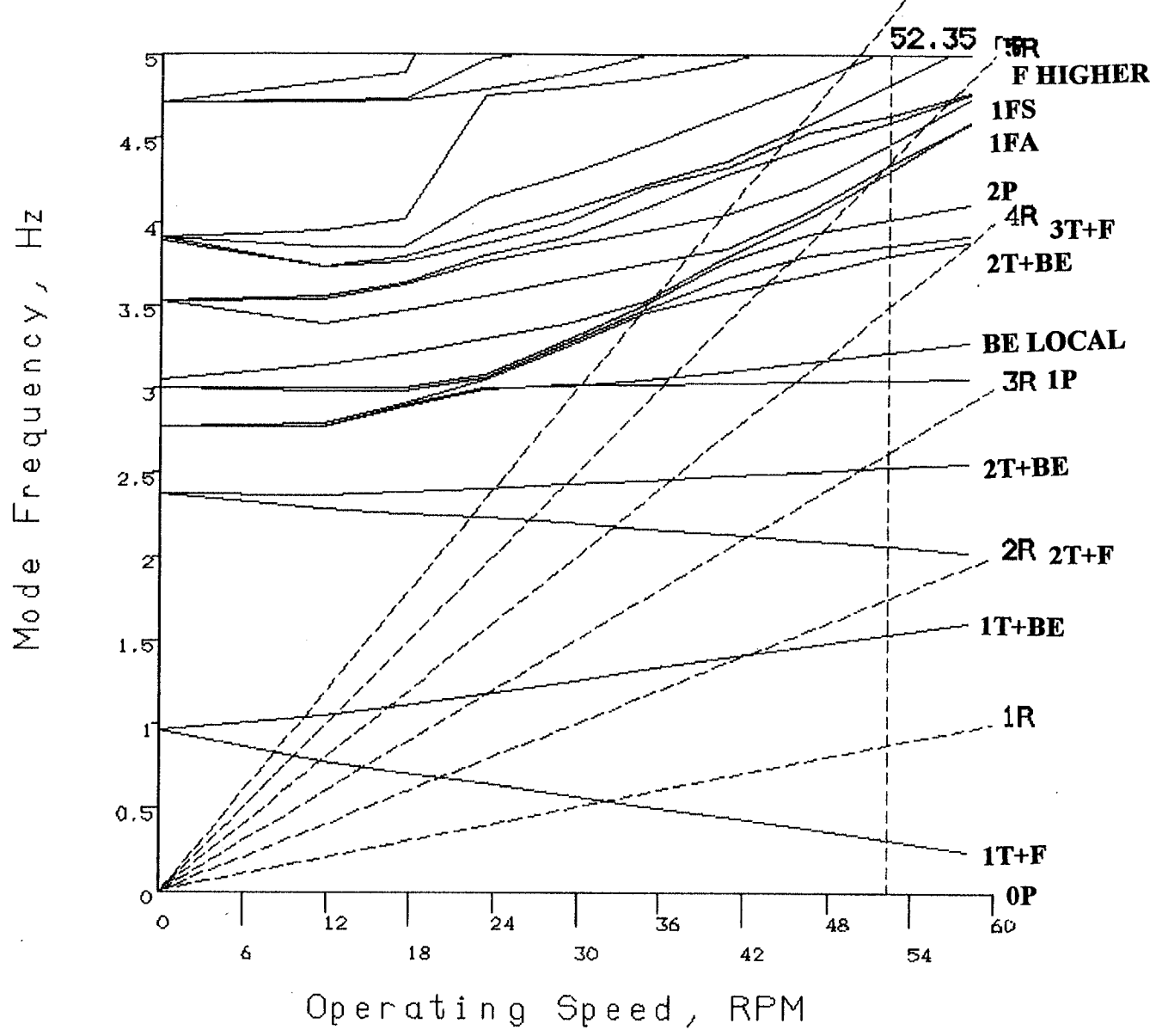
POST26

ZV = 1  
 DIST = 0.75  
 XF = 0.5  
 YF = 0.5  
 ZF = 0.5  
 CENTROID HIDDEN

POST26

ZV = 1  
 DIST = 0.75  
 XF = 0.5  
 YF = 0.5  
 ZF = 0.5  
 CENTROID HIDDEN

# CAMPBELL DIAGRAM



PROTOTYPE MACHINE ITERATION #3, 17.0m with SB24, 18% 27" blades

Figure 61

"B" BLADE

### FLUTTER DAMPING COEFFICIENTS

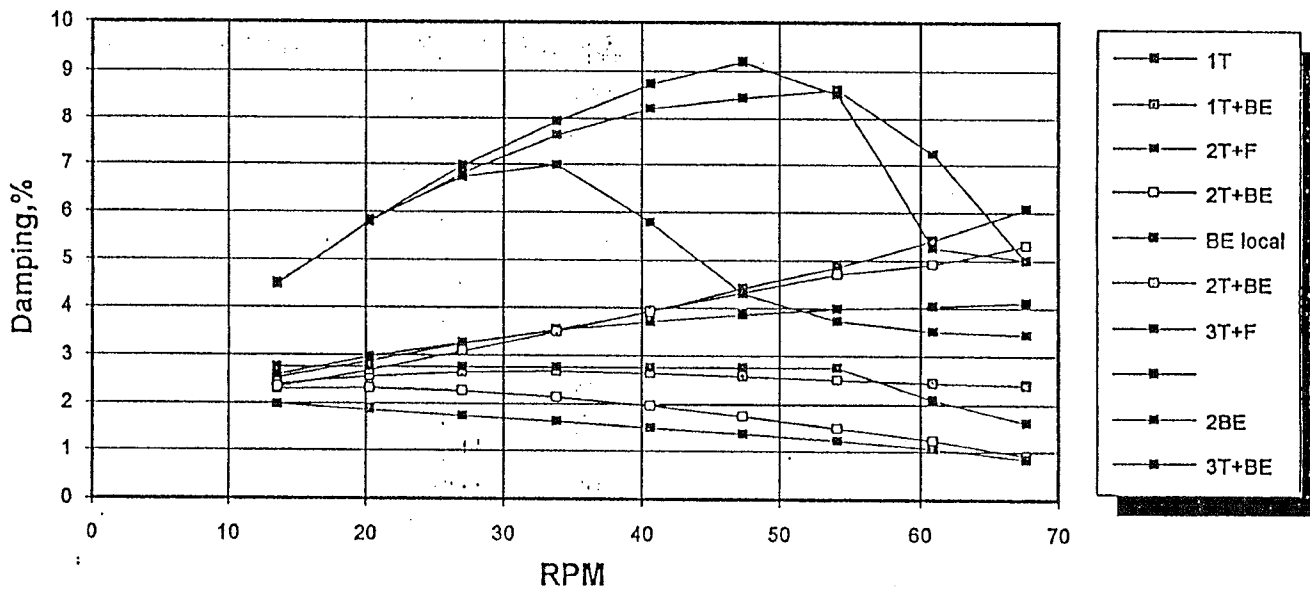


Figure 62

# VISCOUS FLOW SCHEMATIC

( $\alpha = 0^\circ$ )

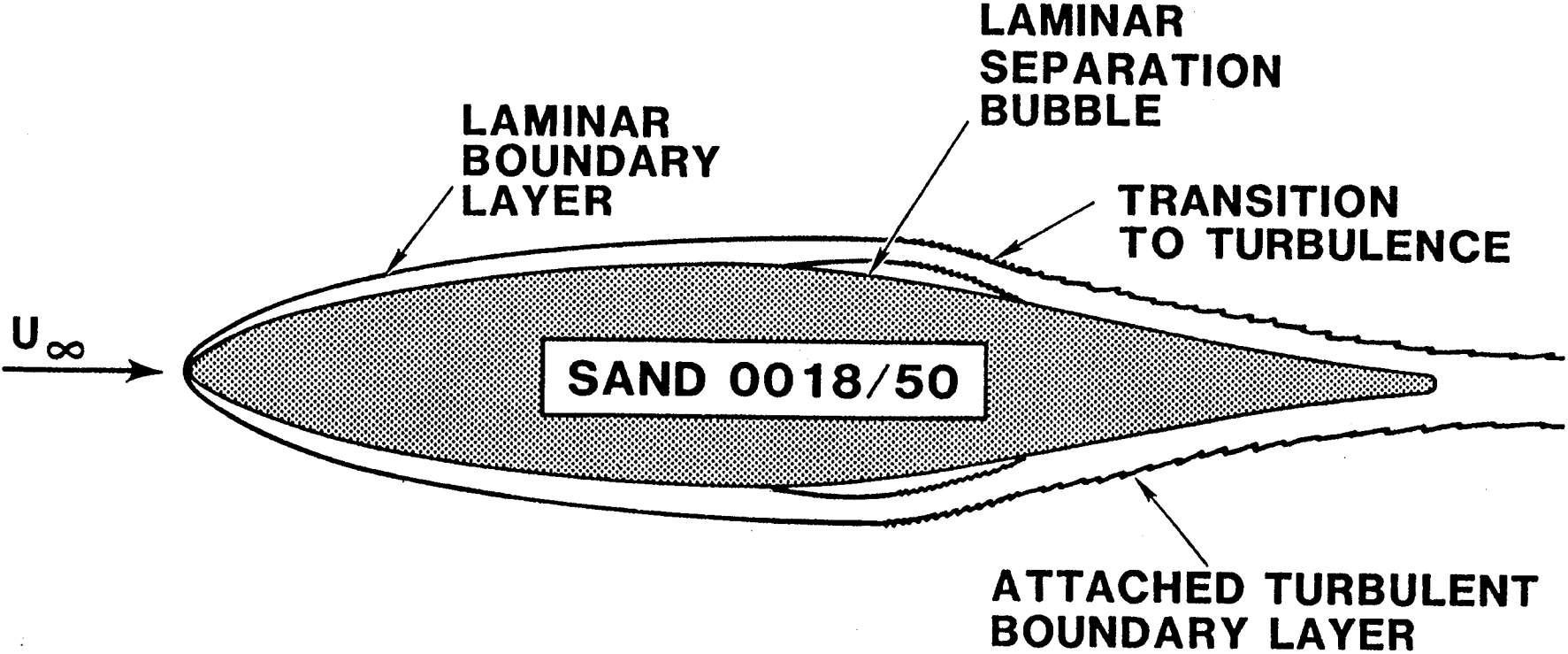


Figure 63

## DISTRIBUTION

B. Bell (10)  
FloWind Corporation  
990 A Street  
Suite 300  
San Rafael, CA 94901

C. P. Butterfield  
NREL  
1617 Cole Boulevard  
Golden, CO 80401

J. Cadogan  
U.S. Department of Energy  
Office of Photovoltaic & Wind  
Technology  
Energy Efficiency & Renewable Energy  
EE-11  
1000 Independence Avenue SW  
Washington, DC 20585

S. Calvert  
U.S. Department of Energy  
Office of Photovoltaic & Wind  
Technology  
Energy Efficiency & Renewable Energy  
EE-11  
1000 Independence Avenue SW  
Washington, DC 20585

P. R. Goldman  
Acting Deputy Director  
Office of Photovoltaic and  
Wind Technology  
Energy Efficiency & Renewable  
Energy, EE-11  
U.S. Department of Energy  
1000 Independence Avenue  
Washington, DC 20585

L. Helling  
Librarian  
National Atomic Museum  
Albuquerque, NM 87185

S. Hock  
Wind Energy Program  
NREL  
1617 Cole Boulevard  
Golden, CO 80401

P. Migliore  
NREL  
1617 Cole Boulevard  
Golden, CO 80401

W. Musial  
NREL  
1617 Cole Boulevard  
Golden, CO 80401

NWTC Library  
NREL  
1617 Cole Boulevard  
Golden, CO 80401

G. Nix  
NREL  
1617 Cole Boulevard  
Golden, CO 80401

D. Sanchez  
U.S. Dept. of Energy  
Albuquerque Operations Office  
P.O. Box 5400  
Albuquerque, NM 87185

R. W. Thresher  
NREL  
1617 Cole Boulevard  
Golden, CO 80401

M.S. 0437	E. D. Reedy, 9118
M.S. 0437	K. E. Metzinger, 9118
M.S. 0439	C. R. Dohrmann, 9234
M.S. 0439	D. W. Lobitz, 9234
M.S. 0557	T. G. Carne, 9741
M.S. 0708	H. M. Dodd, 6214 (50)
M.S. 0708	T. D. Ashwill, 6214
M.S. 0708	D. E. Berg, 6214
M.S. 0708	M. A. Rumsey, 6214
M.S. 0708	H. J. Sutherland, 6214 (5)
M.S. 0708	P. S. Veers, 6214
M.S. 0836	J. H. Strickland, 9116
M.S. 0836	W. Wolfe, 9116
M.S. 0619	Review & Approval Desk, 12630 (2) For DOE/OSTI
M.S. 0899	Technical Library, 4414 (5)
M.S. 9018	Central Technical Files, 8523-2